High Q-factor Metamaterial Duplex Filters in Suspended Stripline Technology

Der Technischen Fakultät
der Universität Erlangen-Nürnberg
zur Erlangung des Grades

D O K T O R - I N G E N I E U R

Shaik Geelani

Erlangen, März 2009

Metamaterial Duplex Filter hoher Güte mit hängenden Streifenleitungen

Als Dissertation genehmigt von
der Technischen Fakultät
der Universität Erlangen-Nürnberg

Tag der Einreichung : 22.12.2008
Tag der Promotion : 05.03.2009

Dekan:

Prof. Dr.-Ing. habil. Johannes Huber

Berichterstatter:

Prof. Dr.-Ing. Georg Fischer

Prof. Dr.-Ing. Jürgen Detlefsen

Contents

List of Figures

List of Tables

Acknowledgements

"In the Name of God, the most Beneficent, and Merciful". The work presented was supported by Alcatel-Lucent, Bell Labs Research, Nuremberg, Germany in co-operation with Friedrich-Alexander-University of Erlangen-Nuremberg and Technical University of Munich, HFS department. My sincere thanks to Prof. Georg Fischer who has given me this opportunity for making my doctoral thesis, his guidance, his appreciation throughout the work is unforgettable, without him I would have never got such an opportunity to work under the supervision of notable world class researcher Prof. Jürgen Detlefsen from Technical University of Munich, Germany. Their initial ideas, their interest and initiativeness gave me much interest and knowledge from beginning of the work till end at each and every point. I would say, without them I could not have make this thesis work. My special thanks to Michael Doubrava, Dr. Michael Söllner and Horst Schenkel for their kind suggestions and help throughout the work. I also thank ALU team Erwin Ruttmann for housing design, Uwe Schacht for PCB support who made this thesis work easy and fast. Also, thanks to the German ministry of research and education (BMBF) for funding part of my thesis work under MARIO project (Metamaterial based flexible duplex filters).

I would like to take this opportunity to thank my parents Mr & Mrs T.S.Abdul Rahaman, my sister and brother-in-law Mr & Mrs R.M.N.Rasool, my brother Shaik Fakhruddin, who supported me morally in any situation during my thesis work.

Abstract

This Doctoral thesis work describes the design of highly selective, low ripple metamaterial (MTM) based microstrip duplex filter (TX Band/RX Band) design for E-GSM 900 base stations. As the requirement for base stations, that are more flexible and their tendency to reduce unwanted transmitted/received signals, leads to the need of sharp edge, low ripple RF bandpass filters. These designs have been implemented using microstrip suspended substrate technology to reach good insertion loss and sharp stopbands. To compare with other microstrip technologies, we have kept our MTM research focussed on exploring suspended substrates for better result achievements. By designing a bandpass filter in microstrip suspended substrate, it is shown that metamaterial structures can be of great advantage for frequency agile RF systems.

During this doctoral thesis, we have proposed a new metamaterial transmission line filter structure with microstrip gap capacitors and open stub inductors (L, C, Quasi-Lumped). This structure is effectively homogenous (means, unitcell $<\lambda/10$) and hence satisfies the principle of metamaterials. At first, we have designed a balanced case of MTM Left-handed (LH) bandpass filter (TX-Band) with three unit cells in a microstrip shielded suspended substrate. This filter is designed for the application of E-GSM 900 base stations within 925 MHz - 960 MHz passband and 915 MHz stopband. The design was done with Agilent's ADS (Advance Design System) software simulator. Simulations are carried out both with circuit simulator (CS) as well with method of moments simulator (MOM). Their respective results are compared. Later, the designed TX-BPF printed circuit board (PCB) is manufactured on ROGERS RO4003 substrate material in a suspended substrate housing to measure and compare with the simulated results. Focus is kept in achieving passband attenuation less than -1 dB maintaining sharp stopbands within narrow range of 35 MHz.

Secondly, we have designed an RX (Receiver) bandpass filter (BPF) with 880 MHz - 915 MHz passband and 925 MHz in stopband using MTM structure in suspended substrate configuration. For the RX filter design, we have used a different structure in comparison with TX-Filter design but focussing on the same goals. This thesis work confines to show the state of art balanced left-handed metamaterial structures and its possible applications in designing RF building blocks like duplex filters within given area of specification. In this research, in contrast to the previous works on metamaterial filter designs with lambda/4 resonators, these have been replaced with lamda/2 resonators. Also, the importance/implications of balanced conditions in metamaterial structures are shown. Hence this thesis work is treated as a scientific approach.

Abstract

Diese Doktorarbeit befasst sich mit dem Entwurf von hochselektiven, welligkeitsarmen Metamaterial basierten Mikrostreifen Duplex Filtern für E-GSM 900 Basisstationen.

Da die Forderung nach mehr Flexibilität und der Wunsch nach Unterdrückung unerwnschter Störaussendungen zu steilflankingen, welligkeitsarmen Bandpassfiltern führt, haben wir solche Filterentwürfe auf Basis hängender Streifenleitungen implementiert, um gute Werte für die Einfügedämpfung und steile Flanken zu erreichen. Im Hinblick auf die verschiedenen Mikrostreifen Technologien haben wir unsere Metamaterial Forschung auf die Untersuchung hängender Streifenleitungen konzentriert um bessere Ergebnisse zu erzielen.

Mit dem Entwurf eines Bandpass Filters unter Nutzung hängender Streifenleitungen können wir zeigen, dass Metamaterial Strukturen von großem Nutzen für frequenzagile Hochfrequenz-Systeme sein können. In dieser Doktorarbeit schlagen wir neue Metamaterial Leitungsstrukturen auf Basis quasi-konzentrierter Elemente (L C Abmessungen $< \lambda/10$) mit Mikrostreifen Schlitz-Kondensatoren und offenen Stichleitungen als Spule vor. Zunächst haben wir ein balanciertes linkshändisches Metamaterial Bandpass Filter für das Sendeband mit 3 Einheitszellen unter Nutzung hängender Streifenleitungen entworfen.

Dieses Filter wurde entworfen für den Einsatz in E-GSM 900 Basisstationen mit einem Durchlassbereich von 925 MHz bis 960 MHz und einem Stoppband unterhalb 915 MHz. Der Entwurf wurde ausgeführt mit Agilents ADS (Advance Design System) Software Simulator. Die Simulationen wurden sowohl mit dem Schaltungssimulator (CS) als auch mit dem Momentensimulator (MOM) durchgeführt. Die Ergebnisse werden verglichen. Später wird das entworfene Sender Bandpass Filter auf Basis ROGERS RO4003 Substratmaterial gefertigt zusammen

mit einem Gehäuse für hängende Streifenleitungen und die Mess-und Simulationsergebnissen verglichen.

Der Schwerpunkt lag darauf, die Durchgangsdämpfung kleiner als -1 dB zu halten und gleichzeitig scharfe Stoppbandkanten innerhalb schmaler Übergangsbereiche von 35 MHz sicherzustellen. Zweitens haben wir einen Empfänger Bandpass mit einem Durchlassbereich von 880 MHz-915 MHz und einem Stoppband ab 925 MHz entworfen. Für den Entwurf des Empfangsfilters haben wir eine andere Struktur im Vergleich zum Senderfilter eingesetzt, aber unter Berücksichtigung der gleichen Optimierungsziele.

Diese Arbeit beschränkt sich darauf den neuesten Stand der Technik bei balancierten linkshändischen Metamaterial Strukturen und ihre potentiellen Anwendungen beim Entwurf von HF Baugruppen wie Duplex Filtern unter Einhaltung der Spezifikation zu zeigen. In dieser Forschung wurden im Gegensatz zu früheren Arbeiten zu Metamaterial Filtern mit $\lambda/4$ Resonatoren diese mit $\lambda/2$ Resonatoren ersetzt. Zudem wird die Wichtigkeit/Anwendung balancierter Betriebsbedingungen bei Metamaterial-Strukturen gezeigt.

Infolgedessen wird diese Doktorarbeit als wissenschaftliche Studie betrieben.

List of Abbreviations

MTM	Metamaterials
BPF	Band Pass Filter
CRLH	Composite Right/Left-Handed materials
TX	Transmitter
RX	Receiver
LH	Left Handed
RH	Right Handed
LHM	Left Handed Materials
RHM	Right Handed Materials
PLH	Pure Left Handed
PRH	Pure Right Handed
E-GSM	Enhanced Global System for Mobile Communications,
RF	Radio Frequency
dB	Decibel
dB[21]	Forward transmission or insertion loss in decibels
dB[11]	Reverse reflection or return loss in decibels
C_{RH}	Right Handed capacitance in [pF]
C_{LH}	Left Handed capacitance in [pF]
L_{LH}	Left Handed inductance in [nH]
λ	Wavelength
L_{RH}	Right Handed inductance in [nH]
R_s	Series resistance in [Ohm]
R_p	Shunt resistance in [Ohm]
ϵ_e	Effective dielectric constant
ϵ_r	Relative permittivity
μ	Permeability
f	Frequency in [MHz]
f_{se}	Series resonant frequency in [MHz]
f_{sh}	Shunt resonant frequency in [MHz]
Q-factor	Quality factor
CS	Circuit simulator

MOM	Method of moments analysis
ADS	Advanced Design System
TL	Transmission Line
L	Inductance in [nH]
$\lambda/4$ TL	Quarter wavelength transmission line
$\lambda/2$ TL	Half wavelength transmission line
NF	Noise Figure
ω	Angular frequency
PCB	Printed circuit board
R	Resistance in [Ohm]
EM	ElectroMagnetic
MCROSS	Microstrip four port connector cross
QOS	Quality of service
MIMO	Multiple Input-Multiple Output
SNR	Signal to Noise ratio
SMA	Sub Miniature A: Standard RF Connector
σ	Conductivity in [S/m]
β	Propagation constant
Γ	Reflection co-efficient
WLAN	Wireless Local Area Network
BW	Band Width
Z	Impedance
v_g	Group velocity
v_p	Phase velocity
Z_L	Load impedance
Z_in	Input impedance
Z_0	Output impedance
Z_c	Characteristic impedance

Chapter 1

Introduction

During the years of infancy for metamaterials (MTMs), which emerged from the first experimental demonstration of a left-handed (LH) structure in 2000, the vast majority of the groups involved in research on MTMs have been focusing on investigation from a physics point of view. The fundamental properties of LH media was predicted by Veselago in 1967 [15]. Not following this trend, the researchers adopted as engineering approach based on a generalized transmission line (TL) theory, with systematic emphasis on developing practical applications. Exhibiting resulted in the elaboration of the powerful composite right/left-handed (CRLH) MTM concept, which has led to novel guided-wave, radiated-wave and refractive-wave devices and structures.

Metamaterials are artificial structures that can be designed to exhibit specific electromagnetic properties that are not commonly found in nature [22]. These metamaterials, which in principle can be synthesized by embedding or including various constituents of novel geometrical shapes and forms in some host media, possess exciting features and interesting electromagnetic properties. Metamaterials with negative permittivity "ϵ" and negative permeability "μ" are commonly referred as left handed materials (LHM) [1]. The general transmission line (TL) approach provides the physical approach of LHM's and hence an efficient tool for LH (Left hand) applications. LHM's are considered to be a more general model

of composite right/left (CRLH) materials, which also occurs naturally as right handed (RH) effects in practical LHM's [5]. A homogenous negative index transmission line (TL) or left-handed (LH) transmission line does not exist in nature, it has to be approached by an artificial structure, which is usually constructed from a series of discontinuous sections operating in a restricted frequency range. A typical realization is found in a quasi-lumped transmission line [50] with elementary cells consisting of a series capacitors and shunt inductors. The unique properties of LHM's have allowed RF and Microwave applications, concepts and devices to be developed.

Precisely, we are implementing a metamaterial structure in the applications of RF duplex filters taking cost and size reductions into consideration as well to prove the state of art. The main task of the duplex filter is to separate transmit and receive frequencies at the antenna port. A typical duplex filter thus has three ports, one for the antenna, the other two for transmitter and receiver respectively. A typical duplex filter is composed of coaxial resonators that require advanced fabrication techniques and materials to achieve high Q-factor (e.g 5000) that are needed to provide high filter selectivity. Filter selectivity is critical in a base station, because very sensitive receivers are operated simultaneously parallel with strong transmitters. In some applications, MIMO systems have proven to ease the cost prohibitive, because of the cost of the duplex filters alone.

1.1 Aims of this work

The requirement for base stations that are more flexible and their multi-band capability leads to the need of RF functional blocks and duplex filters [16]. In base stations, transmit and receive paths have to be separated by a duplexer, which has to handle high power up to 200 W peak and at the same time the sensitivity of the receiver path should not be degraded [23]. For a frequency agile base station, it is required that not only radio and power amplifier are frequency

agile, but also the duplex filter (TX BPP+RX BPF) and the antenna to facilitate a remote alteration of the operating frequency band.

This doctoral thesis includes the design and characterization of MTM RF Duplex filters for the application of E-GSM 900 base stations i.e TX-band (925 MHz-960 MHz) and RX-band (880 MHz-915 MHz) respectively. At first, TX MTM BPF is realized using lumped components and then simulated in Agilent's ADS simulation software. Later, we have implemented the lumped elements in CRLH TL approach with three unit cells in shielded suspended substrate. In this thesis work we have worked using both circuit simulator and method of moments simulators of ADS software and hence compared with the fabricated printed circuit board PCB. A similar approach was followed for the RX BPF design.

In our both designs, we have proposed a new filter structure with microstrip gap capacitors and open stub inductors in context with the previous works [11,24], which includes interdigital capacitors, short stubs and open stubs. Our main goal in this thesis work has been attributed towards achievement of low insertion losses (ripple) and sharp stopband (Edges) and hence to prove the state of art CRLH MTM structures. Also we have kept focus on suspended substrate technology to see the result comparison with the other microstrip technologies and hence to choose the goal oriented suitable technology.

1.2 Thesis Structure

- The second chapter describes, the electromagnetic theory on left handed materials, their basic properties involved and required in designing filters.
- In the third chapter, implementation of transmission line theory on metamaterial structures is explained with respect to their importance in designing bandpass filters.
- In chapter four, we discuss CRLH metamaterial theory on filter applications

along with our new proposed bandpass filter structure in comparison with previously published and practically implemented structures.

- In chapter five, we explain the motivation and application of MTMs in frequency agile RF systems, we introduce theoretical introduction of suspended substrate technology on metamaterial filters. We present a TX Filter design with simulation, measurement board results along with comparisons.

- In the sixth chapter, an RX filter design with simulation and measurement board results is shown.

At the end of the thesis work, we discuss the conclusions along with recommendations on future work.

Chapter 2

Electromagnetic Theory of Left Handed Materials

2.1 Metamaterials

Electromagnetic metamaterials are broadly defined as artificial effectively homogeneous structures with unusual properties not readily available in nature [6]. Where homogeneous structures corresponds to those, whose structural cell size "p" is much smaller than guided wavelength "λ_g" (Typically $\lambda/10$). The nature of the unit cell depends on the constitutive parameters which are related to the refractive index "n" by equation,

$$n = \pm\sqrt{\epsilon_r \mu_r}. \tag{2.1}$$

Where ϵ_r and μ_r are the relative permittivity and permeability related to free space permittivity and permeability by ϵ_0=ϵ/ϵ_r = 8.854x$10^{-12}$and μ_0=μ/μ_r = 4πx10^{-7} respectively. The four possible sign combinations in the pair (ϵ,μ) are (+,+),(+,-),(-,+),(-,-) and are shown in the fig. 2.1. The first three duplets present conventional materials whereas, negative negative combination is referred to as Left handed (LH) materials and are characterized as antiparallel phase and group

velocities or negative refractive index (NRI). Therefore clearly LH structures are MTM and are artificial which exhibits unusual properties.

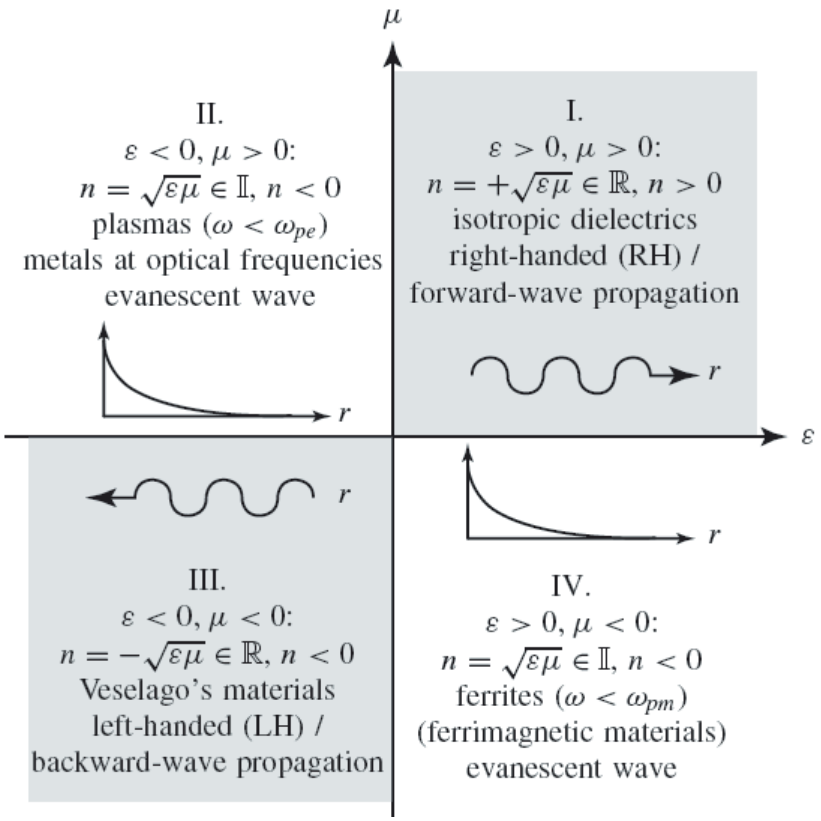

Figure 2.1: Permittivity-Permeability Diagram [16]

Where R and I in the figure represents Real and Imaginary terms and ω_{pe} and ω_{pm} are the electric and magnetic plasma frequencies respectively.

The history of MTM came in to existence in 1960's with the visionary speculation on the existence of negative permittivity ϵ and negative permeability μ by the Russian physicist Viktor Veselago [1]. He concluded that such a media are allowed by Maxwell's equations. J. B. Pendry [2] was the first to theorize a practical way to make a left-handed metamaterial (LHM). Allowing an electromagnetic wave to convey energy (have a group velocity) in the opposite direction to its phase velocity. Pendry's initial idea was that, metallic wires aligned along propagation direction could provide a metamaterial with negative permittivity ($\epsilon < 0$). His

challenge was to construct a material which also showed negative permeability ($\mu < 0$). In 1999, Pendry demonstrated that an open ring ('C' shape) with axis along the propagation direction could provide a negative permeability [3]. In the same paper, he showed that a periodic array of wires and ring could give rise to a negative refractive index.

C. Caloz et al., Iyer and Eleftheriades followed with a transmission line [TL] approach on metamaterials [5], [6] and further theoretical expansions on CRLH (Composite Right/Left Handed) MTM (Metamaterial) structures [9]-[11]. The Caloz/Ithoh research group also applied these results in [9],[11] for bandpass filters (BPF). By taking their ideas into consideration, in this thesis work we have extended metamaterial filter application for high selectivity and high power handling.

2.2 Wave Propagation in Left-Handed Media

In order to show wave propagation in left-handed media, let us reduce Maxwell's equations [39]:

$$\nabla X\overline{E} = -\frac{\partial \overline{B}}{\partial t} - \overline{M_s}.....(Faraday's\,Law) \tag{2.2}$$

$$\nabla X\overline{H} = \frac{\partial \overline{D}}{\partial t} + \overline{J_s}.....(Ampere's\,Law) \tag{2.3}$$

$$\nabla.\overline{D} = Q_e.....(Electric\ Gauss\,Law) \tag{2.4}$$

$$\nabla.\overline{B} = Q_m.....(Magnetic\ Gauss\,Law) \tag{2.5}$$

Where $\overline{E}$ (V/m) is the electric field intensity, $\overline{H}$ (A/m) is the magnetic field intensity, $\overline{D}$ (C/m^2) is the electric flux density, $\overline{B}$ (W/m^2) is the magnetic flux density. And $\overline{M_s}$ (V/m^2) is the fictitious magnetic current density, $\overline{J_s}$ (A/m^2) is

the electric current density, $\overline{Q}_e$ (C/m^3) is the electric charge density, $\overline{Q}_m$ (C/m^3) is the magnetic charge density.

If the medium is linear and non-anisotropic (ϵ, μ doesn't depend on $\overline{E}$, $\overline{H}$), then the vector pairs of [$\overline{D}$, $\overline{E}$] and [$\overline{B}$, $\overline{H}$] are related as [28].

$$\overline{D} = \epsilon_0\overline{E} + \overline{P} = \epsilon_0(1+\chi_e)\overline{E} = \epsilon_0\epsilon_r\overline{E} = \epsilon\overline{E} \tag{2.6}$$

$$\overline{B} = \mu_0\overline{H} + \overline{M} = \mu_0(1+\chi_m)\overline{H} = \mu_0\mu_r\overline{H} = \mu\overline{E} \tag{2.7}$$

where, $\overline{P}$ =$\epsilon_0\chi_e$ and $\overline{M}$ =$\mu_0\chi_m$ are the electric and magnetic polarizations respectively and χ_e, χ_m are the electric and magnetic susceptibilities. Also ϵ_r=1+χ_e and μ_r=1+χ_m are the permittivity and permeability of the material considered and can be written as.

$$\epsilon_r = \epsilon' - j\epsilon'' = \epsilon'(1 - j\tan\delta_e), \tan\delta_e = \frac{\omega\epsilon'' + \sigma_e}{\omega\epsilon'} \tag{2.8}$$

$$\mu_r = \mu' - j\mu'' = \mu'(1 - j\tan\delta_m), \tan\delta_m = \frac{\omega\mu'' + \sigma_m}{\omega\mu'} \tag{2.9}$$

Where σ_m and σ_e are the electrical and magnetic conductivities respectively. The imaginary parts in the above equation represents losses. Assuming harmonic fields with the time dependence e^{+jwt} and defining the corresponding generic phasor $\overline{F}(\overline{r})$ as [17]

$$\overline{F}(\overline{r}, t) = Re[\overline{F}(\overline{r})e^{+jwt}] \tag{2.10}$$

where $\overline{F}$ can represent any physical quantity in eqn. 2.10. Maxwell's equations and the constitutive equations can be written as

$$\nabla X\overline{E} = -j\omega\mu\overline{H} - \overline{M_s} \tag{2.11}$$

$$\nabla X\overline{H} = -j\omega\epsilon\overline{E} - \overline{J_s} \tag{2.12}$$

$$\nabla.\overline{D} = -\rho_e \tag{2.13}$$

$$\nabla.\overline{B} = \rho_m \tag{2.14}$$

and

$$\overline{D} = \epsilon\overline{E} \tag{2.15}$$

$$\overline{B} = \mu\overline{H} \tag{2.16}$$

For a plane wave,

$$\overline{E} = \overline{E}_0 e^{-j\overline{\beta}.\overline{r}} \tag{2.17}$$

$$\overline{H} = \frac{\overline{E}_0}{\eta} e^{-j\overline{\beta}.\overline{r}} \tag{2.18}$$

Where η=$[\overline{E}]/[\overline{H}]$is the wave impedance. Let us assume the medium is loss-less then the above equations can be reduced for our simplicity. i.e ϵ''=μ''=0 and $\overline{H}_s$=$\overline{J}_s$=0.

Then

$$\overline{\beta} X \overline{E} = +\omega\mu\overline{H} \tag{2.19}$$

$$\overline{\beta} X \overline{H} = -\omega\epsilon\overline{E} \tag{2.20}$$

Which is familiar right-handed triad ($\overline{E}$, $\overline{H}$, $\overline{\beta}$) shown in the below figure. In case of left-handed traid as ϵ,μ<0, and therefore[ϵ]=-ϵ>0 and [μ]=-μ>0,[8]

$$\overline{\beta} X \overline{E} = -\omega \left|\mu\right| \overline{H} \tag{2.21}$$

$$\overline{\beta} X \overline{H} = +\omega \left|\epsilon\right| \overline{E} \tag{2.22}$$

As the frequency being always a positive quantity, the phase velocity is [16]

$$\overline{\nu}_p = \frac{\omega}{\beta}\hat{\beta}, where\left(\hat{\beta} = \overline{\beta}/\left|\overline{\beta}\right|\right) \tag{2.23}$$

Then,

$$RHMedium : \beta > 0(\nu_p > 0) \tag{2.24}$$

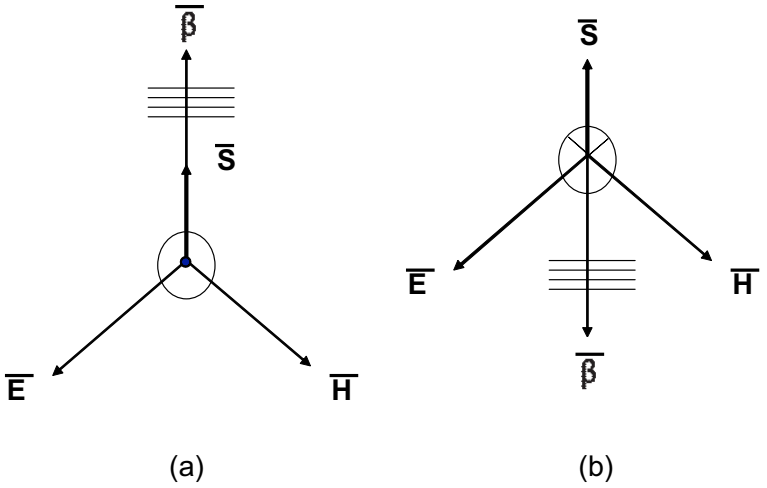

Figure 2.2: Electric - Magnetic Field wave vector (a)Right-Handed Medium (b)Left-Handed Medium [3]

$$LHMedium : \beta < 0(\nu_p < 0) \tag{2.25}$$

Therefore, the eqn. 2.21 and 2.22 can be generalized as,

$$\overline{\beta} X \overline{E} = s\omega \left|\mu\right| \overline{H} \tag{2.26}$$

$$\overline{\beta} X \overline{H} = -s\omega \left|\epsilon\right| \overline{E} \tag{2.27}$$

Where s is "handedness"function which is given as,

$$S = \begin{pmatrix} +1, RH \\ -1, LH \end{pmatrix} \tag{2.28}$$

From eqn. 2.23 in LH medium phase velocity ν_p propagates backward to the source in the opposite direction to that of power, related to group velocity ν_g. The backward propagation implies that the fields have a time-space dependence. Let us assume transverse electromagnetic (TEM) propagation in a homogeneous and isotropic medium,

$$\overline{E}, \overline{H} \approx e^{+j(\omega t + |n| k_0 r)}. \tag{2.29}$$

The propagation constant has only one component that is equal to the wave number k_n in the medium

$$\beta = k_n = nk_0 = n\frac{\omega}{c} \tag{2.30}$$

where,

$$n = \pm\sqrt{\epsilon_r \mu_r} \tag{2.31}$$

In a LH medium, since β<0, eqn. 2.30 and 2.31 reveals that a negative refractive index (NRI), n<0. Which states that the index of refraction is negative in a medium with negative permittivity and permeability. Then in general, the refractive index can be written as,

$$n = s\sqrt{\epsilon_r \mu_r} \tag{2.32}$$

2.2.1 Energy Density and Group Velocity

If the negative values for ϵ and μ are introduced in the usual expression for the time-average density of energy in transparent nondispersive media [26], then U_n is given by

$$U_n = \frac{1}{4}\{\epsilon|E|^2 + \mu|H|^2\} \tag{2.33}$$

which produces the nonphysical result of negative density of energy. It is well known that any physical media other than vaccum must be dispersive[16] and the above equation is valid for very weakly dispersive media. The quasi monochromatic wave packet traveling in a dispersive media is given by [26]

$$U = \frac{1}{4}\{\frac{\partial(\omega\epsilon)}{\partial\omega}|E|^2 + \frac{\partial(\omega\mu)}{\partial\omega}|H|^2\} \tag{2.34}$$

Where the derivatives are evaluated at the central frequency of the wavepacket. Thus, the physical requirement of positive energy density implies, that

$$\frac{\partial(\omega\epsilon)}{\partial\omega} > 0, \frac{\partial(\omega\mu)}{\partial\omega} > 0 \tag{2.35}$$

Which are compatible with ϵ<0 and μ<0, provided $\frac{\partial(\omega\epsilon)}{\partial\omega}> |\epsilon|/\omega$ and $\frac{\partial(\omega\mu)}{\partial\omega}> |\mu|/\omega$. Therefore, physical left-handed media must be highly dispersive. This fact is in agreement with the low-loss Drude-Lorentz model for ϵ and μ, which predicts negative values for ϵ and/or μ in the highly dispersive regions just above resonances.

Backward-wave propagation implies opposite signs between phase and group velocities [32]. In fact,

$$\frac{\partial k^2}{\partial\omega} = 2k\frac{\partial k}{\partial\omega} \equiv 2\frac{\omega}{\nu_p\nu_g} \tag{2.36}$$

where $\nu_p = \omega/k$ and $\nu_g = \partial\omega/\partial k$ are the phase and group velocities respectively. In addition, from $k^2 = \omega^2\epsilon\mu$ and eqn. 2.35:

$$\frac{\partial k^2}{\partial\omega} = \omega\epsilon\frac{\partial(\omega\mu)}{\partial\omega} + \omega\mu\frac{\partial(\omega\epsilon)}{\partial\omega} < 0. \tag{2.37}$$

Finally,

$$\nu_p\nu_g < 0. \tag{2.38}$$

2.2.2 Inverse Doppler Effect

When a moving reflector detects the radiation coming from a source at rest in a uniform medium, the detected frequency of the radiation depends on the relative velocity of the emitter and the receiver which is known as Doppler Effect. If this relative velocity is much smaller than the velocity of light, a non-relativistic analysis suffices to describe such an effect. If the receiver moves towards the source, wavefronts and receiver move in opposite directions. Therefore, the frequency seen by the receiver will be higher than the frequency measured by an observer at rest. If the medium is a left-handed material, then the wave propagation is backward and wavefronts move towards the source. Therefore, both the reflector and the wavefronts move in the same direction, and the frequency measured at

the receiver is smaller than the frequency measured by the observer at rest and can be seen in the figure. 2.3.

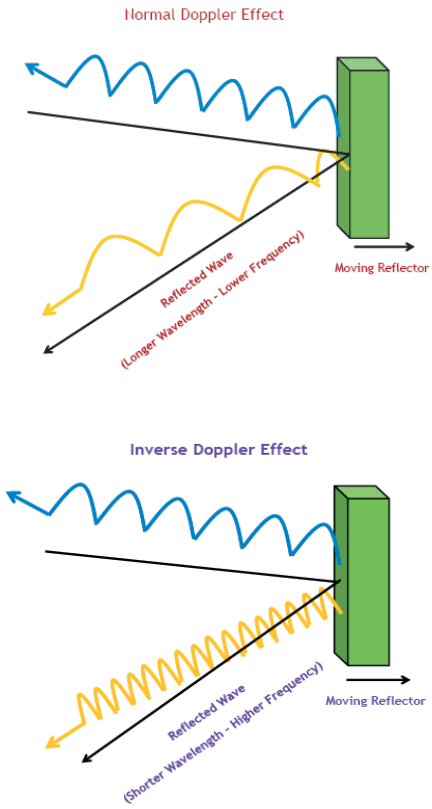

Figure 2.3: Inverse Doppler Effect [17]

The frequency shifts are given by [17]:

$$\Delta\omega = \pm\omega_0 \frac{n\nu}{\nu_p} \tag{2.39}$$

where ω_0 is the frequency of the radiation emitted by the source, ν is the velocity of at which the reflector moves towards the source, ν_p the phase velocity of light in the medium, and the $\pm$ applies to RH/LH media with refractive index 'n'.

Also $\Delta\omega$, is the difference between the frequency detected at the reflector and the frequency of oscillation of the source. More clearly,

$$\Delta\omega = \omega_0 \frac{n\nu}{c} \tag{2.40}$$

For n<0, the frequency shift becomes negative for positive ν.

2.2.3 Backward Cerenkov Radiation

Cerenkov radiation occurs when a charged particle enters an ordinary medium at a velocity higher than the velocity of light in such a medium. If the deceleration of this particle is not too high, its velocity can be considered approximately constant over many wave periods. In figure 2.4 the spherical wavefronts radiated by this particle become delayed with regard to the particle in motion thus giving rise to a shock wave [17], which travels forward, making an angle θ with the particle velocity.

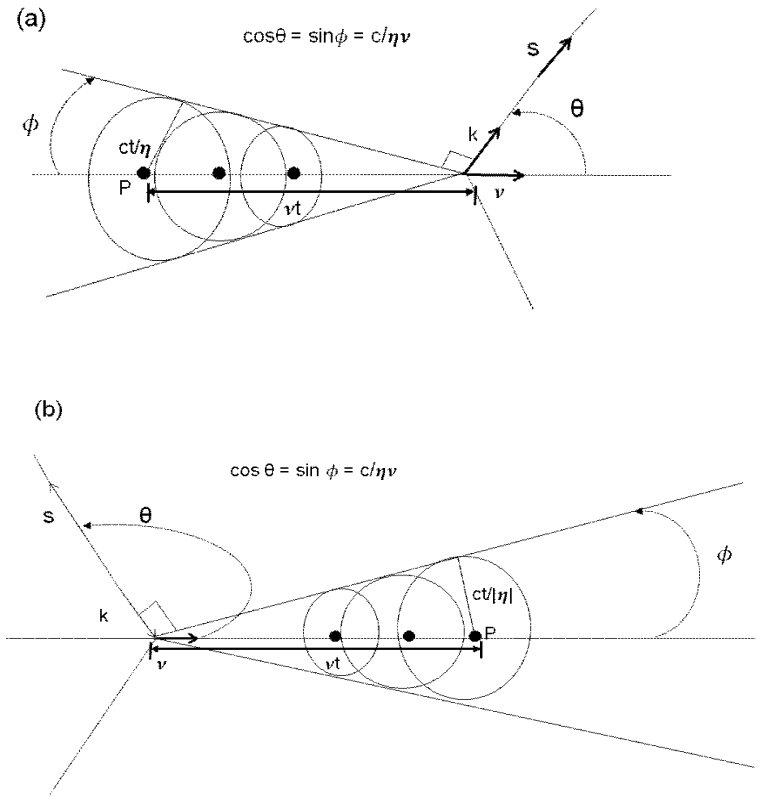

Figure 2.4: Illustration of the formation of Cerenkov shock waves: (a) in an ordinary medium, and (b) in a left-handed medium [33].

This angle is given by,

$$\cos\theta = \frac{c}{n\nu} \tag{2.41}$$

where c/n is the velocity of light in the medium and ν is the velocity of the particle. If the medium has a negative refractive index, wave propagation is backward and the spherical wavefronts corresponding to each frequency harmonic of the radiation move inwards to the source, at a velocity c/[nω]. Therefore each wavefront collapses at the advanced position of the particle shown in the above figure. Thus, the resulting shock wave travels backward at an obtuse angle from the particle motion. The angle is given in eqn. 2.41 as illustrated in the fig. 2.4. Any left-handed medium must be highly dispersive [33], as being restricted to some frequency range. Because the particle radiates at all frequencies, the Cerenkov radiation spectra must show wavefronts moving in both forward and backward directions [6].

2.2.4 Negative Refraction - Reverse Snell's Law

Consider the refraction of an incident optical ray at the interface between ordinary (ϵ>0, μ>0) and the left-handed media. Boundary conditions impose the continuity of the tangential components of the wavevector along the interface. As the left-handed region is considered, the angles of incidence, refraction must have opposite signs and can be seen in the fig. 2.5.

Illustrating Snell's law in left-handed region,

$$\frac{\sin\theta_i}{\sin\theta_r} = \frac{-|k_2|}{k_1} = \frac{n_2}{n_1} < 0 \tag{2.42}$$

where n_1 and n_2 are the refractive indices of the ordinary and left-handed media respectively. Assuming n_1>0 and from the above equation it follows n_2<0 i.e the sign of the square root in the refractive index definition must be chosen to be negative [29]:

$$n = -c\sqrt{\epsilon\mu} < 0 \tag{2.43}$$

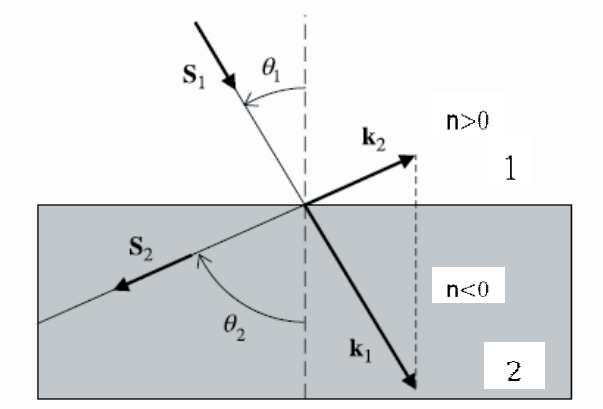

Figure 2.5: Negative Refractive Index [6].

For this reason, the LH materials are referred to as negative refractive index or negative refractive media.

2.2.5 Negative Goos-Hänchen Shift

When a plane wave is incident from a medium "1" of refractive index n=n_1 on to the plane interface of another medium "2" with n=n_2, where $|n_2|<|n_1|$, there is a critical angle $\sin\theta_c=|n_2|/|n_1|$, beyond which total reflection on to the medium 1 occurs. However, fields penetrate into the medium 2 by a small distance, forming a non-uniform plane wave that is evanescent in the direction normal to the interface and propagative along the interface. Power associated with this plane wave flows parallel to the interface in the forward direction for ordinary media and in the backward direction for left-handed media. Thus, when a beam of finite extent is incident from medium 1 to medium 2, the reflected beam experiences a finite lateral shift δ, as a consequence of the energy flow in medium 2. The figure below shows this effect. As energy flow is parallel to wavefront propagation, the Goos-Hänchen shift must be positive in ordinary media. However, if medium 2 is a left-handed medium, energy flow and wavefront propagation are antiparallel. Therefore, the Goos-Hänchen shift must be negative in such media and is depicted in the below fig. 2.6.

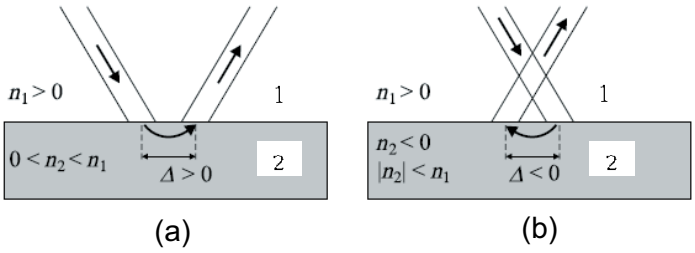

Figure 2.6: (a) Ordinary media (b) Left-Handed media [17].

The Goos-Hänchen shift "Δ" can be calculated by expanding the incident beam in the plane waves, and studying the reflection of these waves at the interface. If the angular spectrum of the beam is not too wide,and the angle of incidence is sufficiently away from the critical and grazing angles, the Goos-Hänchen shift is given by [17]:

$$\Delta = \frac{\partial \phi_r}{\partial k_{\|}}. \tag{2.44}$$

Where ϕ_r is the phase of the reflection coefficient and $k_{\|}$ is the component of the wave-vector parallel to the interface i.e. for lossless left-handed media $|r|$=1, and ϕ_r=-j log r. Therefore by above predictions, the sign of Goos-Hänchen shift agrees with predictions of left-handed media.

2.2.6 Transmission and Reflection Coefficients in LH Media

In this section, transmission and guidance of electromagnetic waves through left-handed side will be analyzed. The method of analysis will be a straight forward extension of the transverse transmission matrix technique [27], the same applies for multilayered structures. For this purpose, plane waves at both sides of a plane interface will be decomposed into propagative positive(+) and negative (-)waves,

with common wave vector component parallel to interface (k_z) and can be seen in below fig. 2.7.

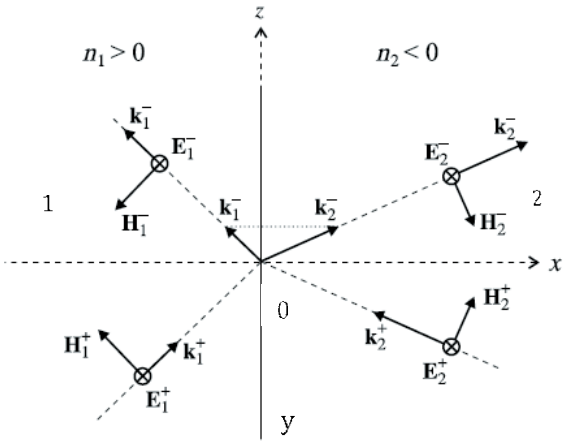

Figure 2.7: Determination of Transverse Transmission Matrix [17]

For considered polarized waves, where E_i=$E_{y,i}$ = E_i^+ = E_i^-, subindex i=1(i=2) stands for the fields at the left/right handed side interface at x=0. Positive waves are defined as those waves carrying energy along the positive axis perpendicular to the interface. Thus if the interface is perpendicular to the x-axis as in the above figure, then the field dependence of positive and negative waves can be summarized as [7]:

$$E_i^{\pm} \equiv E_{y,i}^{\pm} \alpha exp(\mp j k_{x,i} x - j k_z z + j\omega t) \tag{2.45}$$

where k_z is the common wave vector component parallel to the interface. According to backward propagation, in the left-handed half space, $k_{x,2} = \sqrt{\omega^2 \epsilon_2 \mu_2 - k^2}$ chosen with $\mathrm{Re}(k_{x,2} < 0)$. For ordinary media $\mathrm{Re}(k_{x,1} > 0)$ as usual.

The transmission matrix for a left-handed slab of width 'd' is given as [17]:

$$t = \frac{2Z_1 Z_2}{j(Z_1^2 + Z_2^2)\sin(k_{x,2}d) + 2Z_1 Z_2 \cos(k_{x,2}d)} \tag{2.46}$$

and reflection

$$\frac{Z_2^2 - Z_1^2}{Z_1^2 + Z_2^2 - 2jZ_1 Z_2 \cot(k_{x,2}d)} \tag{2.47}$$

Note that ($k_{x,2}d < 0$), so the phase advance through the slab is positive for small values of $k_{x,2}d$, which corrosponds to the propagation of a backward wave inside the slab.

2.2.7 Losses and Dispersion

After showing the propagation in left-handed media, it was claimed that losses and dispersion will destroy many of the previously reported effects. Specifically, negative refraction [6] and super-resolution in Pendry's perfect lens [3] were criticized. The analysis of the refraction of a Gaussian beam at the interface between an ordinary and a left-handed medium showed, without doubt, that negative refraction occurs in such a situation, thus confirming the Veselago analysis [1]. Of more interest are the effects of losses on the perfect lens proposed by Pendry [27]. Let us examine the analysis briefly.

The transmission coefficient of the LH media [17] is given as,

$$t = \frac{4Z}{(1+Z)^2 exp(jk_{x,2}d) - (1-Z)^2 exp(-jk_{x,2}d)} \tag{2.48}$$

where Z=Z_1/Z_2. If $\epsilon/\epsilon_0 \rightarrow$ -1 and $\mu/\mu_0 \rightarrow$ -1, also the wave impedance Z is given as [17]:

$$Z_i = \frac{E_i^+}{H_i^+} = \frac{\omega\mu_i}{k_{x,i}}. \tag{2.49}$$

Where $E_i^+ \equiv E_{y,i}^+$, is the electric field component of the positive wave [Refer above section]. It follows that Z=1, if $K_{x,2}$=-$|K_{x,2}|$ is real, and Z=-1, if $K_{x,2}=\alpha$ is imaginary. Therefore, t$\rightarrow$ exp(j$|K_{x,2}|d$) for propagative waves and t$\rightarrow$ exp (αd) for evanescent waves. In both cases, the phase and amplitude of the incident waves change along the slab just by the amount necessary to produce Fourier harmonics restoration at a distance '2d' from any source which can be seen in below figure.

Let us introduce a small amount of losses in the left-handed slab [30], so that $\epsilon \rightarrow -\epsilon_0(1+\mathrm{j}\delta_\epsilon)$ and $\mu \rightarrow -\mu_0(1+\mathrm{j}\delta_\mu)$and also suppose that $k_z \gg k_0$, so that

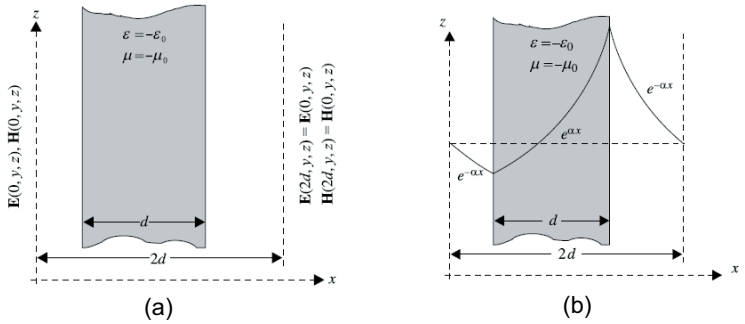

Figure 2.8: (a)Illustration of the perfect lens (b)Amplitude Pattern for an evanescent Fourier harmonic of the perfect lens [27].

$k_{k,2}$=-jα $\rightarrow$ -j$|k_z|$. In such a case taking eqn. 2.48 into account then we obtain:

$$t \rightarrow \frac{4}{4exp(-|k_z|d) - \delta_\mu^2 exp(|k_z|d)}. \tag{2.50}$$

Therefore, for high values of k_z it is still t$\rightarrow$ $exp(|k_z|d) \rightarrow exp(\alpha d)$ provided $\delta_\mu^2 exp(|k_z|d) < 4exp(|k_z|d)$, or:

$$|K_z|d \leq ln(\frac{2}{\delta_\mu}) \tag{2.51}$$

and can also be written as:

$$\frac{\Delta}{d} \geq \frac{2\pi}{k_{max}d} = 2\pi\{ln(\frac{2}{\delta})^{-1}\} \tag{2.52}$$

where $k_{max} \approx \frac{1}{d}ln(\frac{2}{\delta})$; and $\delta = max(\delta_\epsilon, \delta_\mu)$. It is nothing worth that the wavelength of the incident radiation doesn't appear in the eqn. 2.52, only losses and thickness limits the resolution of the device.

2.3 Composite Right-Left Handed Metamaterials (CRLH) MTM's

The concept of CRLH MTMs, developed by Caloz et al. [5] has resulted in numerous microwave applications, including enhanced-bandwidth couplers, dual-band components, leaky-wave antennas and zeroth order mode resonators [11].

However, the wide passband property of CRLH structures, inherent to their (artificial) TL nature, has not been exploited yet beyond their long-wavelength (MTM) frequency band located around the transition frequency between the left-handed (LH) and right-handed (RH) bands. This wideband property turns out to be very suitable for filter applications. In this thesis work we have exploited this structure for narrow band filters which fills the lack.

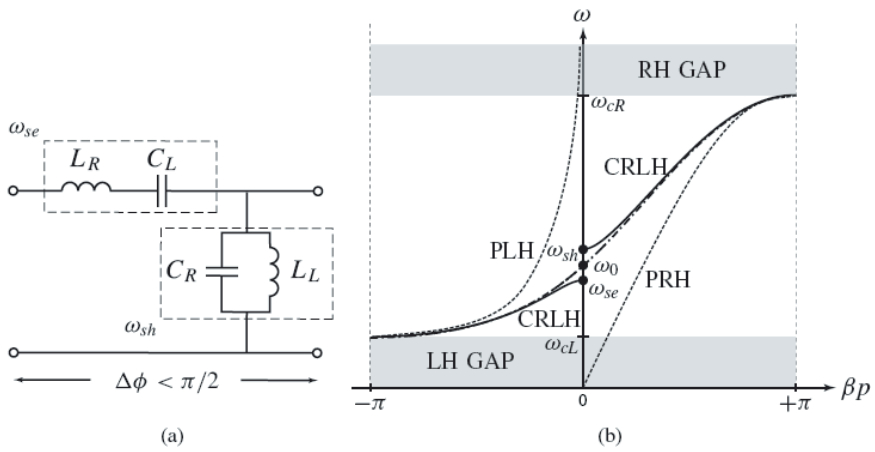

Figure 2.9: (a)Unit Cell (b)LH and RH comparision [16].

The essential characteristics of a CRLH TL MTM can be seen in fig. 2.9. In fig. 2.9(a) L_R, L_L, C_R, C_L represents left/right handed inductances and capacitances respectively which form CRLH structure. At low frequencies, L_R and C_R tend to be short and open, so that the equivalent circuit is essentially reduced to the series-C_L/shunt-L_L which is left-handed (LH) since it has antiparallel phase and group velocities. This LH circuit is of *highpass* nature. Therefore, below certain cutoff frequency a LH stopband is present. At high frequencies C_L and L_L tend to be short and open, then the equivalent circuit is now reduced to series-L_R/shunt-C_R, which has parallel phase and group velocities. This RH circuit is of *lowpass* nature. Therefore below a certain cuttoff frequency a RH stopband is present. In general the series ω_{se} and shunt ω_{sh} are different, so that a gap exists between the LH and the RH ranges. However, if these resonances are made equal

or balanced, this gap disappears and an infinite wavelength $\lambda_g = 2\pi/|\beta|$ (where $|\beta| \rightarrow 0$) propagation is achieved at ω_0. Despite its filter behavior, the CRLH structure is never operated at the edges of Brillouin zone, where p$\approx \lambda_{g/2}$ but only at the transition frequency where effective homogeneity is ensured p$< \lambda_{g/4}$ [16] (where "p" is cell size). Also, as the CRLH structure has both LH and RH range, their dispersion curve in each case differs from PLH (Pure Left-Handed) and PRH (Pure Right-Handed) as shown in the fig. 2.9b. This happens due to the combined effects of LH and RH contributions at all frequencies.

Chapter 3

Transmission Line theory of Metamaterials

3.1 Introduction

A transmission line (TL) is perfectly uniform and homogenous [9], which means it has an invariant cross section along the direction of propagation. It can transmit signals from zero to infinite frequencies. RH homogenous TLs are commonly used as coaxial or microstrip lines, but LH and CRLH is not possible due to unavailability of real homogeneous LH or CRLH materials, but can be possible to construct effectively homogeneous artificial LC TL structures or MTM TLs, that perfectly behave as ideal TLs in a restricted range of frequencies. The difference between a perfectly homogeneous TL and an effectively homogeneous TL is that in the former case we have an incremental length $\Delta Z \rightarrow 0$, whereas in the latter case we must consider the restriction [16]

$$\Delta z \ll \lambda_g \left[\Delta z < \frac{\lambda_g}{4}\right] \; Typically \; \frac{\lambda_g}{10} \tag{3.1}$$

where λ_g represents the guided wavelength and Δz is typically equal the average unit cell size p. Loss-Less and Lossy CRLH TLs are discussed further in the next section.

3.2 Loss Less CRLH TLs

The below figure is a loss less ideal CRLH TL model consisting of per-unit length impedance $Z'(\Omega/m)$ constituted by per-unit length inductance L'_R (H/m) in series with a LH times-unit length capacitance C'_L(Fxm) and a per-unit length admittance Y' (S/m) constituted by a RH per-unit-length capacitance C'_R(F/m) in parallel with a LH times-unit length inductance L'_L (Hxm) and is:

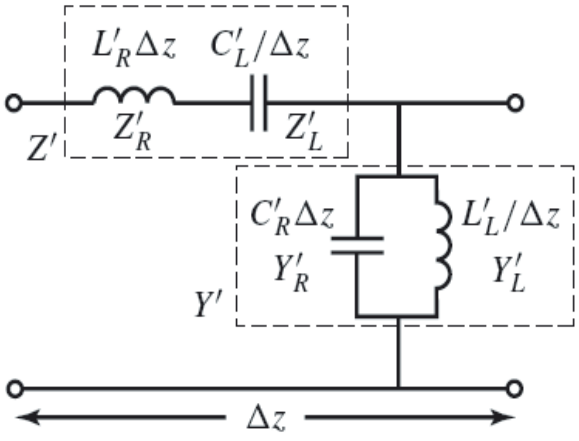

Figure 3.1: Ideal CRLH TL [16]

$$Z' = j\left(\omega L'_R - \frac{1}{\omega C'_L}\right) \tag{3.2}$$

$$Y' = j\left(\omega C'_R - \frac{1}{\omega L'_L}\right). \tag{3.3}$$

If LH immittances are zero, $Z'_L = -j/(\omega C'_L)$=0 or $C'_L = \infty$ and $Y'_L = -j/(\omega L'_L)$=0 or $L'_L = \infty$, only the RH immittances $Z'_R = j\omega L'_R$ and $Y'_R = j\omega C'_R$ are present which reduces to the conventional RH TL model otherwise LH TL model.

The behavior of the CRLH TL can be detailed by the asymptotic consideration. At low frequencies $(\omega \to 0), Z'_R \to 0, Y'_R \to 0$ so that the CRLH TL becomes equivalent to a PLH (Pure Left-Handed) TL ($L'_R = C'_R = 0$). At high frequencies

$(\omega \to \infty), Z'_L \to 0, Y'_L \to 0$, So that CRLH TL becomes equivalent to a PRH (Pure Right-Handed) TL ($L'_L = C'_L = \infty$). At all other frequencies the transmission characteristics depend on the combination of LH and RH contributions.

Let us generalize CRLH TLs using the Telegraphist's equations, For a steady-state sinusoidal waves based on cosine phasors:

$$\frac{dU}{dz} = -Z'I = -j\omega\left(L'R - \frac{1}{\omega^2 C'_L}\right)I \tag{3.4}$$

$$\frac{dI}{dz} = -Y'U = -j\omega\left(C'R - \frac{1}{\omega^2 L'_L}\right)U \tag{3.5}$$

Where U and I are the position-dependent voltage and currents [V=V(z)] and [I=I(z)] along the line respectively. By solving eqn. 3.4 and 3.5, we get the following wave equations for U and I[11]:

$$\frac{d^2V}{dz^2} = -\gamma^2 = 0 \tag{3.6}$$

$$\frac{d^2I}{dz^2} = -\gamma^2 = 0. \tag{3.7}$$

Where γ (l/m) is the complex propagation constant and can be expressed in terms of the per-unit-length immittances Z' and Y' as:

$$\gamma = \alpha + j\beta = \sqrt{Z'Y'}. \tag{3.8}$$

The characteristic impedance Z_c (Ω), relating to voltage and currents on the line (propagating wave equations with +ve and -ve voltages and currents) is:

$$Z_C = R_C + jX_c = \frac{Z'}{\gamma} = \sqrt{\frac{Z'}{Y'}} = Z_c(\omega). \tag{3.9}$$

Let us use variables:

$$\omega'_R = \frac{1}{\sqrt{L'_R C'_R}}(radxm)/s. \tag{3.10}$$

$$\omega'_L = \frac{1}{\sqrt{L'_L C'_L}} rad(mxs). \tag{3.11}$$

$$\kappa = L'_R C'_L + L'_L C'_L (s/rad)^2. \tag{3.12}$$

and the series and shunt resonance frequencies are[5]

$$\omega'_{se} = \frac{1}{\sqrt{L'_R C'_L}} rad/s. \tag{3.13}$$

$$\omega'_{sh} = \frac{1}{\sqrt{L'_L C'_R}} rad/s. \tag{3.14}$$

respectively. By inserting eqn. 3.2 into eqn. 3.8 and using eqn. 3.10, we get the following expression for complex propagation constant[16]:

$$\gamma = \alpha + j\beta = js(\omega)\sqrt{\left(\frac{\omega}{\omega'_R}\right) + \left(\frac{\omega'_L}{\omega'}\right)^2 - \kappa\omega_L^2}. \tag{3.15}$$

Where $s(\omega)$ is the following sign function:

$$s(\omega) = -1 \; ; If \;\; \omega < min(\omega_{se}, \omega_{sh}) \;\; ..... LH \;\; Range \tag{3.16}$$

$$s(\omega) = +1 \;\; ; If \;\; \omega > max(\omega_{se}, \omega_{sh}) \;\; ..... RH \, range \tag{3.17}$$

The negative term in the eqn. 3.15 shows that the propagation constant γ is not necessarily purely imaginary [5] $\gamma = j\beta$ (Pass band); it can be purely real $\gamma = \alpha$ (stop band) in some frequency ranges despite the fact that the line is loss-less.

3.3 Dispersion/Attenuation

The dispersion/attenuation curve is in fig. 3.2a shows the CRLH dispersion and attenuation curves for energy propagation along both the positive and negative z direction, whereas, fig. 3.2b shows the CRLH dispersion comparison with PRH and PLH at lower and higher frequencies. The gap is due to the different series and shunt resonances $(\omega_{se}, \omega_{sh})$ respectively, if this happens then the CRLH TL

is said to be *unbalanced*. If the resonances are equal then CRLH TL is said to be *balanced* and the gap closes with nonzero group velocity [16].

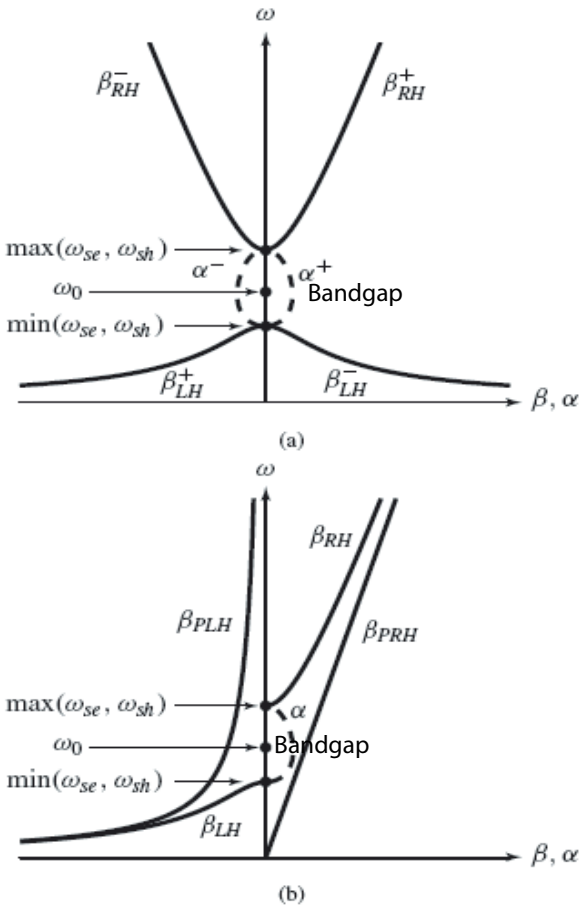

Figure 3.2: Dispersion/Attenuation Curves: (a)Energy propagation along +z and -z directions. (b) Comparison of the CRLH, PLH (β_{PLH}) and PRH (β_{PRH}) TLs for energy propagation along the +z direction (vg $>$ 0) [16]

From the curves, when $\omega < min(\omega_{se}, \omega_{sh})$, TL is LH with negative group velocity and positive phase velocity and that β is therefore negative. Similarly, when $\omega > max(\omega_{se}, \omega_{sh})$ they will posses positive group and phase velocities and hence positive propagation i.e. β.

The frequency of maximum oscillation ω_0 (i.e. bandgap occurs at ω_0) for CRLH can be derived from eqn. 3.15 by differentiating it with respect to ω *i.e.* $\frac{d\gamma}{d\omega}$ and

this yields to:

$$\omega_0 = \sqrt{\omega'_R \omega'_L} = \frac{1}{4\sqrt{L'_R C'_R L'_L C'_L}} \tag{3.18}$$

.

The CRLH characteristic impedance is obtained by inserting eqn. 3.13 and 3.14 in eqn. 3.9, then we get:

$$Z_c = Z_L \sqrt{\frac{(\omega/\omega_{se})^2 - 1}{(\omega/\omega_{sh})^2 - 1}}. \tag{3.19}$$

Where PLH (pure left handed) and PRH (pure right handed) impedances are,

$$Z_L = \sqrt{\frac{L'_L}{C'_L}} \tag{3.20}$$

and

$$Z_R = \sqrt{\frac{L'_R}{C'_R}}. \tag{3.21}$$

From eqn. 3.19, it can be noted that the characteristic impedance has a zero and a pole at $\omega = \omega_{se}$ and $\omega = \omega_{sh}$ respectively,

$$Z_c(\omega = \omega_{se} = 0) \tag{3.22}$$

$$Z_c(\omega = \omega_{sh} = \infty) \tag{3.23}$$

The characteristic impedance curves differentiation between CRLH, LH and RH behavior are shown in fig. 3.3:

The fundamental transmission quantities like guided wavelength λ_g, phase velocity ν_p and group velocity ν_g of CRLH TL are defined from the following equations as,

$$\lambda_g = \frac{2\pi}{|\beta|} = \frac{2\pi}{\sqrt{(\omega/\omega'_R)^2 + (\omega'_L/\omega)^2 - \kappa\omega'^2_L}} \tag{3.24}$$

and,

$$\nu_p = \frac{\omega}{\beta} = s(\omega) \frac{\omega}{\sqrt{(\omega/\omega'_R)^2 + (\omega'_L/\omega)^2 - \kappa\omega'^2_L}} \tag{3.25}$$

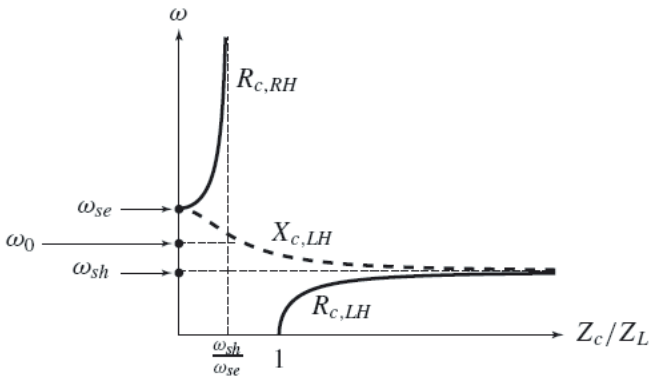

Figure 3.3: Characteristic Impedance [9]

and,

$$\nu_g = \left(\frac{d\beta}{d\omega}\right)^{-1} = \frac{|\omega\omega_R'^{-2} - \omega^{-3}\omega_L'^2|}{\sqrt{(\omega/\omega_R')^2 + (\omega_L'/\omega)^2 - \kappa\omega_L'^2}} \tag{3.26}$$

The above properties can be seen for CRLH and PLH in the below figures as PRH is well known for the constant properties.

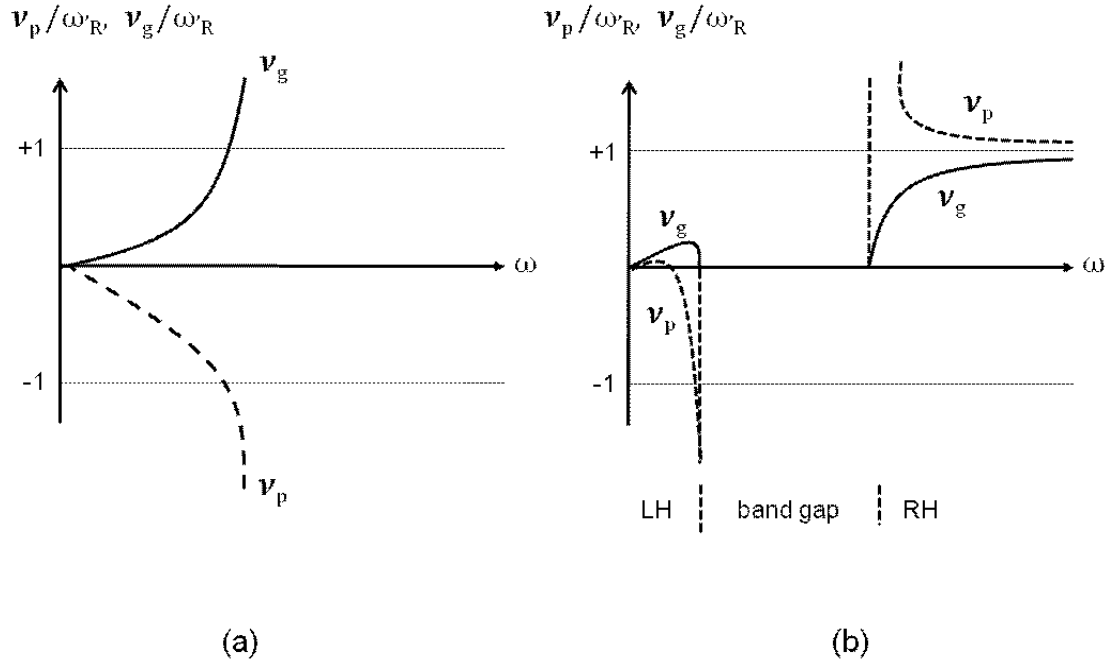

Figure 3.4: (a)PLH TL Properties (b)CRLH Properties [16]

3.4 CRLH TL equivalent MTM Constitutive Parameters

The CRLH TL parameters (L_R, C_R, L_L, C_L) can be related to constitutive parameters ϵ and μ of a real material exhibiting the same propagation characteristics by mapping the telegraphists's equations to maxwell's equations and such a matching is possible only if the electromagnetic waves in the MTM are propagating in *transverse electromagnetic mode* (TEM) [36], where the longitudinal components of the electric and magnetic fields are both zero ($E_Z = 0$ *and* $H_Z = 0$, Z direction of TL), For this let us consider a parallel plate wave guide structure filled with CRLH material shown in the fig. 3.5 [38]:

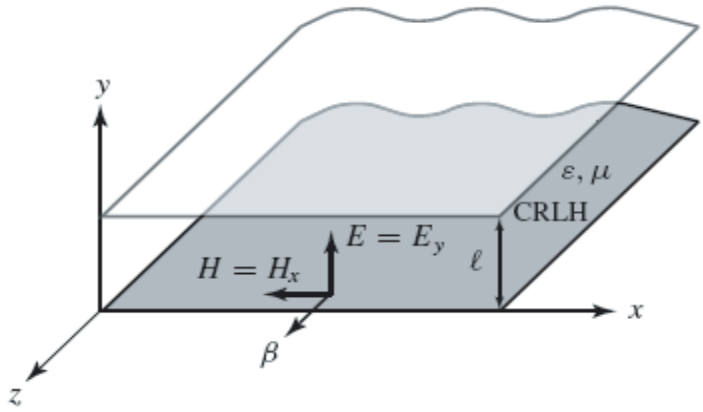

Figure 3.5: Parallel Plate wave guide filled with CRLH Material [16]

Now imposing Maxwell's equations,

$$\frac{dE_y}{dz} = -Z' H_x = -j\omega\beta\mu H_x \tag{3.27}$$

$$\frac{dH_x}{dz} = -Y' E_y = -j\omega\beta\epsilon E_y. \tag{3.28}$$

which are identical to Telegraphist's equations[38] eqn's. 2.2 and eqn. 2.3, if the following mapping:

$$E_y \rightarrow V \tag{3.29}$$

$$H_x \rightarrow I \tag{3.30}$$

and,

$$\mu = \mu(\omega) = L'_R - \frac{1}{\omega^2 C'_L} \tag{3.31}$$

$$\epsilon = \epsilon(\omega) = C'_R - \frac{1}{\omega^2 L'_L}. \tag{3.32}$$

where $\epsilon = \epsilon_r \epsilon_)$ (H/m) and $(\mu = \mu_r \mu_0)$ (F/m). Which represents equivalent constitutive parameters of CRLH TL MTM. Finally we can derive CRLH TL equivalent refractive index as:

$$n = n(\omega) = \sqrt{\mu_r \epsilon_r} = c\sqrt{\mu\epsilon}. \tag{3.33}$$

This equivalent refractive index is related to TEM propagation constant β by

$$\beta = nk_0 \tag{3.34}$$

where $k_0 = \omega/c$.

3.4.1 CRLH TL Balanced and Unbalanced Resonances

Considering fig. 3.1, the CRLH TL is said to be *balanced*, when their resonance frequencies are equal [16], .i.e:

$$\omega_{se} = \omega_{sh} \tag{3.35}$$

The characteristic impedances of series and shunt cancel each other suppressing resonance effect.

$$L'_R C'_L = C'_L L'_L \tag{3.36}$$

As a consequence the gap between them closes and the characteristic impedance becomes a frequency-independent quantity

$$Z_c = Z_L = Z_R \tag{3.37}$$

which means, that the balanced condition allows matching over an infinite bandwidth. And the transition frequency is given as:

$$\omega_0 = \sqrt{\omega'_R \omega'_L} \tag{3.38}$$

where ω'_R, ω'_L are LH and RH resonant frequencies. Also the propagation constant:

$$\beta = \frac{\omega}{\omega'_R} - \frac{\omega'_L}{\omega}. \tag{3.39}$$

On the other side, if the series and the shunt resonances are unequal then the CRLH TL is *unbalanced* where,

$$\omega_{se} \neq \omega_{sh} \tag{3.40}$$

Which means we have zero immittances when the TL is fed by a signal with either frequency $\omega = \omega_{se}$ or $\omega = \omega_{sh}$. Introducing a pole and a zero in the characteristic impedance, i.e.:

$$Z_c(\omega = \omega_{se}) = 0 \tag{3.41}$$

and

$$Z_c(\omega = \omega_{sh}) = \infty. \tag{3.42}$$

This impedance conditions corresponds to the zero group velocities i.e. $v_g = 0$ where there is no power transfer and propagation. The TL resonances result in the emergence of stopband or bandgap.

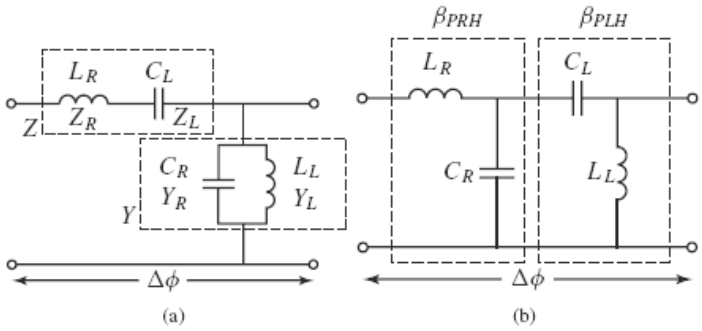

Figure 3.6: (a)Balanced unit Cell (b)Unbalanced unit cell [16]

Fig. 3.6 shows the difference between balanced and unbalanced structures. The balanced structure has a lot of advantages over unbalanced structure [40] like:

- It is simpler because of series combined LH and RH contributions are decoupled from each other.
- The balanced TL is gapless which facts Z_c and β from eqn's. 3.37 and 3.39 are real at all frequencies from $\omega = 0$ to $\omega = \infty$.
- The balanced TL has non zero phase and group velocities, where unbalanced TL has zero phase and group velocities.
- The characteristic impedance Z_c of the balanced TL is a constant frequency independent quantity, for which the balanced TL can be matched over a broad bandwidth. Where in unbalanced case, it matches to a single frequency.

In this thesis work we have preferred balanced structure over unbalanced due to the advantages.

3.4.2 Lossy CRLH TL Case

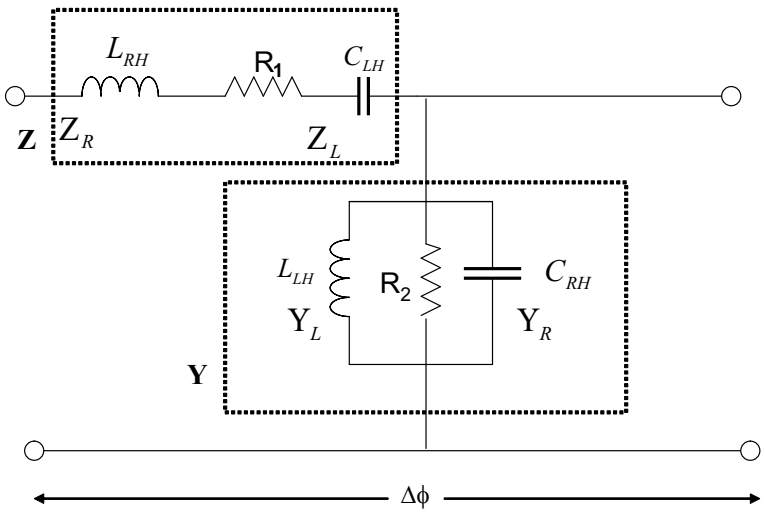

Figure 3.7: Lossy CRLH TL

The lossy CRLH TL structure is shown in fig. 3.7. The per-unit length immittances can be written as [9]:

$$Z' = R' + jX'; X' = \left(\omega L'_R - \frac{1}{\omega C'_L}\right) \tag{3.43}$$

$$Y' = G' + jB'; B' = \left(\omega C'_R - \frac{1}{\omega L'_L}\right). \tag{3.44}$$

Here the complex propagation constant and characteristic impedance are given as:

$$\gamma = \alpha + j\beta = \sqrt{Z'Y'} = \sqrt{(R'G' - X'B') - j(R'B' + G'X')} \tag{3.45}$$

$$Z_c = R_0 + jX_0 = \frac{Z'}{Y'} = \frac{R' + jX'}{G' + jB'} \tag{3.46}$$

.

To obtain some insight into the lossy effects, let us consider PLH TL. Using equation (3.45) with $L'_R = C'_R = 0$ in (3.43), we obtain the propagation constant γ_L for the PLH lossy TL.

$$\gamma_L = -j\frac{\sqrt{1 - R'G'(\omega/\omega'_L)^2 + j\omega(C'_L R' + L'_L G')}}{\omega/\omega'_L} = \gamma_L + j\beta_L \tag{3.47}$$

Which has both a real and imaginary part at all frequencies ($\alpha \neq 0, \beta \neq 0 \vee \omega$). In practical low-frequency microwave structures, ohmic and dielectric losses are relatively small [41], and the parameters

$$A = R'G'(\omega/\omega')^2 \tag{3.48}$$

$$B = \omega(C'_L R' + L'_L G') \tag{3.49}$$

are typicall such that $A \ll B < 1$. Therefore **A** can be neglected and the remaining square root may be approximated by its first order Taylor expansion, so that

$$\gamma_L = -j\frac{1}{\omega/\omega'_L}\left[1 + \frac{j}{2}(C'_L R' + L'_L G')\right] \tag{3.50}$$

from which

$$\beta_L \approx -\frac{\omega'_L}{\omega} \tag{3.51}$$

$$\alpha_L \approx \frac{1}{2}\left[R'Y_0 + G'Z_c\right] \tag{3.52}$$

Where $Z_c = Z_L = \sqrt{L'_L/C'_L}$ and $Y_0 = Y_L = 1/Z_c$, We observe that a weakly lossy LH TL exhibits the same propagation constant as a loss-less LH TL and same attenuation factor as that of the conventional RH TL [16]. Which facts that, the loss mechanism is the same in both LH TL and RH TL. From eqn. 3.46, the characteristic impedance is,

$$Z_c = \sqrt{\frac{R' - j/\omega C'_L}{G' + j\omega L'_L}}\omega \to 0 \approx \frac{L'_L}{C'_L}. \tag{3.53}$$

which is identically equal to eqn. (3.37) of loss-less LH TL and essentially behaves in the same manner and hence the same applies to CRLH TL including both LH and RH contributions. It has been observed that, the reduction of group velocity over a bandwidth is due to the introduction of losses. Which increases, as the amount of losses is increased and nullifies the real part of the characteristic impedance at the transition frequency.

The characteristic impedance and propagation constant of the CRLH lossy TL are shown in the fig's. 3.8, 3.9 for the balanced and unbalanced cases, respectively.

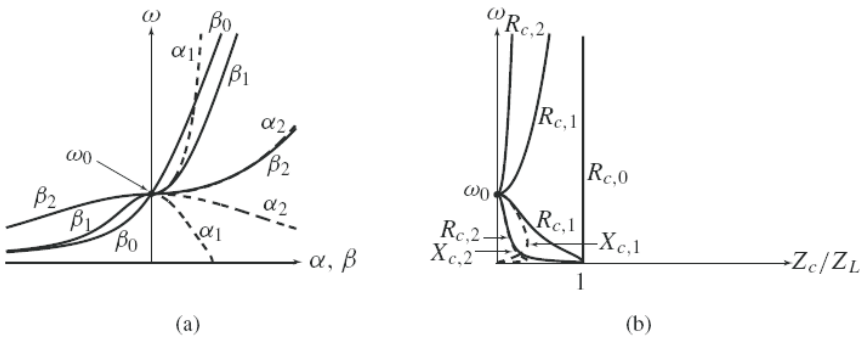

Figure 3.8: Effects of losses in the ideal balanced CRLH TL. (a) Dispersion and attenuation. (b) Characteristic impedance. The indexes 0, 1, 2 refer to a loss-less, weakly lossy, and strongly lossy TL, respectively [17].

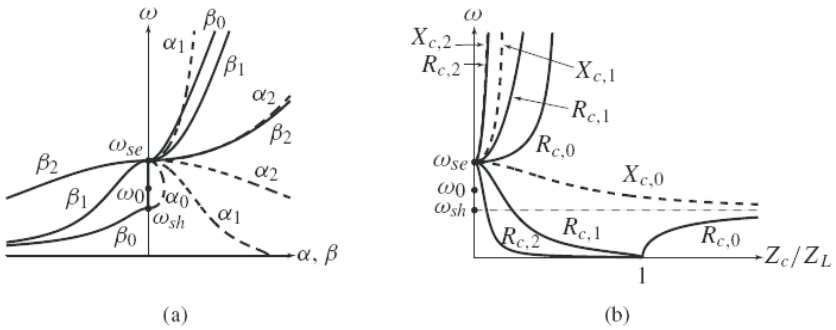

Figure 3.9: Effects of losses in the ideal unbalanced CRLH TL for $\omega_{sh} < \omega_{se}$. (a) Dispersion and attenuation. (b) Characteristic impedance. The indexes 0, 1, 2 refer to a loss-less, weakly lossy, and strongly lossy TL, respectively. [16].

We find from eqns. 3.45 and 3.46, that in the CRLH TL [8] $Z'(\omega_0) = B'(\omega_0) = \sqrt{R'/G'}$, this value can be shown to represent a minimum of Z_c in the balanced case in fig . 3.9. We also observe that in the unbalanced case, $X'(\omega_{se}) = 0$, leading to a minimum value of Z_c at $\omega = \omega_{sh}$.

3.5 LC Network Implementation

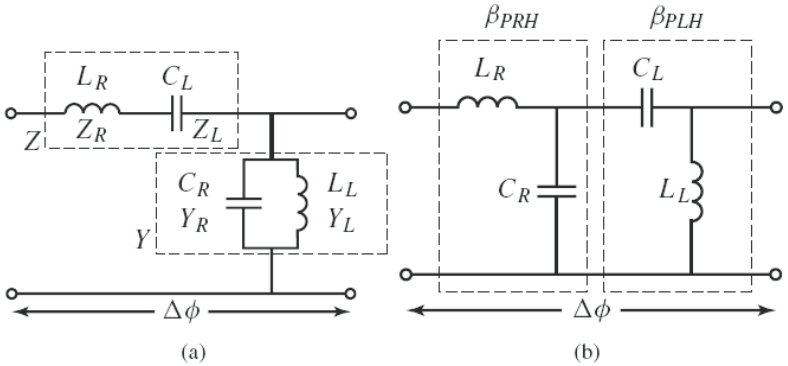

Figure 3.10: Unit cell of an LC CRLH TL. (a) General (unbalanced). (b) Balanced ($L_R C_L = L_L C_R$) [5]

The LC unit cell is shown in fig. 3.10. It consists of an impedance $Z(\omega)$ constituted

by a RH inductance $L_R(H)$ in series with a LH capacitance $C_L(F)$ and of an admittance $Y(\omega)$ constituted by a RH capacitance $C_R(F)$ in parallel with a LH inductance $L_L(H)$ [40]:

$$Z = j\left(\omega L_R - \frac{1}{\omega C_L}\right) = j\frac{(\omega/\omega_{se})^2 - 1}{\omega C_L} \tag{3.54}$$

and

$$Y = j\left(\omega C_R - \frac{1}{\omega L_L}\right) = j\frac{(\omega/\omega_{sh})^2 - 1}{\omega L_L}. \tag{3.55}$$

Where the series and shunt resonance ω_{se} *and* ω_{sh} can be written in similar manner to that of the ideal homogenous case [16].

$$\omega_{se} = \frac{1}{\sqrt{L_R C_L}} \tag{3.56}$$

and

$$\omega_{sh} = \frac{1}{\sqrt{L_L C_R}} \tag{3.57}$$

The phase shift induced by the unit cells is noted as $\Delta\phi$. This is due to the practical circuital implementation of inductors and capacitors which will occupy a physical length varying with technology used. If the footprint of the unit cell is p in length (fig. 3.10), then we can write the immittances along ΔZ as,

$$\frac{Z}{p} = j\left[\omega\left(\frac{L_R}{p}\right) - \frac{1}{\omega(C_{LP})}\right] \tag{3.58}$$

and

$$\frac{Y}{p} = j\left[\omega\left(\frac{C_R}{p}\right) - \frac{1}{\omega(L_{LP})}\right] \tag{3.59}$$

The comparisons of eqn's. 3.2 and 3.3 with eqn's. 3.58 and 3.59 reveals that, if $p = \Delta Z \to 0$, the immittances for the length p become $Z/p \to Z', Y/p \to Y'$ which means that the LC implementation of fig. 3.10 is equivalent to the incremental structure of fig. 3.1.

3.5.1 Difference with conventional filters

The difference between MTM bandpass filters and conventional filters are:

- MTM filters are quasi-lumped, while conventaional filters are directly converted TLines.
- CRLH TL in the balanced case, can be regarded as the central section part of a low-ripple high order chebyshev BPF [13].
- In MTM filters, only passband is directly useful the stopbands are usually parasitics.
- MTM filters usually satisfies effective homogenous condition (unit cell order of lamda/10 and unit cell phase shift less than $\pi/2$), but in conventional filters there may be node to node phase shifters of order larger than $\pi/2$.
- A MTM structures can be 1D, 2D, 3D and behave as bulk media, but conventional are 1D and behave as a electric circuits.
- A MTM filter can be made up of identical cells repeating and hence periodic, where as in conventional filters each cell has generally different LC values to match the specification of given prototype.

3.6 Symmetric and Asymmetric Structures

Lossless symmetric and asymmetric CRLH TL structures are shown in fig. 3.11 and 3.12 respectively. *Symmetric* configuration has the same input and output impedances i.e Z_{in}=Z_{in}, therefore symmetric network is preferred. *Asymmetric* configuration has different input and output impedances i.e $Z_{in} \neq Z_{in}$, therefore it requires different port impedances for matching, which is impractical. Also, there are mismatch effects at the connections with external ports. In this thesis, we

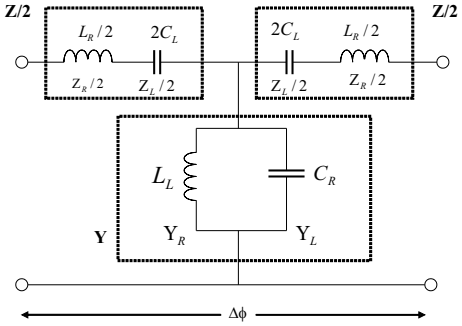

Figure 3.11: Symmetric CRLH TL Structure

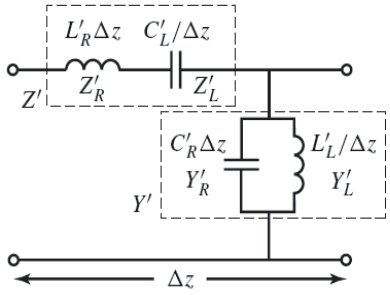

Figure 3.12: Asymmetric CRLH TL Structure

have implemented symmetric configuration due to its advantages over asymmetric configuration.

Chapter 4

Metamaterial CRLH TL Applications for Filters

4.1 CRLH Metamaterial theory on Filter Application

Fig. 4.1, shows the LC equivalent circuit model for an ideal unit cell of an CRLH TL (Transmission Line). Considering the balanced condition of the circuit where the series resonance equals the shunt resonance i.e $\omega_{se} = \omega_{sh}$ [42],

the series resonance frequency of the unit cell is

$$f_{se} = \frac{1}{2\pi\sqrt{L_{RH}C_{LH}}} \tag{4.1}$$

and the shunt resonance is

$$f_{sh} = \frac{1}{2\pi\sqrt{L_{LH}C_{RH}}}. \tag{4.2}$$

On the left handed side (LHS) when $\omega \to 0$, then $|Z| \to \frac{1}{\omega_{C_{LH}}} + R1 \to \infty$ and $|Y| \to \frac{1}{\omega_{L_{LH}}} + \frac{1}{R2} \to \infty$ therefore, we have a stop band due to the high pass nature of LH elements. On the other side which is right handed side(RHS), as $\omega \to \infty$, $|Z| \to \omega_{L_{RH}} \to \infty$ and $|Y| \to \omega_{C_{RH}} \to \infty$

Due to the low pass nature of RH elements, again stopband behavior is found. Between these two stopbands a perfectly matched passband can be achieved at balanced conditions [16]. In this thesis work we have chosen balanced case for filter design due to the advantages over unbalanced structure. This is an important findings and thus an essential conclusion for a structured filter design approach.

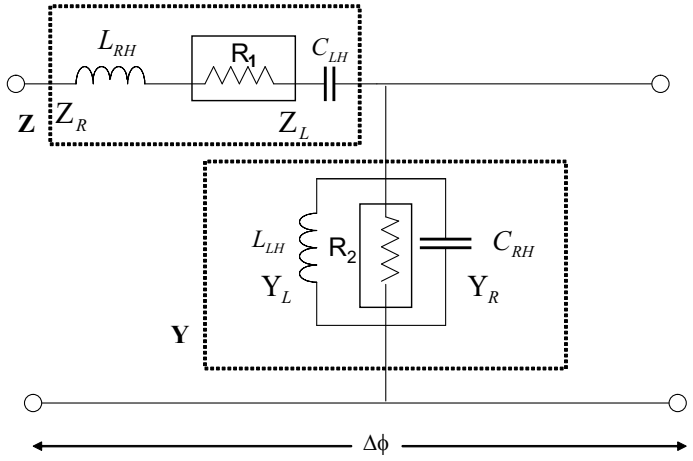

Figure 4.1: Ideal lossless CRLH TL

So, the LC equivalent of CRLH TL can be implemented for bandpass filters which is fully characterizable in terms of its propagation constant β and Characteristic impendence Z_c in its passband. where [16]

$$\beta = \sqrt{\begin{array}{l} \frac{C_{RH}}{C_{LH}} + \frac{L_{RH}}{L_{LH}} + \frac{R_l}{R_2} - \omega^2 * L_{RH} * C_{RH} \\ -\frac{1}{\omega^2 * L_{LH} * C_{LH}} + j * \{\omega * [R_1 * C_{RH} + \frac{L_{RH}}{R_2} \\ -\frac{R1}{\omega^2 * L_{LH}} - \frac{1}{\omega^2 * L_{RH} * C_{RH}}]\} \end{array}} \tag{4.3}$$

and

$$Z_c = \sqrt{\frac{L_{RH} + \frac{R_1}{j*\omega} - \frac{1}{\omega^2 * C_{LH}}}{C_{RH} + \frac{1}{R_2 * j * \omega} - \frac{1}{\omega^2 * L_{LH}}}} \tag{4.4}$$

Fig. 4.2 reflects the practical symmetric unit cell of an LC CRLH TL, where the Input and Output impedances are matched simultaneously with the same value and is preferred over asymmetric unit cell which has opposite properties [16].

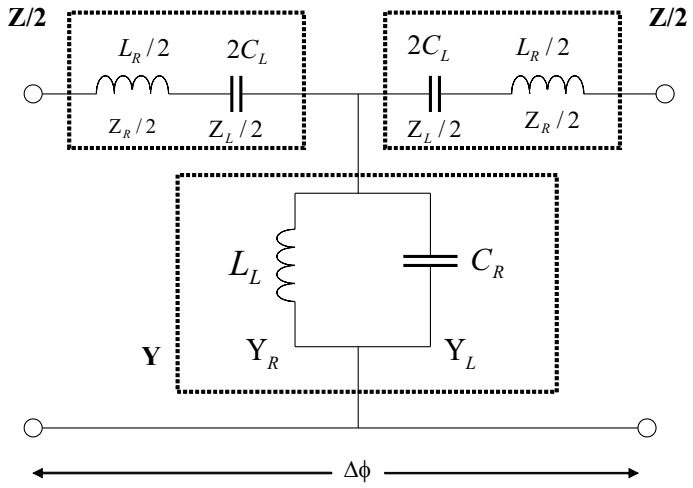

Figure 4.2: Lossless symmetric Unit Cell

4.2 Microstrip Implementation of MTM

Fig. 4.3 depicts a typical microstrip CRLH TL constituted by interdigital capacitors and stub inductors shorted to the ground plane by via. This structure is the first distributed MTM TL structure and its equivalent T-network is shown in the fig.4.4. It was introduced by Caloz et.al. in 2002 and subsequently used in various applications[42].

For such structure, the equivalent unit cell in fig. 4.3 is shown in fig. 4.2. Its equivalent T-network is shown in fig. 4.4. The unit cell, centered in the plane defined by the axis of the stub, represents a T-network with two impedance branches $2C_L$ and inductance $L_R/2$ and by admittance branch with inductance L_L and capacitance C_R. The contributions C_L and L_L are provided by interdigital capacitors and stub inductors whereas, the contributions C_R and L_R comes from their parasitic reactances[5]. The parasitic inductance L_R is due to magnetic flux generated by the currents flowing along the digit fingers of the capacitor and the parasitic capacitance C_R is due to the parallel-plate voltage gradients existing between the trace and the ground plane. First approximation formulas for the inductance L_L and capacitance C_L may be obtained as follows.

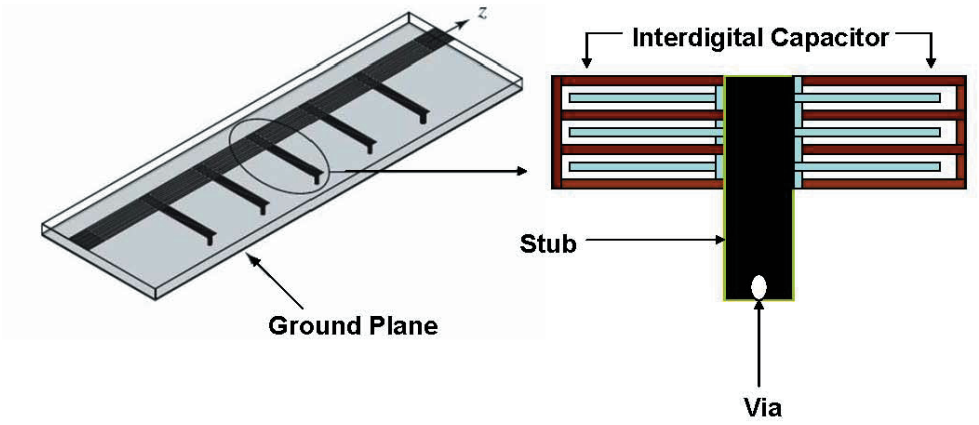

Figure 4.3: Microstrip CRLH TL using interdigital capacitors and shorted stub inductors [5]

The shorted stub corresponds to a shorted TL, with input impedance[16] $Z_{in}^{si} = jZ_C^{si}\tan(\beta^{si}l^{si})$, where Z_{in}^{si}, β^{si}, and l^{si} represents the characteristic impedance, propagation constant and the length of the stub respectively. Equating with the ideal impedance of inductor, $j\omega L_L$, we get

$$L_L \approx \frac{Z_C^{si}}{\omega}\tan(\beta^{si}l^{si}) \tag{4.5}$$

and is independent of frequency. The approximation formula for the capacitance of the interdigital capacitor is,

$$C_L \approx (\epsilon_r + 1)l^{ic}[(N-3)A_1 + A_2](pF) \tag{4.6}$$

where,

$$A_1 = 4.409\tanh\left[0.55\left(\frac{h}{\omega^{ic}}\right)^{0.45}\right]10^{-6}(pF/\mu m) \tag{4.7}$$

and

$$A_2 = 9.92\tanh\left[0.52\left(\frac{h}{\omega^{ic}}\right)^{0.5}\right]10^{-6}(pF/\mu m) \tag{4.8}$$

where l^{ic},ω^{ic} and h represent the length of the interdigital capacitor, the overall width of its finger, and the height of the substrate respectively. The obtained

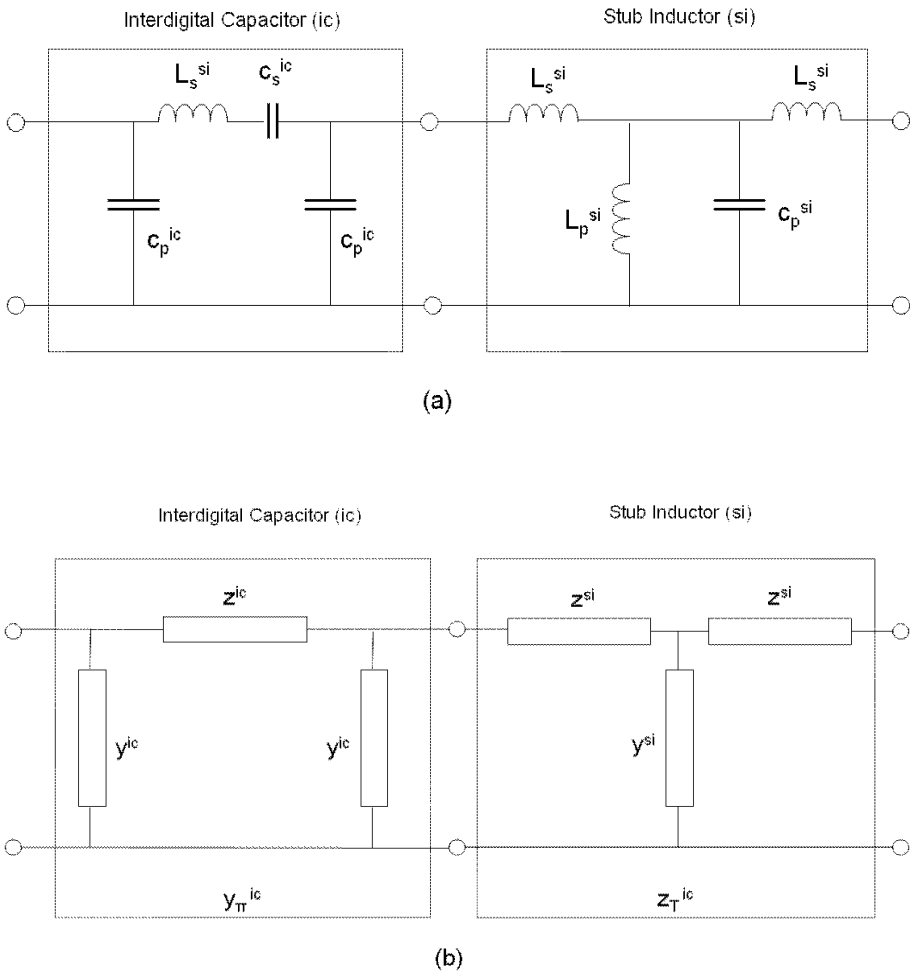

Figure 4.4: Circuit models for the parameters extraction of the unit cell (a) Equivalent circuit. (b) Auxiliary equivalent T and π networks [11]

parameters are approximations.

For the above unit cell, the accurate approach to extract parameters are using S,Y and Z parameters from [16], using full-wave simulation process,

$$L_R = L_S^{si} \tag{4.9}$$

$$C_R = 2C_P^{ic} + C_P^{si} \tag{4.10}$$

$$L_L = L_P^{si} \tag{4.11}$$

$$C_L = C_S^{ic} \tag{4.12}$$

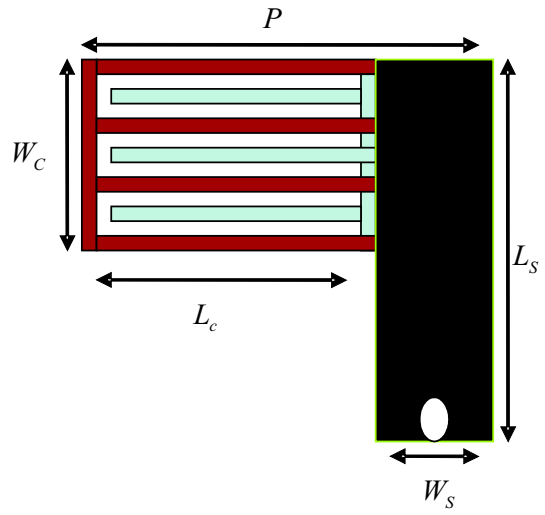

Figure 4.5: CRLH MTM TL Unit Cell with Interdigital Capacitor and stub inductor [16]

The above theoretical method was practically demonstrated and proved for a broad bandwidth bandpass filter by C.Caloz/I.Ithoh in their publications for both balanced and unbalanced conditions respectively [5] [11],[42]. Their fabricated board with interdigital capacitors and stub inductors for 24 unit cells are depicted in fig. 4.6 and their results in fig. 4.7 [16].

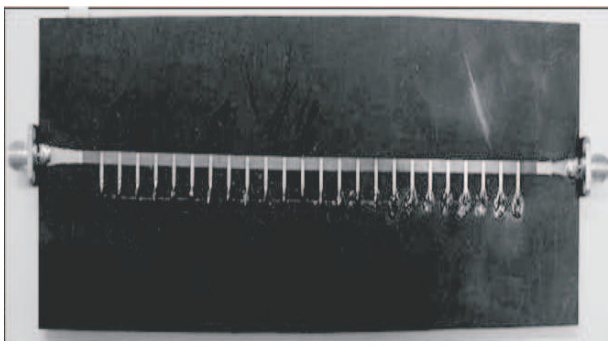

Figure 4.6: Caloz/Itoh practical board [16]

With the success of their theory, they concluded that left-handed materials are possible and constitute a very promising new paradigm for microwave and optical engineering [43]. Further in 2007, Islam/Eleftheriades [24] in their publications

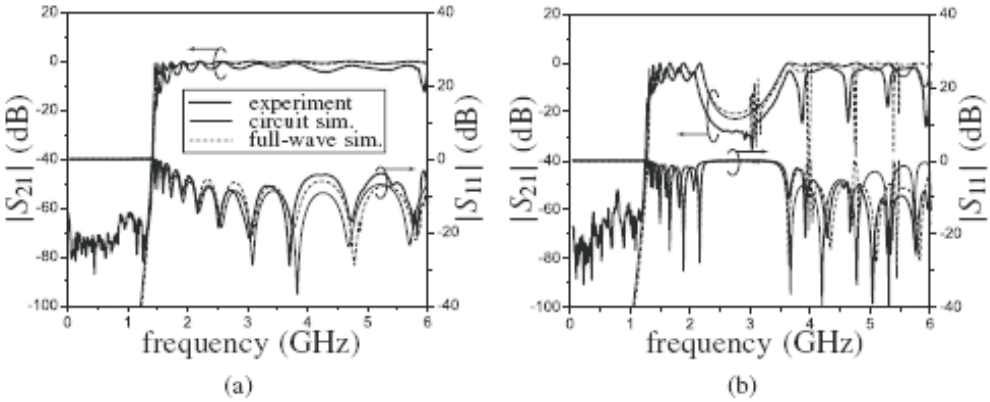

Figure 4.7: Caloz/Itoh practical board Results(a) Balanced circuit(b) Unbalanced [16]

presented these new metamaterial TL structures with interdigital capacitors and open stub inductors for narrow bandwidth bandpass filters.

4.3 Negative Refractive Index Narrow bandwidth Bandpass Filter

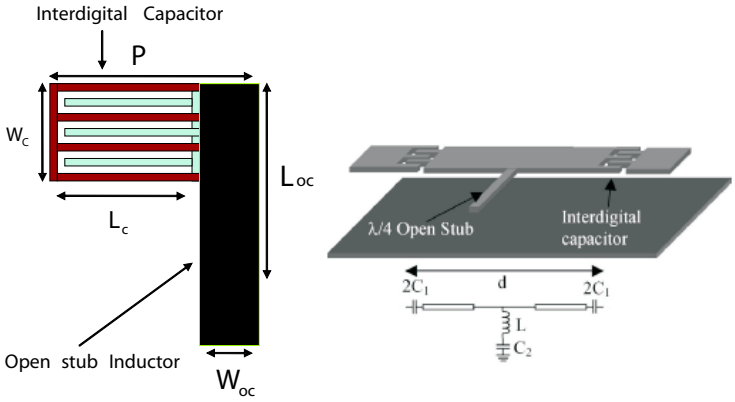

Figure 4.8: Islam/Eleftheriades structure with Interdigital Capacitors and Open-stubs [24]

Islam/Eleftheriades in their publication presented the above new left-handed structure called for narrow bandwidth bandpass filter design. The single high-pass unit cell configuration is too broadband to allow a sharp cut-off response required by a duplexer. An attenuation-pole can be introduced by replacing the shorted-stub $\lambda/4$ from Caloz/Itoh structure with a $\lambda/2$ open stub. Above its resonant frequency, the $\lambda/4$ stub is inductive and a negative refractive index unit-cell can be obtained [24]. The interdigital capacitor and length "d" of the filter is adjusted to match to the characteristic impedance of the system. Also, parallel open stubs instead of series interdigital capacitors are used to provide the matching network. Practical implementation for their mentioned structured single unit cell filter has obtained a narrow passband insertion loss of 1.26 dB at 2.03 GHz and his results are depicted in fig. 4.9.

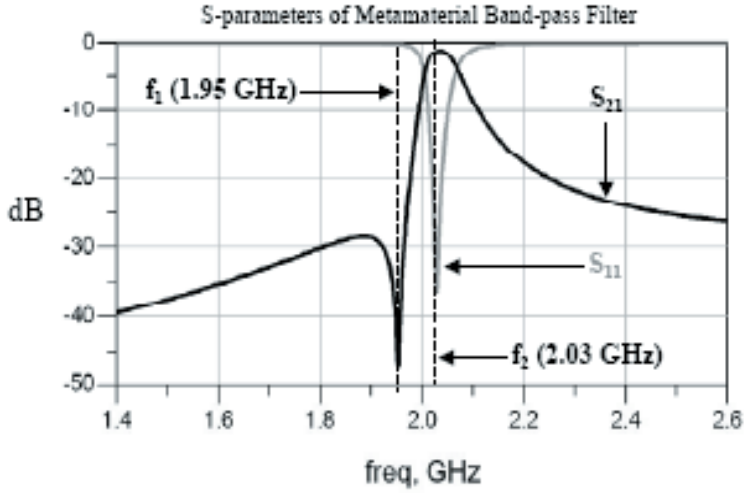

Figure 4.9: Islam/Eleftheriades Structure [11]

4.4 Metamaterial TL Narrow bandpass filter structures using Microstrip Gaps and Open stubs

As a left-handed transmission line does not exist in nature, It has to be approached by artificial structure which is usually constructed from a series of discontinuous sections operating in a restricted frequency range. A typical realization is found in a quasi-lumped transmission line [50] with elementary cells consisting of series capacitors and shunt inductors.

C. Caloz and T. Itoh in their publications [5] presented periodical Composite Right/Left Handed [CRLH] Metamaterial [MTM] Transmission Line [TL] bandpass filter design with interdigital capacitors and short stub inductors for broad bandwidths. In their periodical structure they got the same amount of left handed [LH] and right handed [RH] resonance frequencies dependently on the amount of cells which was discussed in the previous section of this chapter. Islam/Eleftheriades [24] in their publications presented these new metamaterial TL structures with interdigital capacitors and open stub inductors for narrow bandwidth bandpass filters. By taking this idea into consideration in this doctoral thesis work, we have proposed narrow bandwidth filter design using microstrip gap capacitors and open stubs inductors which equates with CRLH MTM TL. Fig. 4.10, shows a microstrip MTM CRLH TL bandpass filter structure with series microstrip gap (slots) capacitor and shunt open stub inductor.

4.4.1 Using $\lambda/2$ resonators

As mentioned earlier we have replaced $\lambda/4$ resonator (short stubs) with $\lambda/2$ resonator (open stubs). On the large scale both resonators show similar behavior. A $\lambda/2$ resonator with a very long stub and virtually large-valued ground capacitor acts exactly like a $\lambda/4$ resonator. The long lengths of the openstubs could be of disadvantage, but the strips may be meandered to minimize lengths. As we are

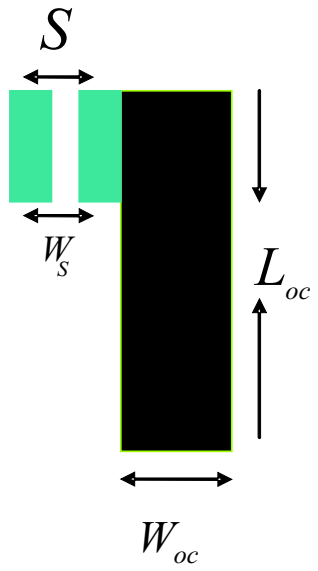

Figure 4.10: CRLH MTM TL structure with Gaps and open stubs

using suspended substrate technology where the conductive housing fulfill the gap between this to resonators.

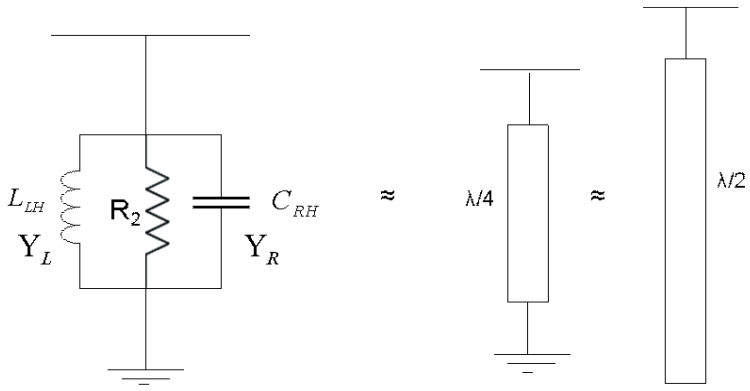

Figure 4.11: $\lambda/2$ resonator equivalence

The advantage is that it does not require via conductor. We are using suspended substrate technology, where the housing is a critical issue. This could be a possibility for minimizing effects (losses/shift) on mechanically fabricated board, which is studied further in this thesis work. Secondly, to prove CRLH MTM structural behavior with $\lambda/2$ resonators for better results in filter design. The equivalence

of open stub inductor can be seen in fig. 4.11

4.4.2 Microstrip Open Stub and Gap Equivalent CRLH Structure -Tx Filter

The structure assumes, the modeling of the metamaterial equivalent CRLH TL which is equivalent of fig. 4.2. The metamaterial (or left handed) line is represented by periodical arrangement of serial capacity and shunt inductivity. The serial capacitance is represented in the layout by slots and shunt inductivity by open stubs. The equivalent microstrip gap circuit is shown in fig. 4.12a, which is symmetric and equal to C_{even} (i.e. $C_{even} = 2C_1$) [44]. The position of the resonances in the frequency domain is determined by the length of the side wings which exhibits right handed inductance. By changing the length of the short wings (left and right wings between slots) we can also steer the position of the LH-resonances to each other. Moreover, the distance between the slots is mainly determined by the width of the side wings. If the distance between the slots is different from the width of the side wings, which is not particularly a rule. But this has a big influence on the behavior. The width of the side wings has also huge influence on the bandwidth. The wider the side wings the narrower the filter effect tends to be. The side wing inductors are used for the presence of RH (Right Handed) inductance during low frequency approximations as well to maintain the characteristic impedance "Z_C" of the unit cell. In order to concentrate all the possible frequencies in a narrow frequency range, we have used the gaps (slots), where the width of the gaps steers the bandwidth of the filter. The smaller the capacity (width of the gap), the more narrow is the bandwidth [18]. To avoid via conductor in short stubs we have used open stubs long lengths and dispersion could be disadvantageous.

But could be of interest, if any solution arises during research to overcome the drawbacks. For parameter extraction [from fig. 4.2 and fig. 4.12], neglecting ex-

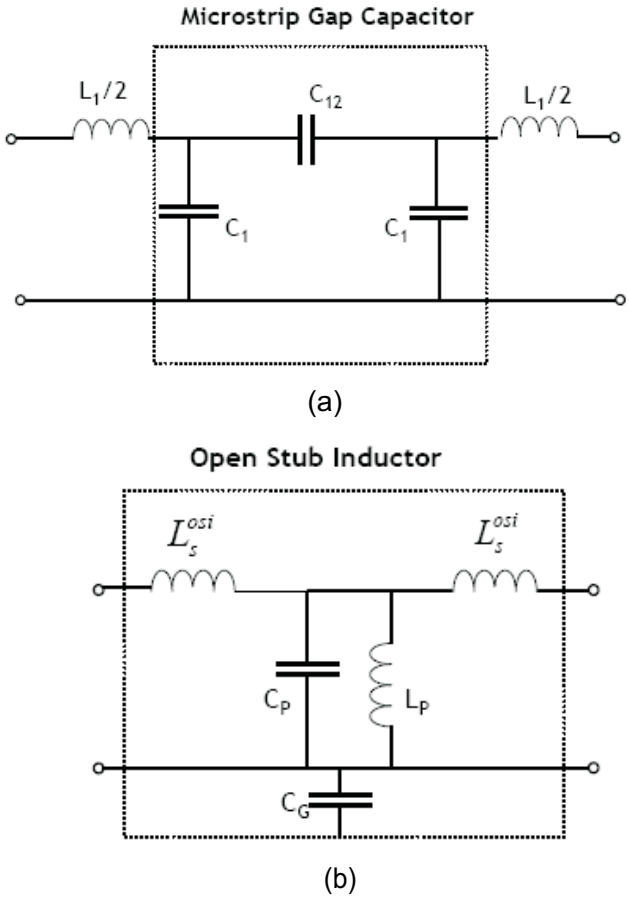

Figure 4.12: Equivalent (a)Gap capacitor (b)Open stub Inductor

tremely small inductance L_s^{osi}, we obtain four CRLH parameters as [16],

$$L_{RH} = L_1/2 + L_1/2 \tag{4.13}$$

$$C_{RH} = C_P + C_G \tag{4.14}$$

$$L_{LH} = L_P \tag{4.15}$$

$$C_{LH} = C_{12} \tag{4.16}$$

By reducing the capacity in serial branch we reduce the distance between resonances in the frequency domain. But the values of gap width and spacing can be optimized using Agilent's ADS software with goal constraints. The low-frequency

approximation for the inductance of open stub [39] is:

$$L_L = -Z_C^{os}(\cot \beta_l^{os})/\omega \tag{4.17}$$

where $\cot \beta_l^{os}$ is the electrical length of stub [16]. The schematic of the new CRLH MTM TL structure is shown in fig. 4.13 in the resonant frequency range. We have proposed this structure to prove the state of art metamaterials in designing TX bandpass filters for E-GSM 900 base station applications.

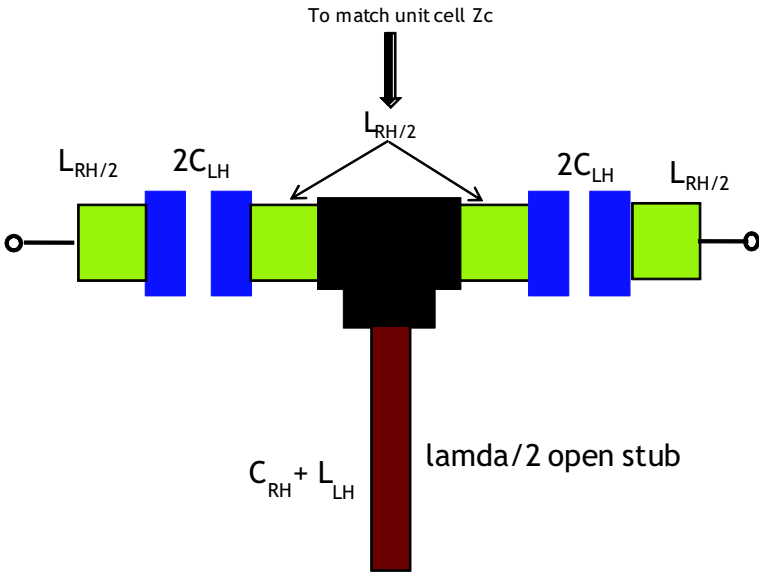

Figure 4.13: MTM CRLH TL Unit cell

4.4.3 Microstrip Open Stub and Gap Equivalent CRLH Structure -Rx Filter

We have used a different structure with similar gaps and open stubs as per the requirement for Rx filter. In this structure the series resonance is replaced by $\lambda/2$ resonator and the shunt path is obtained by coupling microstrip gap with open stub inductor separated by short TL.

In case of ***series resonant*** circuit we have converted simple RLC circuit to $\lambda/2$ TLine [45], first taking center frequency into consideration, then optimizing for a

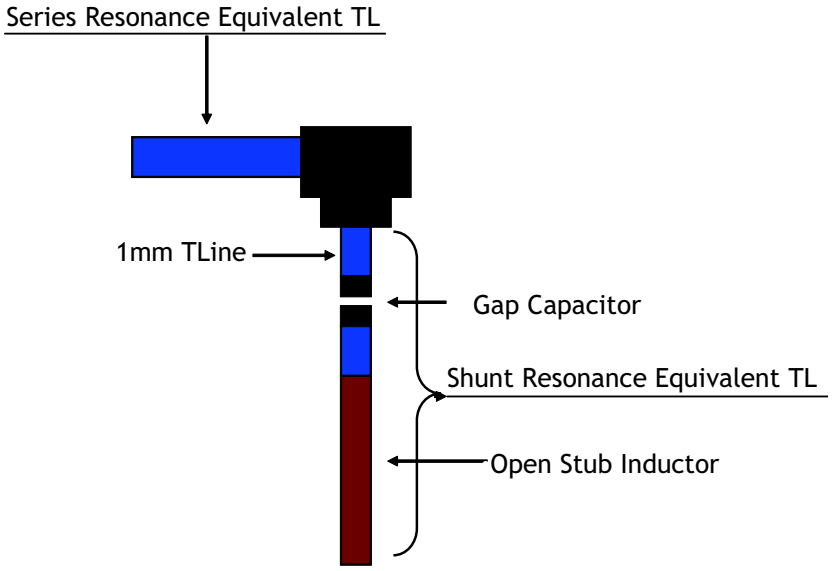

Figure 4.14: Rx BPF - Structure

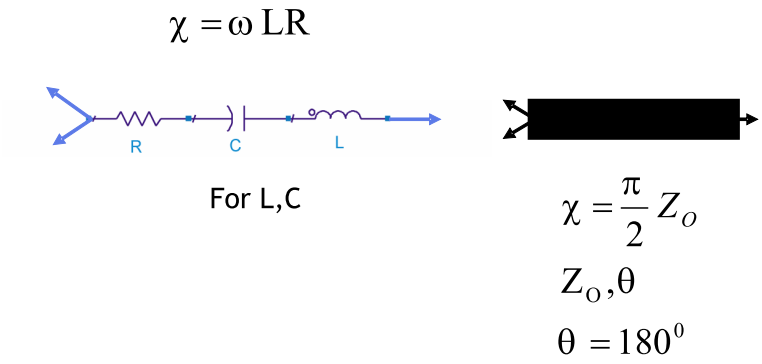

Figure 4.15: Series Resonant Circuit Equivalent

required band of frequency and its equivalent is shown in fig. 4.15. Right handed inductance L_{RH} and left handed capacitance C_{LH} can be obtained through calculations.

In case of ***shunt resonant*** circuit microstrip gap capacitor is converted to open stub inductor, by using fig. 4.2. For shunt resonance, neglecting small inductances and capacitances we get:

$$C_{RH} = 2C_1 + C_P + C_G \tag{4.18}$$

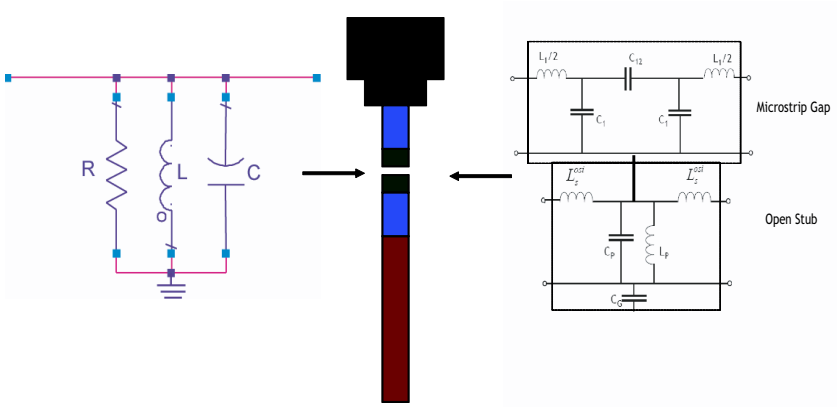

Figure 4.16: Shunt Resonant Circuit Equivalent

$$L_{LH} = L_P. \tag{4.19}$$

In fig. 4.14, we have used 1mm Tline to separate the gap from the T-shape interconnect to avoid change of reference plane problem during momentum simulations. The metamaterial behavior of such structure is further discussed in chapter 6 and the unit cell can be seen in fig. 4.17. The open-stub extensions and microstrip gap spacing are responsible in narrowing the passband, with respect to our design requirements.

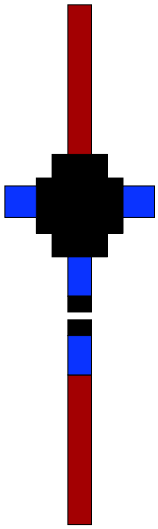

Figure 4.17: Rx BPF Unit Cell

Chapter 5

Left Handed TX RF bandpass filter design

5.1 Introduction

In this chapter we have designed an RF TX-bandpass filter for 925 MHz-960 MHz (35 MHz narrow bandwidth) for E-GSM applications using our new proposed structure with gaps and open stubs with simulation, measurement board results along with the comparisons. Also we have discussed the difference made by the suspended substrate technology in achieving low passband and sharp stopband which is used in this design. We picturised the applications of metamaterial structures in base stations.

5.2 RF Frequency Agile Systems

Fig. 5.1 gives a vision on what level MTM structures can be applied in RF systems [23]. In telecommunication systems, a large geographically distributed network coverage area is typically partitioned into a multiplicity of mobile communication regions, called as cells, where each cell includes a communication node,

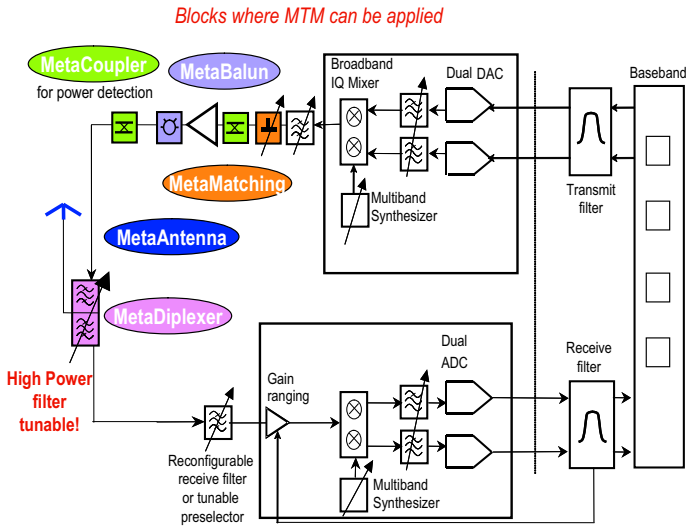

Figure 5.1: Applications of Metamaterials in RF Systems [18]

such as a base station to realize wireless communications with one or more mobile stations or wireless devices within that cell. The network coverage area is commonly based on wireless links that are designed to operate at a minimum level consistent with Quality of Service (QoS) in an area where the mobile station has sufficient power to achieve a target signal-to-noise (SNR) ratio at a cell site that includes the base station. Due to continued growth in the number of users in mobile communications, many wireless network operators or service providers must find new ways of increasing the capacity of their networks. Antenna systems represent an area that may be developed to increase capacity in mobile communication networks [46].

Specifically, many traditional installations of mobile communication base-station antennas make use of space-diversity techniques (e.g., Multiple Input Multiple Output (MIMO) systems), which require at least two antennas pointing in the same direction and separated from each other. A typical base station may now employ as many as six transmitting and six receiving antennas, each requiring its own duplex filter. Typically 4 paths.

The main task of the duplex filter is to separate transmit and receive frequen-

cies at the antenna port shown in fig. 5.2. A typical duplex filter thus has three ports, one for the antenna, one for the transmitter and one for the receiver. A typical duplex filter is composed of coaxial resonators that require advanced fabrication techniques and materials to achieve high Q-factors (e.g. 5000) [18] that are needed to provide high filter selectivity. Filter selectivity is critical in a base station because very sensitive receivers are operated simultaneously with strong transmitters. In some applications. MIMO systems have proven to be cost prohibitive because of the cost of the duplex filters alone.

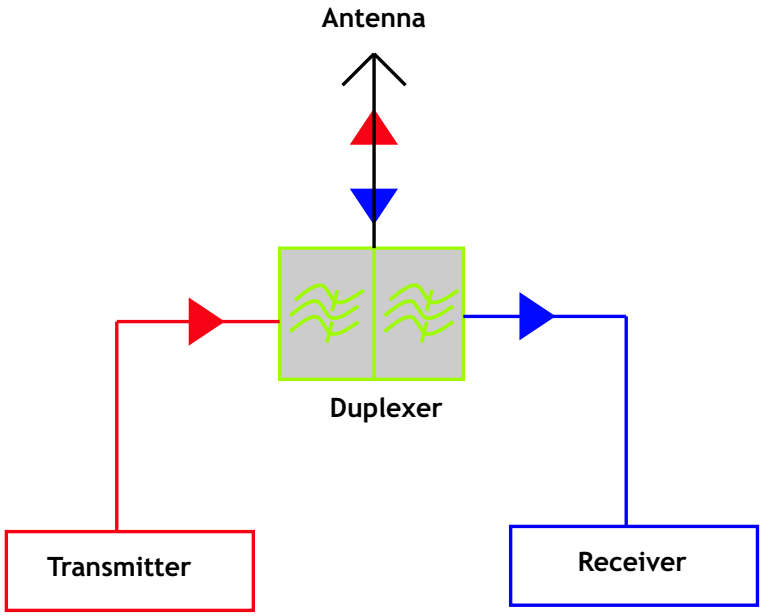

Figure 5.2: Duplex Filter Block

5.3 Left Handed MTM RF Tx Filter Design

5.3.1 Requirements

A Duplex filter is defined as a filter where an individual TX and RX filter shares one antenna with an isolation between them. They have to handle high tranmist power levels up to 49 dBm from transmitter(TX) to Antenna and very weak

receive level around -118 dBm from Antenna to Receiver(RX).

The requirement for E-GSM 900 Alcatel-Lucent base station with minimum 80 dB attenuation for RX-band and maximum 1 dB insertion loss in TX-band is to be enhanced during this thesis work. Fig. 5.3, shows a typical duplex filter with high Q-factor (5000) with very tough housing of 360 mm x 240 mm x 50 mm size, complex fabrication process and hence it is much expensive. Therefore we have adapted state of art metamaterial structures taking cost-efficient concepts seriously into consideration and hence to overcome the current coaxial duplex filter [47].

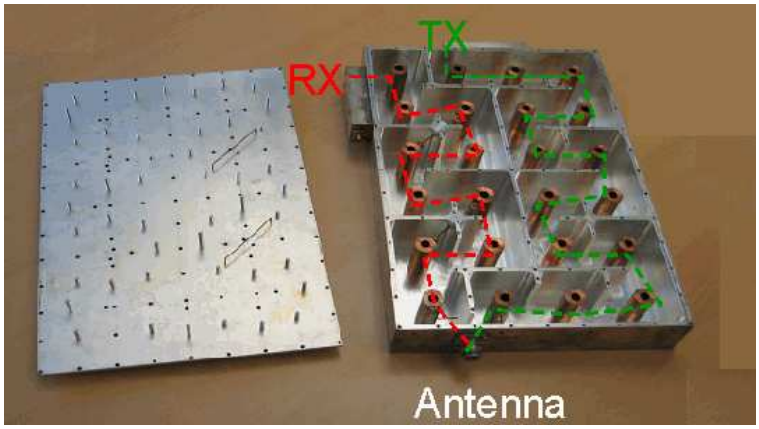

Figure 5.3: Duplex Filter [Alcatel-Lucent]

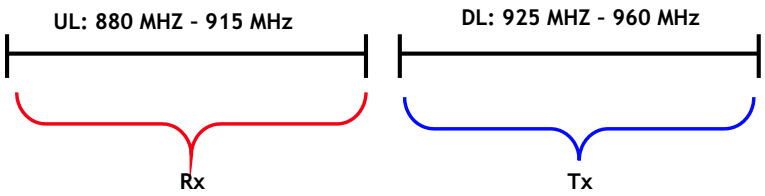

Figure 5.4: E-GSM 900 Band

In this thesis work we have proposed new MTM CRLH structure for filter designs by using new structure with microstrip gap capacitors and open stub inductors, discussed in sec. 4.4, of chapter 4. We have designed narrow bandwidth RF bandpass filter (TX band, 925 MHz - 960 MHz) in shielded suspended substrate for

E-GSM base station applications. We have used balanced structure for our design due to its advantages over unbalanced structures as discussed in chapter 3. Our main goal is to achieve an insertion loss of less than 1 dB with sharp stopbands considering form factor and cost in the state of art MTM structures and its practical application.

To validate the new structure design and analysis, the three unit cell BPF filter layout board was fabricated and measured and hence to prove the state of art MTM CRLH structures. The schematic of the new CRLH TL structured unit cell bandpass filter is shown in fig. 5.5. It has been observed during simulation that, the unit cell impedance at the ports resembles as 75Ω, so the impedance transformer [17] is used to step it down to 50Ω for perfect matching with the 50Ω ports.

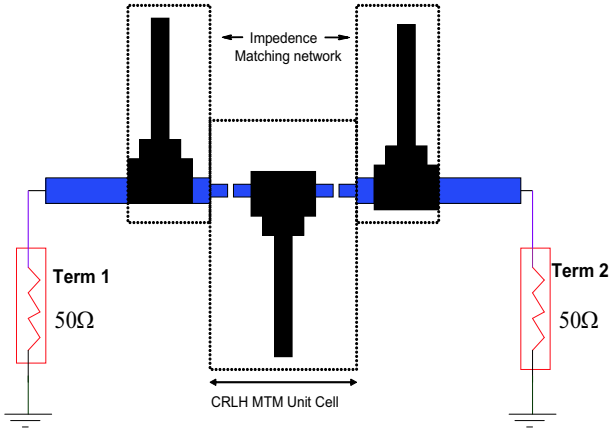

Figure 5.5: TX MTM unit cell

5.3.2 Lumped Circuit Design and Quality Factor

We have started our MTM BPF design following the design rules starting from lumped then switching to distributed which includes our new structure equivalence. Fig. 5.9. shows the single MTM unit cell which is lumped. We have tuned the values of series and shunt left/right handed lumped elements with respect

to our design frequencies i.e. 925 MHz - 960 MHz. Serial and shunt resonance frequencies define edges of the band gap and characteristic impedance in LH and RH section [16]. According to our theoretical calculations in smith chart with respect to the center frequency, as well as tuning lumped parameters in Agilent ADS software we have realized the series/shunt elements separately.

Quality Factor is a very important factor [48] as we are strictly dealing with series and shunt resonances, there are many definitions based on

- -3dB Bandwidth

$$Q_{3dB} = \frac{f_{center}}{BW_{3dB}} \tag{5.1}$$

- Phase Steepness

$$Q_{Phase} = \left[\omega \left|\frac{d\psi(\omega)}{d\omega}\right|\right]_{\omega=\omega_{res}} \tag{5.2}$$

- Energy

$$\frac{2\omega\left(\Sigma\omega_e + \Sigma\omega_m\right)}{\Sigma P_{loss}} \tag{5.3}$$

- From the values of the complex impedances e.g. $\frac{\omega L}{R}$

Each of the definitions has the sensible meaning only at the resonance or in close range to the resonance. If we want to show the quality factor over a frequency range (e.g. in the whole pass band) the easiest one to implement in the simulations and measurements is based on the phase steepness. So if we have the course of the phase of the S21 curve, with simple mathematical operations we are able to calculate the quality factor of the resonant structure. All diagrams, which show the quality factor, are calculated based on this definition.

5.3.3 Series/Shunt Resonant Element Verification

The values realized for the **series** resonant circuit are:

- $C_{LH} = 2.12pF$
- $L_{RH} = 925nH$
- $R_S = 0.05\Omega$
- $Q - Factor = 1220$

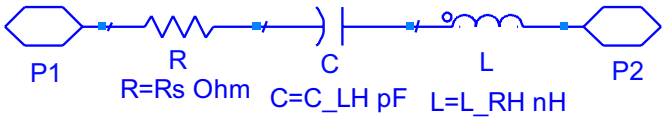

Figure 5.6: Series Resonant Circuit Verification

As mentioned above, the simulated series resonator Quality Factor with respect to phase steepness is shown in fig. 5.7. Which is 70 less than what we have shown in the calculations.

In case of **shunt** it is not possible to individually realize of L and C values due to restrictions in the form factor given by $(\lambda/20)$ [18]. Therefore we tuned the values and the shunt lumped model is seen in fig. 5.8.

- $C_{RH} = 0.032pF$
- $L_{LH} = 1.16nH$
- $R_P = 10,00000\Omega$
- $Q - Factor = 5252$

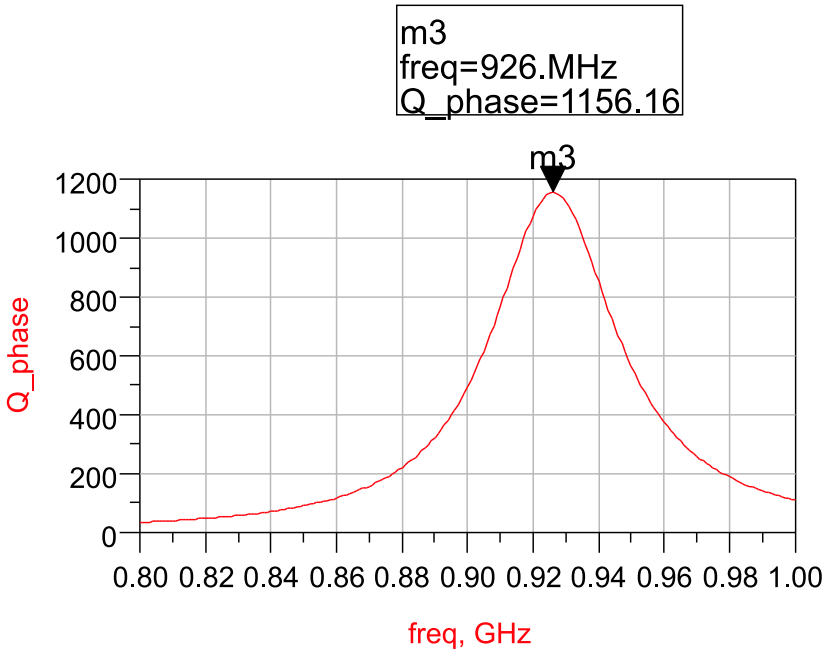

Figure 5.7: Series Resonant Q-Factor

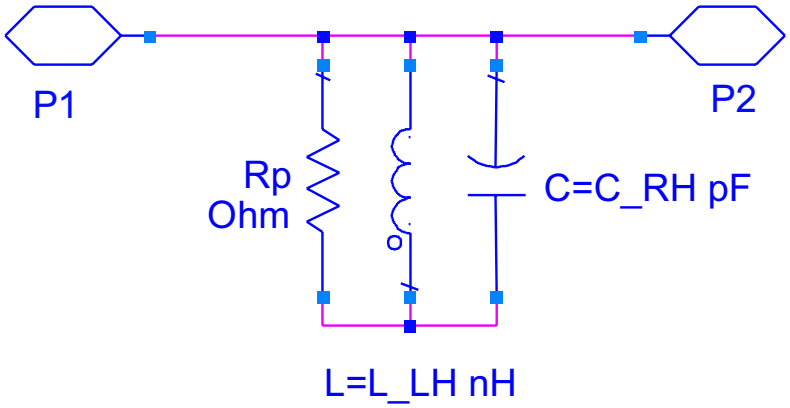

Figure 5.8: Shunt Resonant Circuit Verification

Using the above lumped series/shunt element values we have transformed these into metamaterial unit cell which is depicted in fig. 5.9. The quality factor for the unit cell, is shown in fig. 5.10.

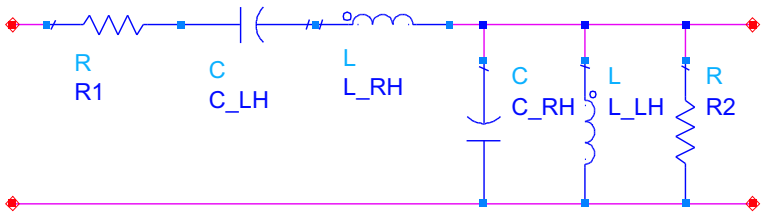

Figure 5.9: MTM Unit Cell Lumped

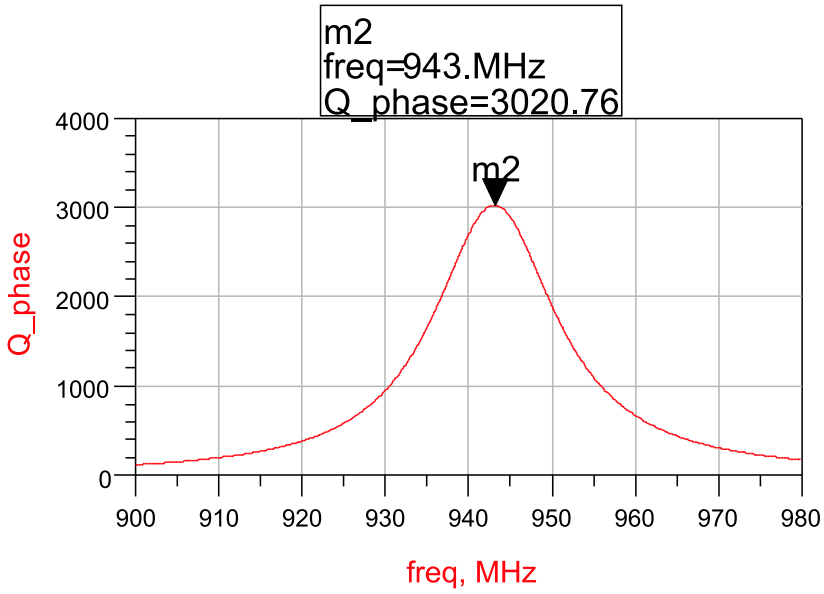

Figure 5.10: Unit Cell - Quality Factor

Also for a single unit cell an insertion lossless than -0.03 achieved and is shown in fig. 5.11. With respect to our attention till we reach the measurement board. i.e less than 1 dB insertion loss. Also increasing number of unit cells remind to keep insertion loss less than 1 dB.

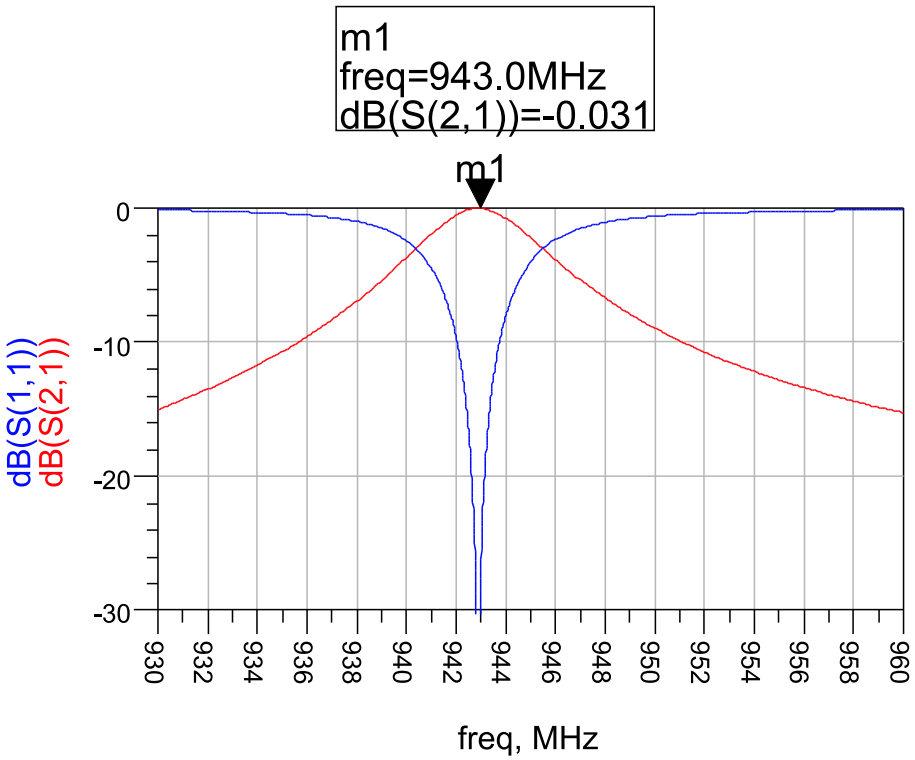

Figure 5.11: Left Handed TX Unit Cell - Insertion Loss

5.3.4 Zero-Order Resonance/Bandgap definition by serial and parallel resonance frequency - 3 unit cells

The series and shunt resonance frequencies define the edges of the bandgap [16] and characteristic impedance in LH and RH sections which is fully characterizable in terms of its propagation constant β and characteristic impendence Z_c in its passband for bandpass filters. where [18]:

$$\beta = \sqrt{\begin{array}{l} \frac{C_{RH}}{C_{LH}} + \frac{L_{RH}}{L_{LH}} + \frac{R_l}{R_2} - \omega^2 * L_{RH} * C_{RH} \\ -\frac{1}{\omega^2 * L_{LH} * C_{LH}} + j * \{\omega * [R_1 * C_{RH} + \frac{L_{RH}}{R_2} \\ -\frac{R1}{\omega^2 * L_{LH}} - \frac{1}{\omega^2 * L_{RH} * C_{RH}}]\} \end{array}} \tag{5.4}$$

and

$$Z_c = \sqrt{\frac{L_{RH} + \frac{R_1}{j*\omega} - \frac{1}{\omega^2 * C_{LH}}}{C_{RH} + \frac{1}{R_2 * j * \omega} - \frac{1}{\omega^2 * L_{LH}}}}. \tag{5.5}$$

Zero-order resonance frequency is the frequency which is independent of physical size i.e ($\beta = 0$). β is complex by formula 5.4 so $Re\beta = 0$ and is one of the proof for metamaterial behavior. It is also defined as a resonance, where the Q-factor is not susceptible to losses and survives with increasing losses. It can be proved by means of localization of phase constant with voltage measurement(i.e $\beta = 0$), aswell with the parametric study by introducing losses (i.e. R). In case of series resistance, the zero order resonance is found at the center of the passband where as in parallel resonance at the edges of either RH section. Fig. 5.12 depicts three unit cell lumped circuit. To observe the zero-order resonances the circuit is simulated (fig. 5.13). For the distributed structure, the zero-order resonance has been found nearly at 960 MHz and can be seen in fig. 5.14 and and its location can be revived from fig. 5.15. Also it was observed in fig. 5.14, with an increase of R_s (Series Resistance) the phase steepness (indicator for Q-factor) is not reduced and even improves at high values of R_s and hence proved the properties of state of art MTM structure.

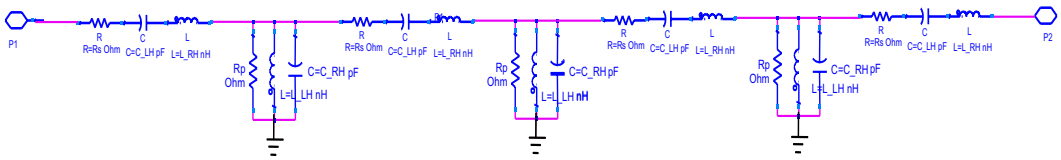

Figure 5.12: Three Unit Cell - Lumped

Further simulation for passband insertion and stopband attenuation can be seen in fig. 5.13. Where the insertion loss was found to be better achieved less than -0.1 dB in 35 MHz band 925 MHz - 960 MHz with -23dB as a stopband. The series and shunt resonances found are:

$$\omega_{se} = 943\, MHz \tag{5.6}$$

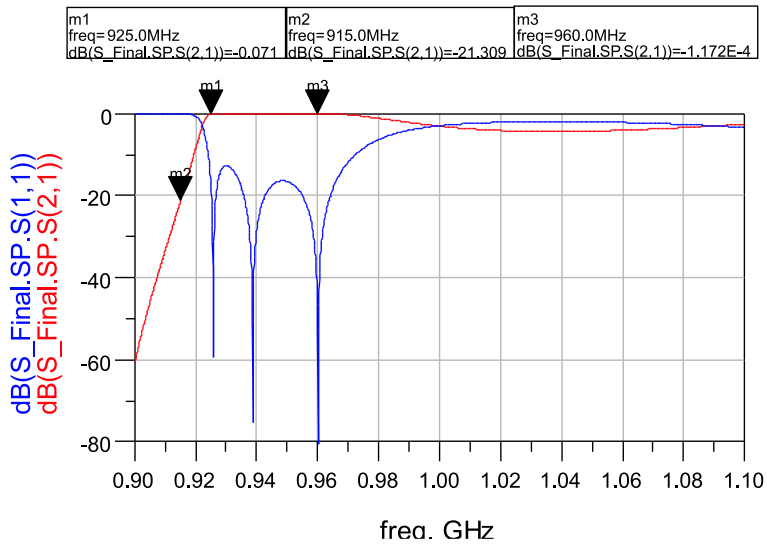

Figure 5.13: Lumped Circuit-Simulation Results - Three Unit Cells

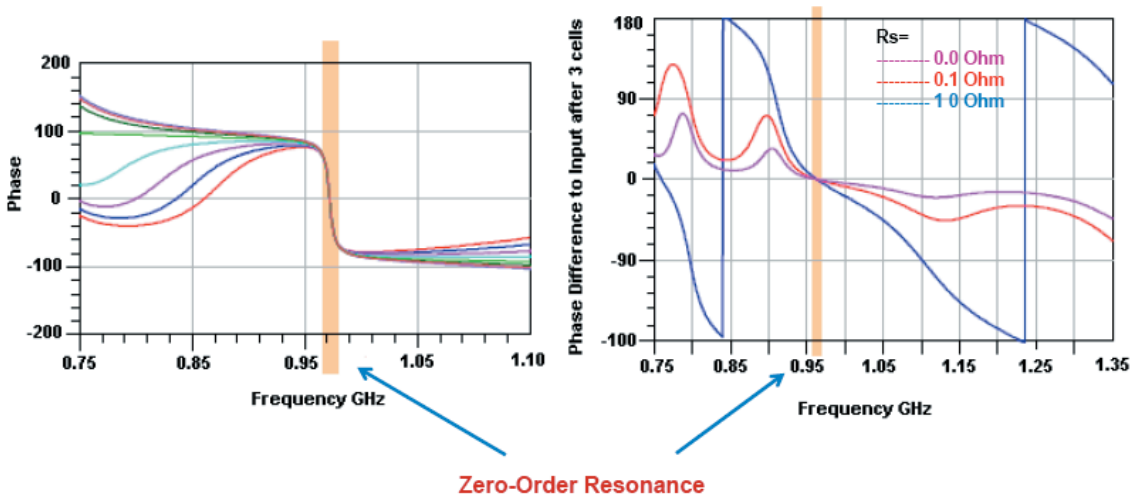

Figure 5.14: Zero-Order Resonance Proof

$$\omega_{sh} = 960\,MHz. \tag{5.7}$$

Which means the circuit is bit unbalanced, as gap existed due to, losses but near to balance conditions. The behavior of this filter obtained is purely left-handed, hence this filter is a left-handed MTM filter. With these simulation results, using 11 unit cells, we are able to reach a TX filter with -80 dB stop band and less than

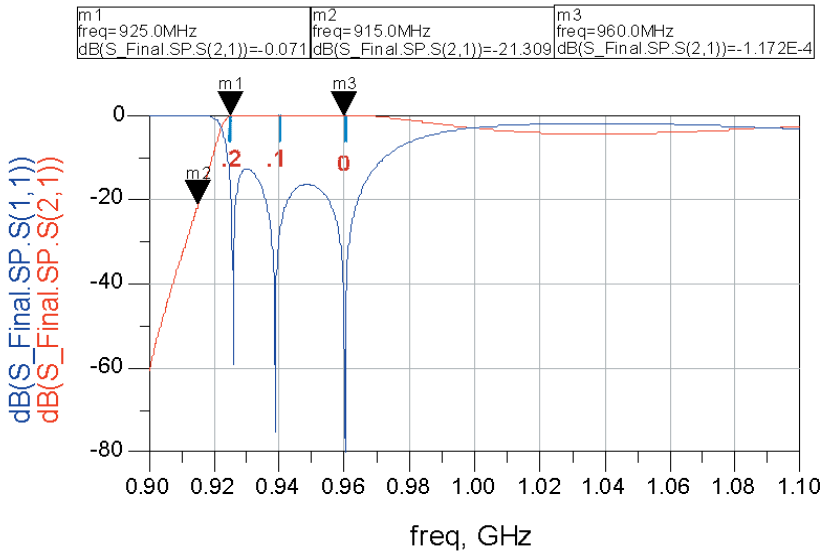

Figure 5.15: Zero-Order location

1 dB insertion loss. Moreover, we convert these lumped elements to transmission lines based on our new structure using suspended substrate technology which can be explained further.

5.4 Microstrip Shielded Suspended Substrate

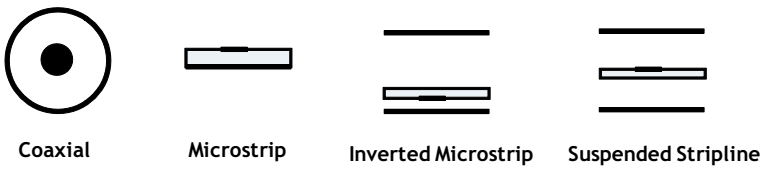

Figure 5.16: Line Configurations

The main important factor in filter design is the insertion loss. Where the substrate has a very big influence. The fig. 5.16 shows the classification. Coaxial cables

have the lowest losses but problematic on integration of tuning/reconfiguration elements. Planar are compatible to radio/PA manufacturing and hence compatible for tuning. Where as, microstrip lines are lossy. Microstrip inverted substrate are formed by turning the substrate over 180 degree to the ground plane in order to concentrate the electromagnetic field mainly in the air. Which are helpful in demonstrating with nbg. Shielded suspended substrates are very close to coaxial with much higher Q-factors. We have used shielded suspended substrate for the filter designs. Suspended strip line is an excellent transmission line media [14]. Increased cross-section together with a relatively thin substrate are responsible for reduced ohmic and dielectric losses. A large portion of the fields in air results in low dispersion and hence the radiation is prevented with shielding [13],[14]. Suspended and inverted microstrip lines are among the principal transmission media used in the upper microwave and lower millimeter-wave bands. Most of the microstrip components, such as power dividers, transistor amplifiers, directional couplers, receiver mixers, and frequency multipliers are manufactured using suspended substrate lines. Due to the symmetrical shielding, the suspended substrate line is particularly useful for integrated circuits with waveguide components, and the wide range of impedance values achievable makes these media particular suitable for filters. It's clear that thinner and less lossy is the substrate, the smaller the insertion loss and thus more narrow the filter effect.

In comparison with the planar microstrip, the suspended substrate line has many advantages [49]. The most interesting aspect is that the presence of an air gap between the substrate and the ground plane reduces the effects of dispersion on the propagation constant, generally to such an extent that the quasi-static results remain useful even at very high frequencies. Structural inaccuracies have a smaller effect due to the wider conductors, so also electrical properties are more precise. Because more of the field is in the air, higher characteristic impedances Z_L can be realized.

The disadvantages are difficulties in miniaturization, critical housing technology

(because the housing also acts as an electrode) and the increased complexity of utilizing hybrid elements. So, although suspended and inverted microstrip lines have many good properties, they are large and difficult to produce. In this thesis work we have worked with symmetric shielded microstrip line for better results and high Q-factor.

5.4.1 Symmetric shielded suspended substrate

The structure of the suspended substrate microstrip line with side walls is presented in fig. 5.17. These equations from [21] are used when the structure is symmetric.

The equations are divided into two ranges. For narrow strips ($0 < \omega < a/2$),

$$Z_0 = \frac{\eta_0}{2\pi}\left[V + R\ln\left(\frac{6}{\omega/b} + \sqrt{1 + \frac{4}{\omega/b}^2}\right)\right] \tag{5.8}$$

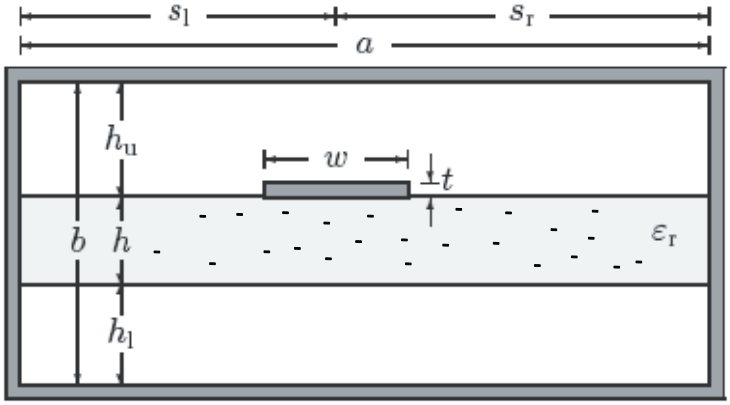

Figure 5.17: Symmetric Shielded Suspended Substrate structure

$$\epsilon_{eff} = \frac{1}{\left[1 + \left(E - F\ln\frac{\omega}{b}\right)\left(\frac{1}{\sqrt{\epsilon_r}}\right)\right]^2} \tag{5.9}$$

Where,

$$V = 1.7866 - 0.2035\frac{h}{b} + 0.4750\frac{a}{b} \tag{5.10}$$

$$R = 1.0835 + 0.1007\frac{h}{b} - 0.09457\frac{a}{b} \tag{5.11}$$

$$E = 0.2077 + 1.2177\frac{h}{b} - 0.08364\frac{a}{b} \tag{5.12}$$

$$F = 0.03451 - 0.1031\frac{h}{b} + 0.01742\frac{a}{b} \tag{5.13}$$

For wider strips, $(a/2 < \omega < a)$

$$Z_0 = \eta_0 \left[V + \frac{R}{\frac{\omega}{b} + 1.3930 + 0.6670 \ln\left(\frac{\omega}{b} + 1.444\right)} \right] \tag{5.14}$$

and

$$\epsilon_{eff} = \frac{1}{\left[1 + \left(E - F \ln\frac{\omega}{b}\right)\left(\frac{1}{\sqrt{\epsilon_r}}\right)\right]^2} \tag{5.15}$$

Where,

$$V = -0.6301 - 0.07082\frac{h}{b} + 0.247\frac{a}{b} \tag{5.16}$$

$$R = 1.9492 + 0.1553\frac{h}{b} - 0.5123\frac{a}{b} \tag{5.17}$$

$$E = 0.464 + 0.9647\frac{h}{b} - 0.2063\frac{a}{b} \tag{5.18}$$

$$F = -0.1424 + 0.3017\frac{h}{b} - 0.02411\frac{a}{b} \tag{5.19}$$

The above relations are valid for $1.0 \leq a/b \leq 2.5, 1.0 \leq \omega \leq 4$, and $0.1 \leq h/b \leq 0.5$. The results of the wide strip equations agree with those obtained using finite differential techniques to $\pm 3\%$, the narrow strip agreement is $\pm 2\%$.

5.4.2 Suspended Substrate Implementation

To achieve less insertion low we have implemented suspended substrate whose quality is described previously. We have tested planar, shielded and inverted substrate models to choose the least insertion loss model at our design frequency level.

Fig. 5.19 shows a 30 cm long microstrip line of Rogers RO 4003 substrate material with thickness of 0.813 mm simulated in Agilent's ADS environment to choose the

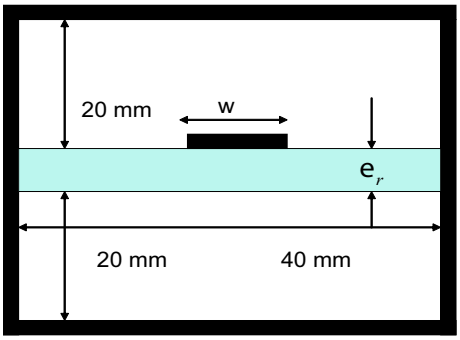

Figure 5.18: Shielded Suspended Substrate 40 mm spacing

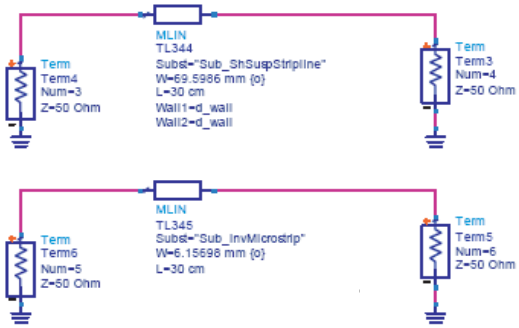

Figure 5.19: Substrate Test - 30 cm TL Line

better substrate model for low losses for our filter design in state of art Metamaterial structure. The simulation curves in fig. 5.20. represents, shielded microstrip suspended substrate, inverse suspended substrate and planar microstrip line simulation results respectively. In relation to its low insertion losses dB [S21] from graph, we have chosen suspended substrate for our design and its symmetric displacement is 40 mm, where the substrate is 20 mm apart from the both sides of the metallic shielding can be seen in fig. 5.18.

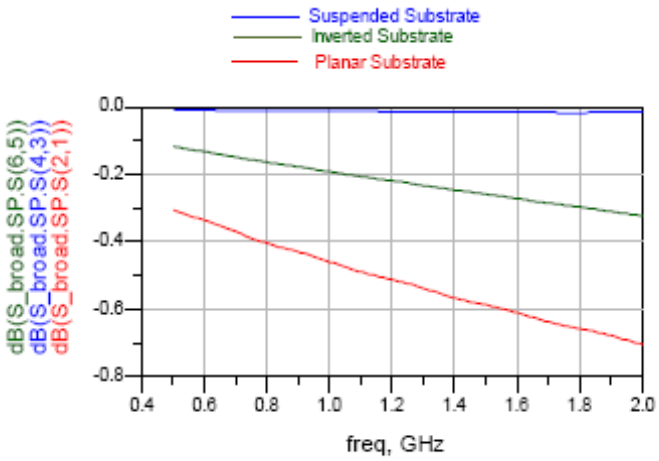

Figure 5.20: Substrate Simulation Results - 30cm TLine

5.5 Lumped to Microstrip Transmission Line Conversion

We have converted the lumped MTM unit cell circuit into Microstrip TL with the new proposed structure explained in the previous chapter and this is completely in suspended stripline with $E_{eff} = 1.04$, substrate Rogers 4003, Tanδ=0.0021 height 0.813 mm with 20 mm to top and bottom with conductor thickness of 0.1 mm,. The values are calculated with respect to center frequency and later optimized in passband, now the TLine **series** equivalent of lumped is shown in below fig. 5.21.

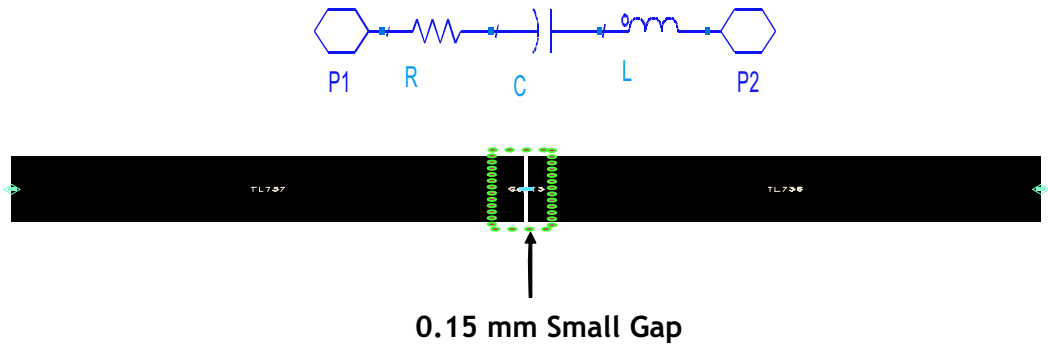

Figure 5.21: Lumped Series Equivalent Microstrip TL

- Length L = 14 mm both sides
- Width W = 3 mm
- Gap Spacing S = 0.15 mm

The lumped equivalent of shunt resonant circuit is shown in fig. 5.22 and the values of the TLines are:

- Short Open Stub Length Loc1 = 1.2 mm
- Long Open Stub Length Loc2 = 274 mm

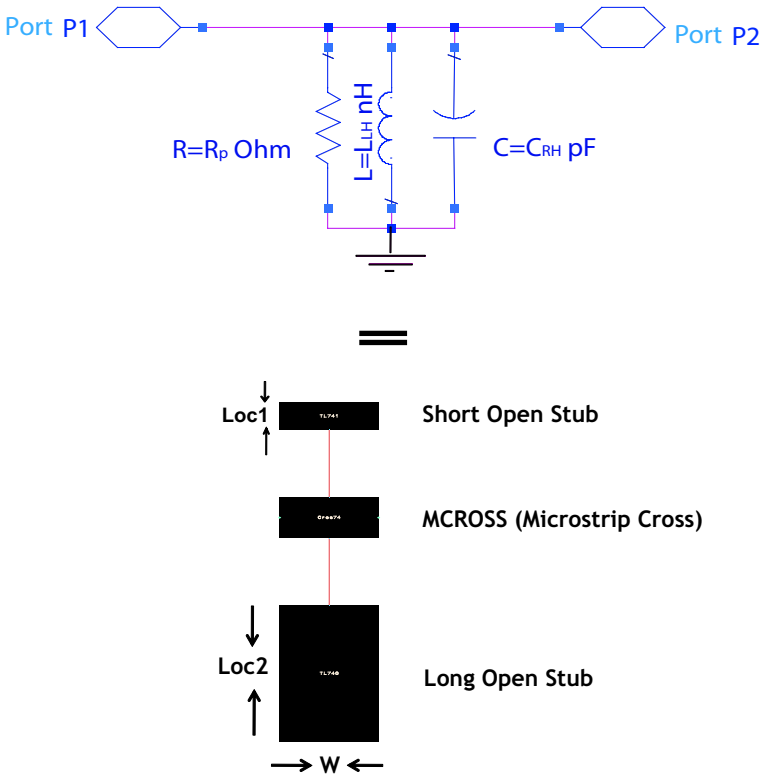

Figure 5.22: Lumped Shunt Equivalent Microstrip TL

- Width W = 5 mm
- MCROSS is a four port connecting network.

The extension of open stubs are meant for narrowing bandwidth. The converted lumped to microstrip TL MTM unit cell and its Q-factor is shown in below fig. 5.23 and fig. 5.24. The quality factor in the simulation shows 2039, which is better than the lumped element unit cell, This might be due to various reasons of the suspended substrate technology and due to impedance transformer.

Figure 5.23: MTM TL Unit Cell

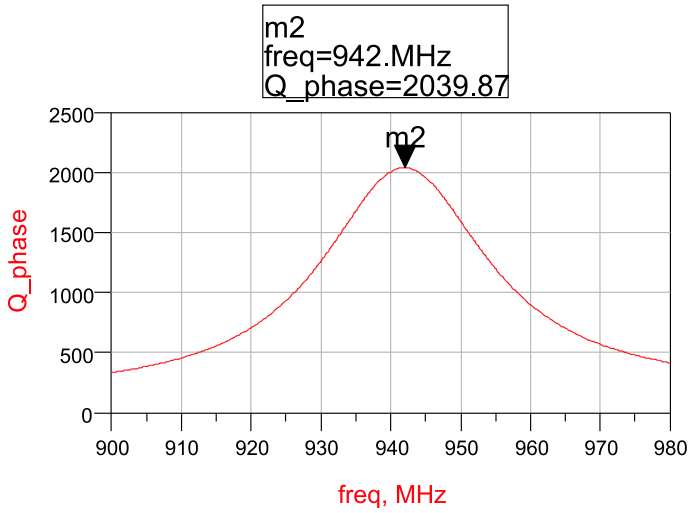

Figure 5.24: MTM TL Unit Cell- Quality Factor

5.6 3 Unit Cells TX Filter Design - Simulation, Momentum, Measurement Results

Fig. 5.25 shows a technology of three unit cell CRLH MTM BPF filter in a shielded suspended substrate with impedance transformers to match the ports to 50Ω environment. The circuit design simulations are carried out in Agilent's ADS Software. Besides circuit simulator we have also simulated the layout in method

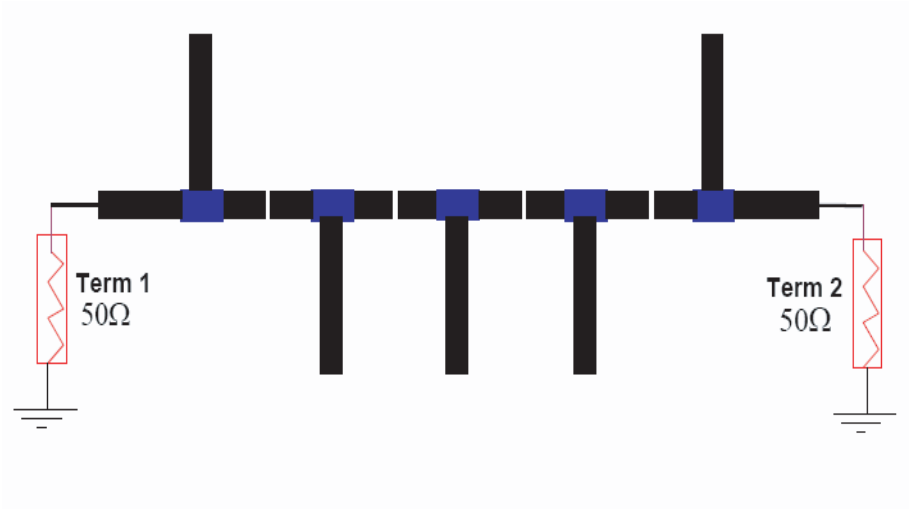

Figure 5.25: 3 unit cell Left-handed Tx-Filter

of moments analysis simulator (MoM) in the absence of any active devices, which is expected to reveal results closer to measurement results.

5.6.1 Circuit Simulator Results

As in the pervious section, we have discussed the meta behavior of our filter structure and its proof is shown by the electrical distributions of currents in fig. 5.26. It shows, that these resonances has left handed behavior with a uniform current distribution. The right pole shows zeroth order resonance and thus the bandgap. Therefore, this structure must a the CRLH one.

We have many possibilities to optimize the structure to the desired performance:

- Width of the slots
- Width of the side wings
- Number of unit cells
- Properties of the substrate (i.e. holder of the structure)
- Distance between slots (independent of the width of the side wings)

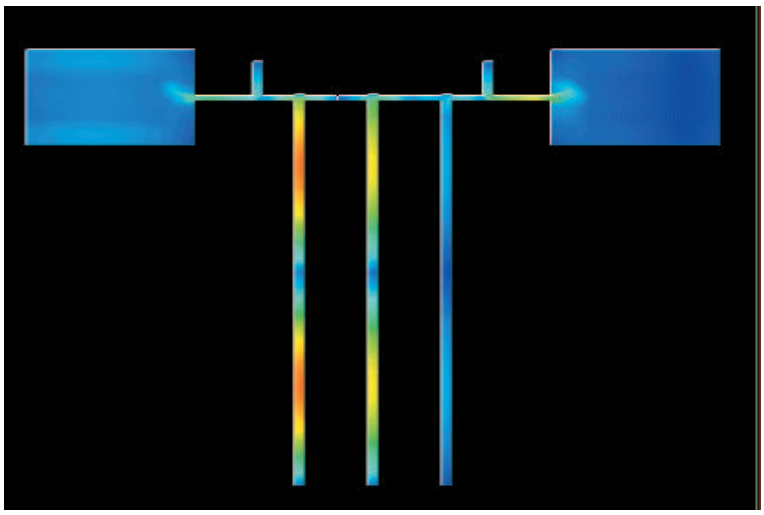

Figure 5.26: Electromagnetic Current Distributions

- Distance of the structure to the ground plane
- Distance of the substrate to the upper electrical shield
- Width of the strips.

The circuit simulator shows an average insertion loss (ripple) less than -0.25 dB (925 MHz - 960 MHz) with a sharp stopband of -23 dB (at 10 MHz offset) with three poles within 35 MHz range and is depicted in fig. 5.27.

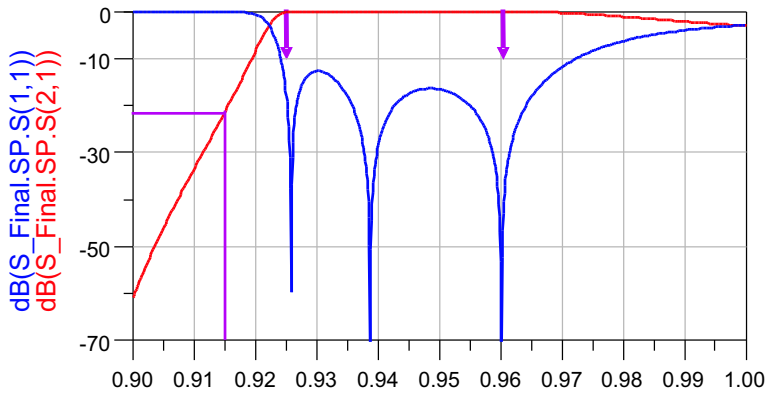

Figure 5.27: Left-handed 3 unit cell Tx BPF-Simulation Results

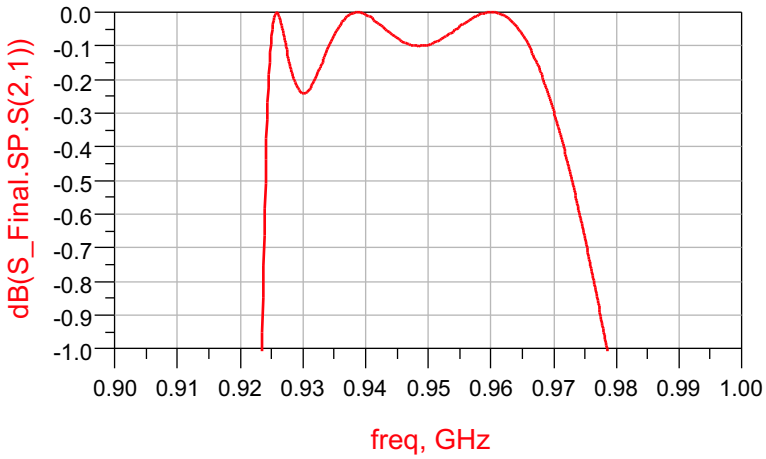

Figure 5.28: Simulation Results - Closer View

Band ripple can be viewed in fig. 5.28. One can realize the concept in metamaterials, that the number of unit cells makes the edges sharper [14], but has influence in the increment of insertion loss. From simulation result with this structure it can be concluded, that with 11 unit cells less than -80 dB stopband can be achieved together with below -1 dB insertion loss. Which would be required for various industrial products. Housing in three-dimensional view can be seen in fig. 5.29 which gives an idea how the substrate has been placed.

Method of moments simulator analysis results can be seen in fig. 5.30 and the close view in fig. 5.31. On comparison with circuit simulator, the momentum results are -0.3 dB and -13 dB more in ripple and edges (stopband), which is again much better hope to go for measurement board to prove the state of art left-handed MTM new structure and its applications in RF communication systems.

The layout board 33 cm x 37 cm in fig. 5.32 is fabricated using ROGERS RO4003 material with substrate thickness of 0.813 mm and conductor thickness of 0.1 mm respectively in a close conductive housing of shielded suspended substrate, separated by 20 mm symmetric walls on top and bottom from the center of BPF. The cross-section can be seen in fig. 5.33, closed box view in fig. 5.34 respectively. The measurement board of MTM CRLH BPF results in fig. 5.35 shows a stopband of

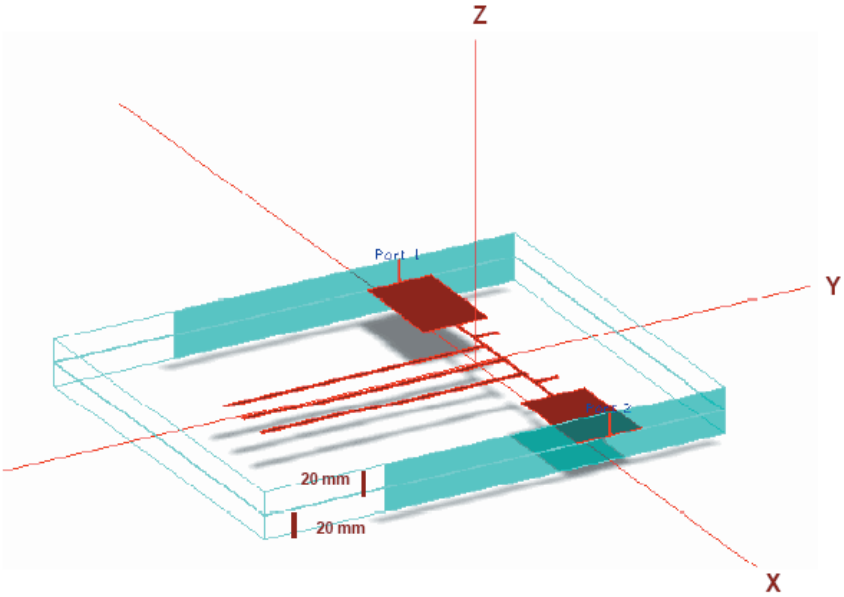

Figure 5.29: 3-Dimensional Suspended Housing

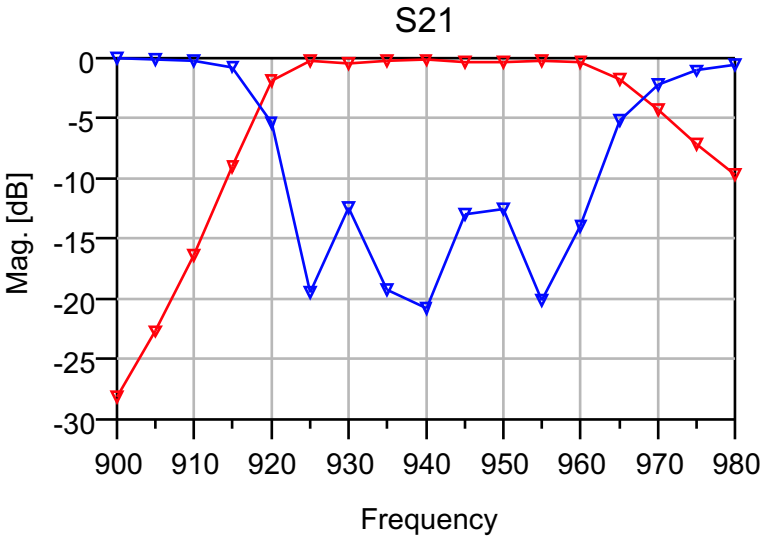

Figure 5.30: TX Filer - Momentum Simulator - Results

nearly -10 dB at 918 MHz with an average passband less than -0.76 dB between 928 MHz - 964 MHz within 35 MHz bandwidth. The frequency range is displaced about 3-4 MHz due to critical housing of the suspended substrate, and can be ad-

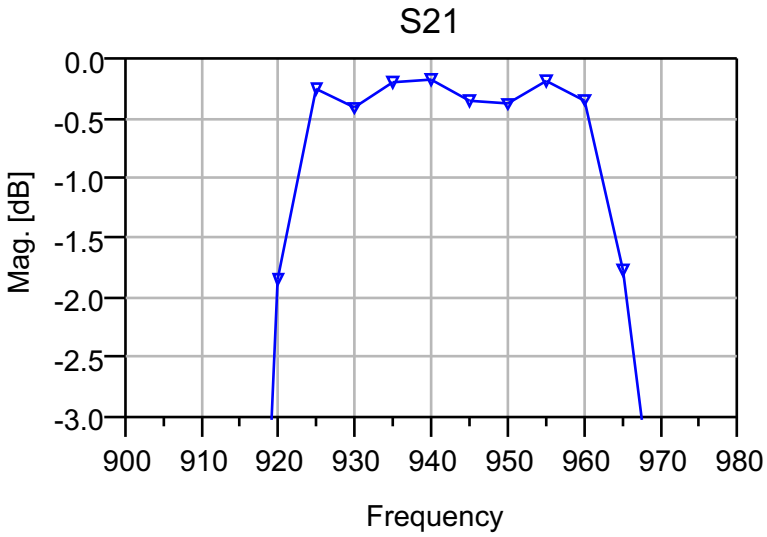

Figure 5.31: Momentum Results - Closer View

justed by tuning the metallic housing screws to set our frequency range of design i.e. 925 MHz - 960 MHz respectively. The results in this range achieved -0.7 dB insertion loss in passband and -10 dB stop band at 915 MHz and can be seen in fig. 5.36. Fig.5.37 shows the comparison between circuit simulator, momentum simulator and measurement results and are tabulated in table. 5.1. The obtained fabricated board results are almost equal in the stopband and 0.4 dB higher in the passband in comparison with method of momentum analysis simulator than circuit simulator and hence satisfy our goal of reaching passband loss less than -1 dB. This gives an idea, that the measurement results can be improved better with momentum simulator optimization techniques. Moreover sharper stopband can be achieved by increasing number of unit cells [16], which is our future research task along with size reduction in the state of art MTM structures.

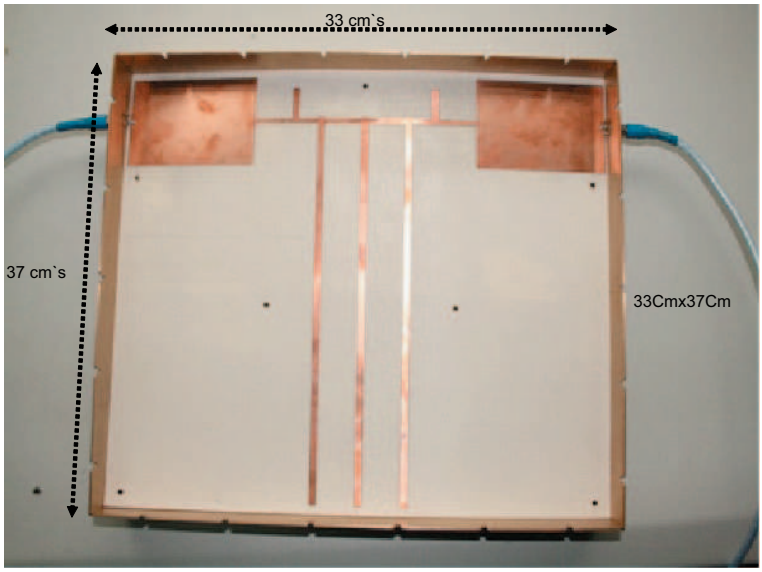

Figure 5.32: MTM TX-BPF - Measurement Board

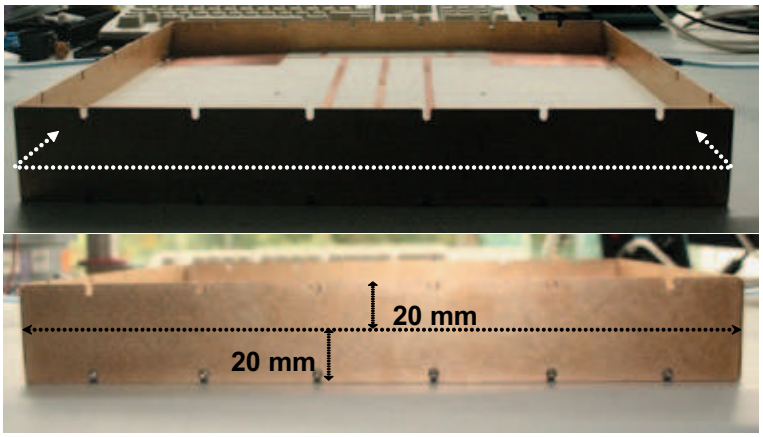

Figure 5.33: Board Cross-Section

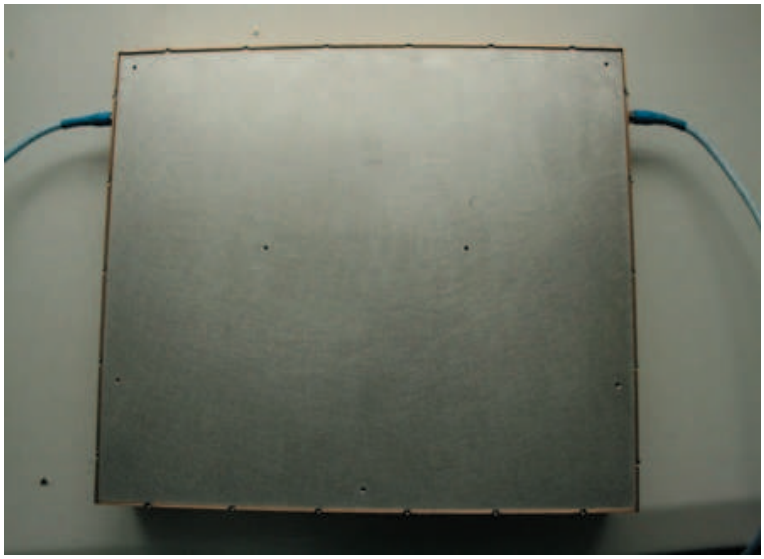

Figure 5.34: Conductive Closed View

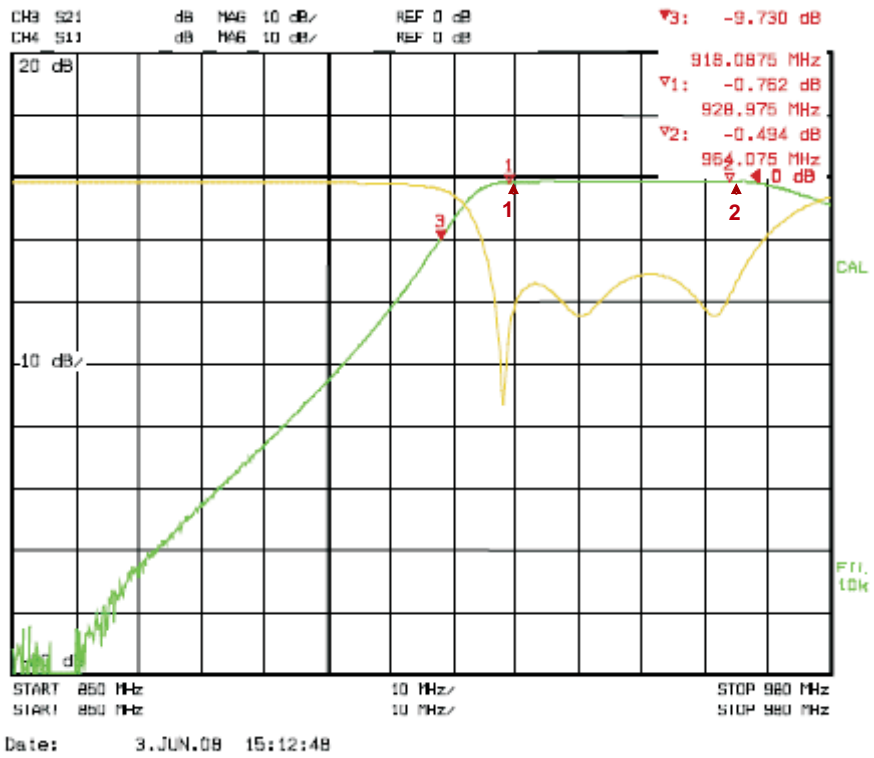

Figure 5.35: MTM TX-BPF- Measurement Board Results

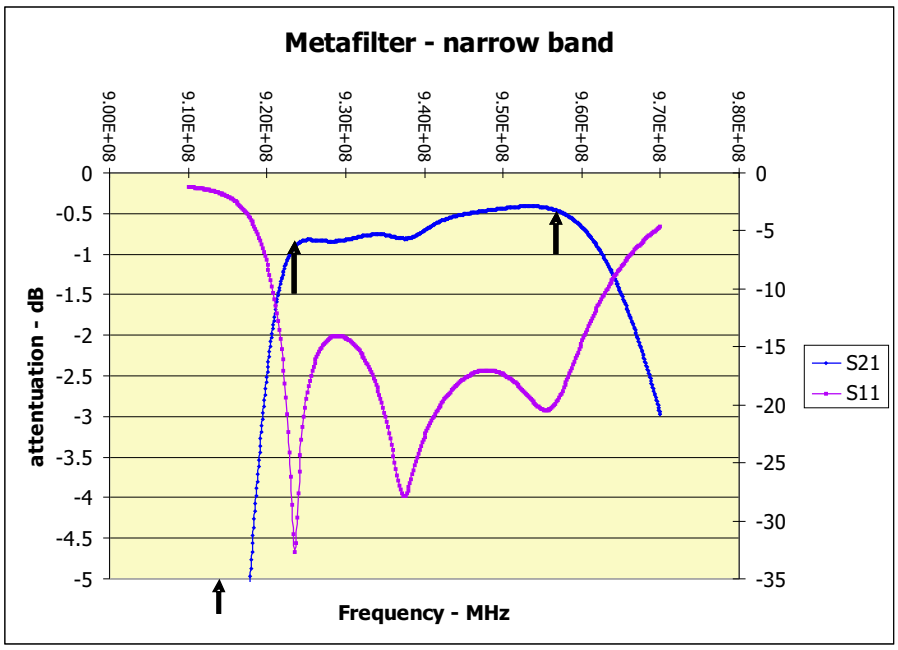

Figure 5.36: MTM TX-BPF- Measurement Board Results -(925MHz-960MHz)

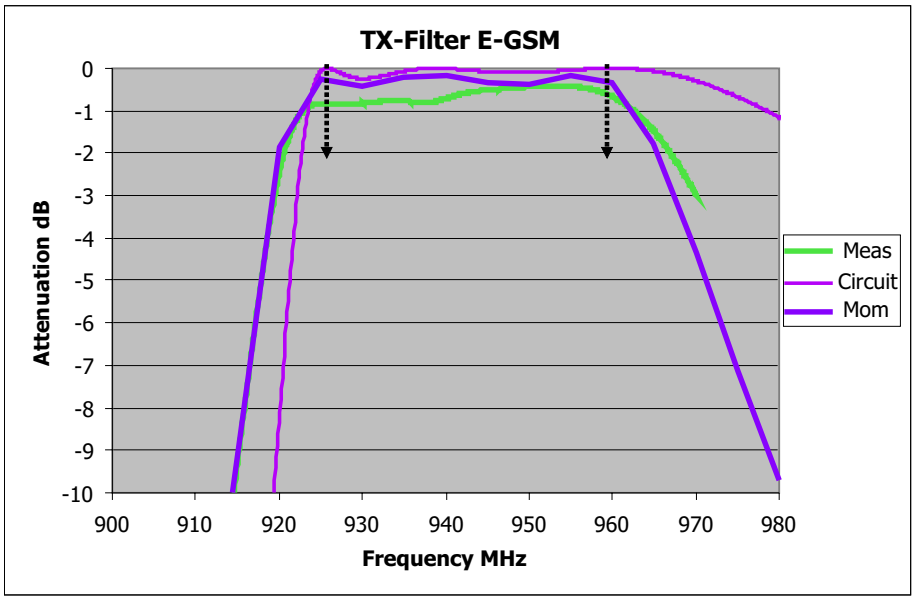

Figure 5.37: Result Comparison

Freq	CS Results	MoM Results	Measured Results
925 MHz Passband dB[S21]	-0.07 dB	-0.25 dB	-0.7 dB
960 MHz Passband dB[S21]	-0.03 dB	-0.26 dB	-0.4 dB
915 MHz Stopband dB[S21]	-23 dB	-10 dB	-10 dB

Table 5.1: TX-Result Comparison Table

5.7 conclusion

It was shown by designing a TX-bandpass filter, that left handed TLines with suspended substrate implementation are very beneficial in terms of providing low insertion losses, which are very much needed for E-GSM base stations. The obtained board measurement result is very good in agreement with momentum simulation results and with respect to circuit simulator results. Future work on metamaterial CRLH structures for microwave filters will continue for much better results using this new structure with open stubs and gaps taking size reduction into consideration.

Chapter 6

MTM RX bandpass filter design

6.1 Introduction

After the design of MTM TX BPF, in this chapter we have designed metamaterial RX Bandpass filter for E-GSM applications 880 MHz - 915 MHz. We have used the inverse of the TX structure for series and shunt resonances which was explained

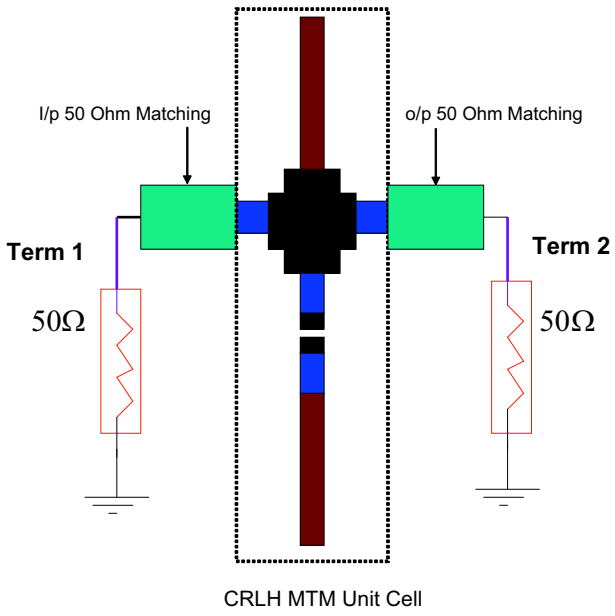

Figure 6.1: Rx BPF Unit Cell - MTM Structure

in the previous chapter. A unit cell structure of such metamaterial RX filter can be seen in fig. 6.1. Our first aim is to design the RX filter in MTM structure and secondly to keep the insertion loss less than -1 dB with sharp stop bands. We first design this filter using Lumped elements to verify simulation results, Q-Factor and Zero-order resonances which are responsible for the metamaterial behavior. Then we transform into our proposed structure using TLines in suspended substrate technology. Circuit simulator, momentum simulator and finally the measurement board results are presented.

6.2 RX - Series/Shunt Resonant Element Verification - Lumped

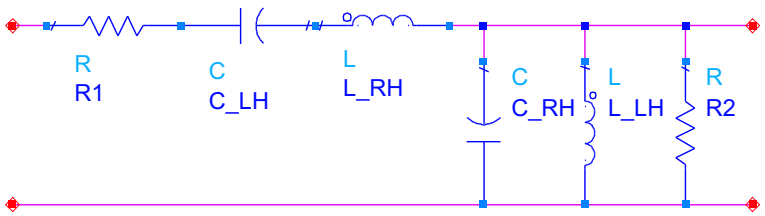

Figure 6.2: MTM Unit Cell Lumped

For the above Lumped RX MTM unit cell, the values for series and shunt resonances can be realized in simulation by tuning each element with respect to the desired frequency. Therefore the realized **series** resonant circuit values with their calculated Q-factors are:

- $C_{LH} = 2.2\,pF$
- $L_{RH} = 932\,nH$
- $R_S = 0.05\Omega$

- $Q - Factor = 1220$

and for the **shunt** resonant

- $C_{RH} = 0.034\,pF$
- $L_{LH} = 1.2\,nH$
- $R_P = 10,00000\Omega$
- $Q - Factor = 5252$ (Which is pretty high, when compared to co-axial resonators)

6.3 RX-Lumped Circuit Design and Quality Factor

6.3.1 Unit Cells-Simulation Results, Q-Factor

Fig. 6.3 shows the quality factor for the single unit cell RX filter. For a single unit cell, the quality factor at the center frequency is about 2986, which is subsequently less than TX single unit Cell Q-factor.

Also, for a single unit cell an insertion loss less than -0.03 is achieved and is shown in the fig. 6.4. Our intention is to keep insertion loss less than -1 dB with the measurement board.

6.3.2 Three Unit Cells-Simulation Results,Zero-order Resonance

As with TX filter, all the principles will be applied to this filter as well, For three unit cells (fig. 6.5) the simulation result show an insertion loss of less than -0.1 dB

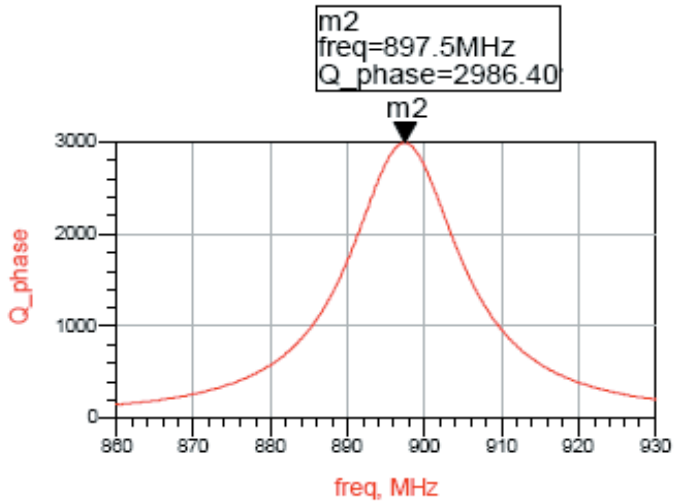

Figure 6.3: Q-Factor - unit cell

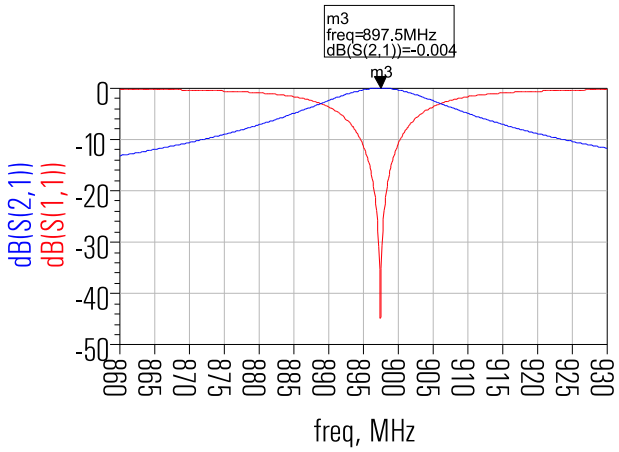

Figure 6.4: Insertion Loss dB[S21] - unit cell

.

with -17 dB stopband respectively and can be seen in the fig.6.6. The zero-order has been shown in fig. 6.7, and fig. 6.8 which is defined as the frequency which is independent of physical size i.e($\beta = 0$). This filter is also a bit unbalanced

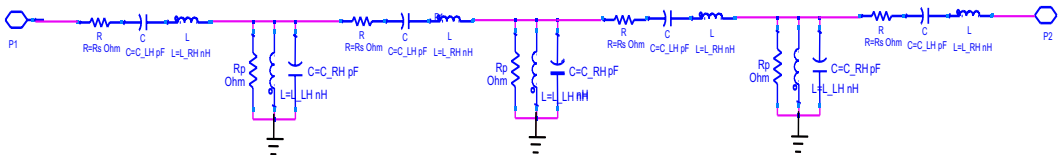

Figure 6.5: Three Unit Cell - Lumped

structure like TX filter, where the resonant frequency for both series and parallel circuits are not equal.Hence their zero-orders are clearly shown to prove that this structure is a CRLH MTM.

$$\omega_{se} = 897\,MHz \tag{6.1}$$

$$\omega_{sh} = 915\,MHz. \tag{6.2}$$

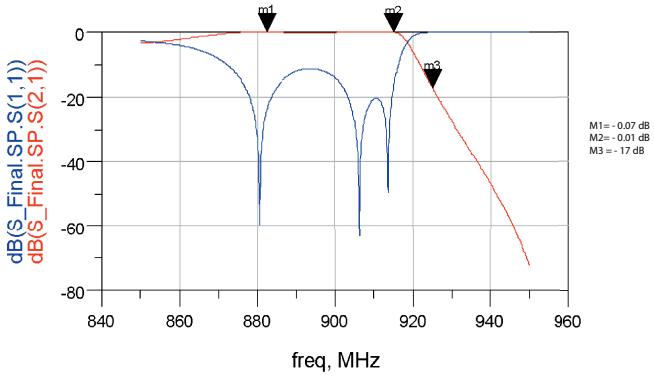

Figure 6.6: Three Unit Cell - Lumped - Simulation Results

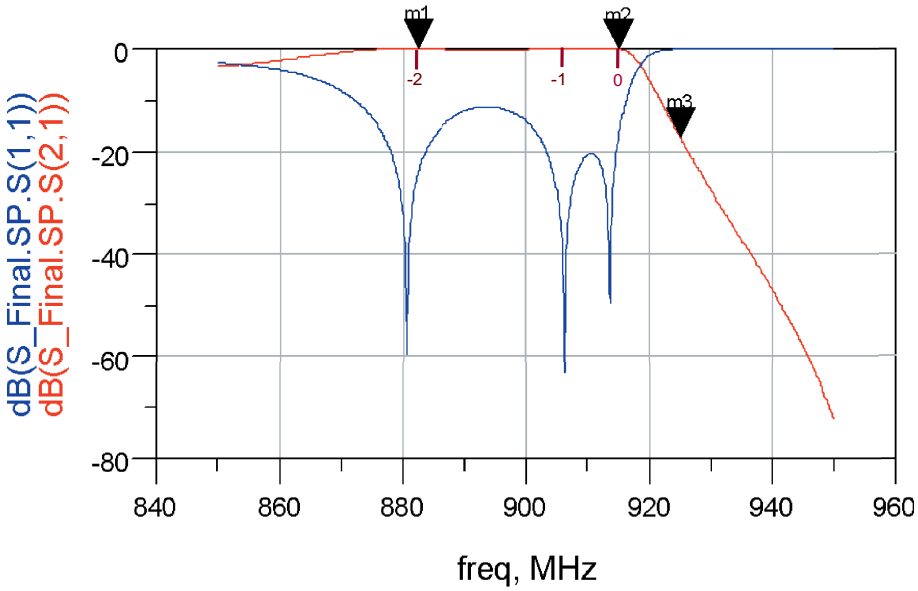

Figure 6.7: Zero-Order Resonance Location

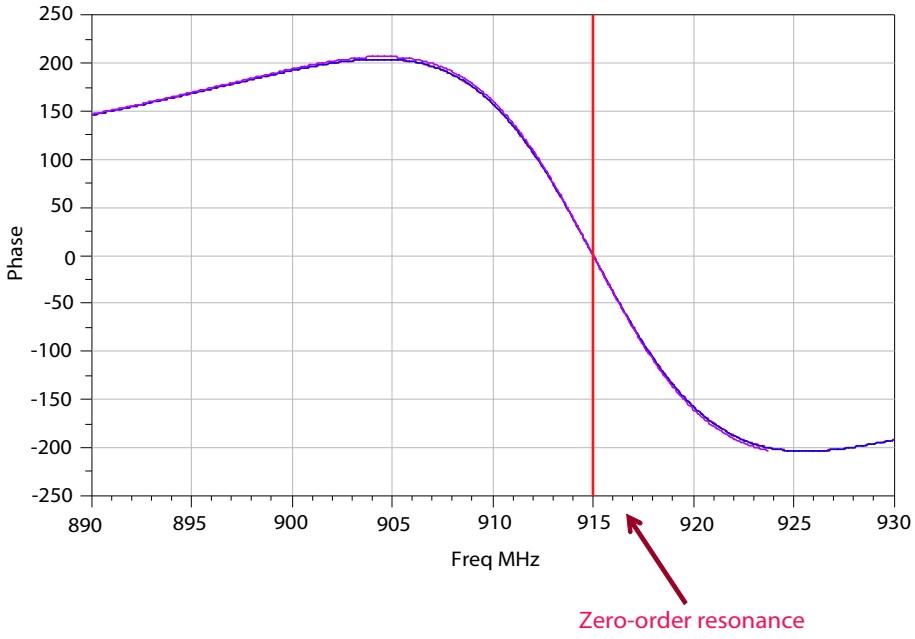

Figure 6.8: Zero-Order Resonance Proof

6.4 Lumped to Microstrip Transmission Line Conversion

We have converted the lumped MTM unit cell circuit into microstrip metamaterial TL with the new proposed structure explained in the previous chapter 4 to achieve RX form. This is enclosed in shielded suspended substrate with $\epsilon_{eff} = 1.04$ using Rogers 4003 with $Tan\delta = 0.0021$, height 0.813 mm with 20 mm displacement from top and bottom with conductor thickness of 0.1 mm. The values are calculated with respect to center frequency and later optimized in passband. The single unit cell is shown in the fig. 6.9.

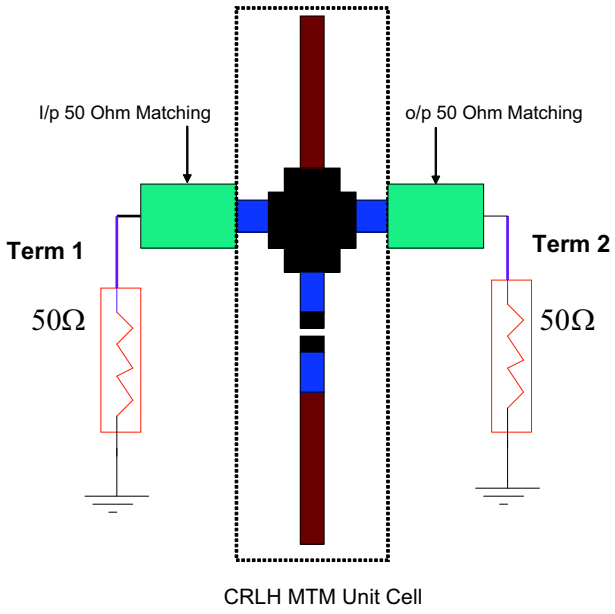

Figure 6.9: RX BPF Unit Cell - MTM Structure

The equivalent series and shunt circuits are shown in fig. 6.10 and fig. 6.11, the series circuit [12] is an approximation value for single frequency which is a center frequency but has been optimized over a 35 MHz range.

The values of *series resonance* TL obtained after calculations and optimizations are:

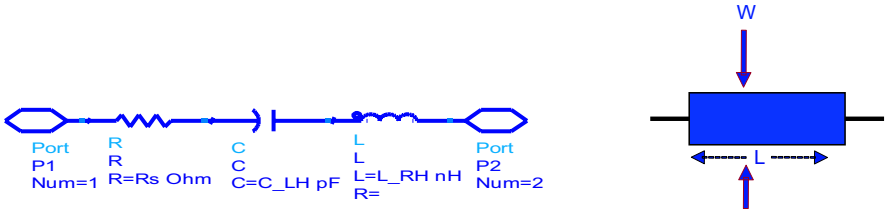

Figure 6.10: Series Resonance - Equivalent

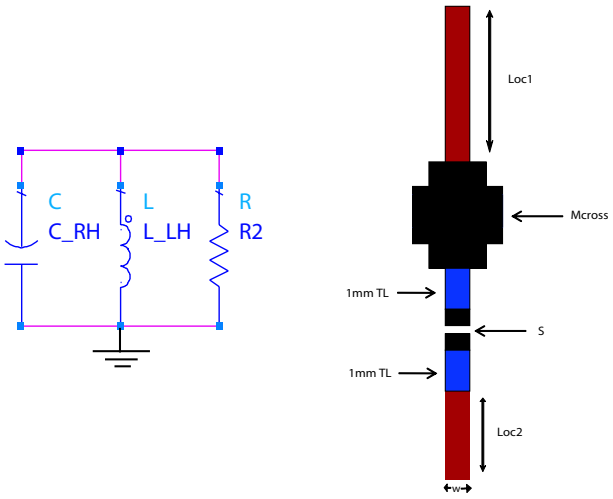

Figure 6.11: Shunt Resonance - Equivalent

- Length L = 14 mm , both sides
- Width W = 3 mm.

The values of *Shunt resonance* are:

- First Open Stub Length Loc1 = 1.2 mm
- Second Open Stub Length Loc2 = 274 mm
- Width W = 5 mm
- Gap Spacing S = 0.2 mm.

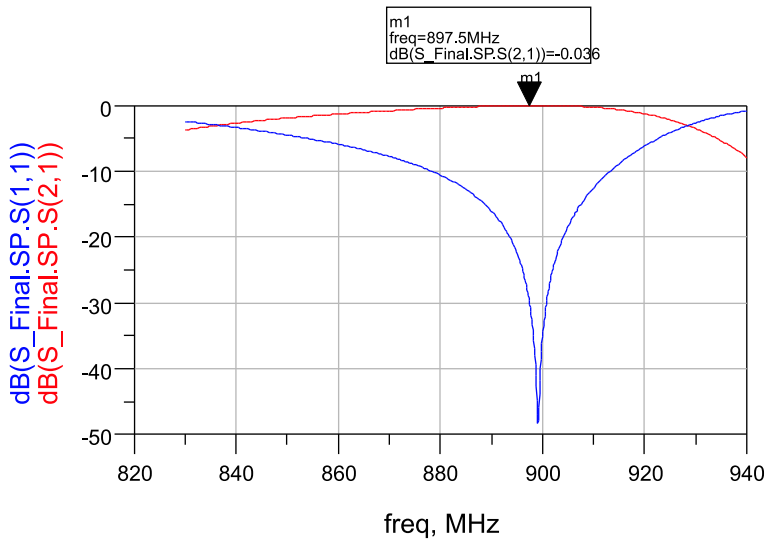

Figure 6.12: Meta RX TL - unit cell- Simulation

The converted lumped to microstrip TL MTM unit cell is simulated and the values depicted in fig. 6.12 with -0.036 dB insertion loss and the Q-factor of 2600 respectively.

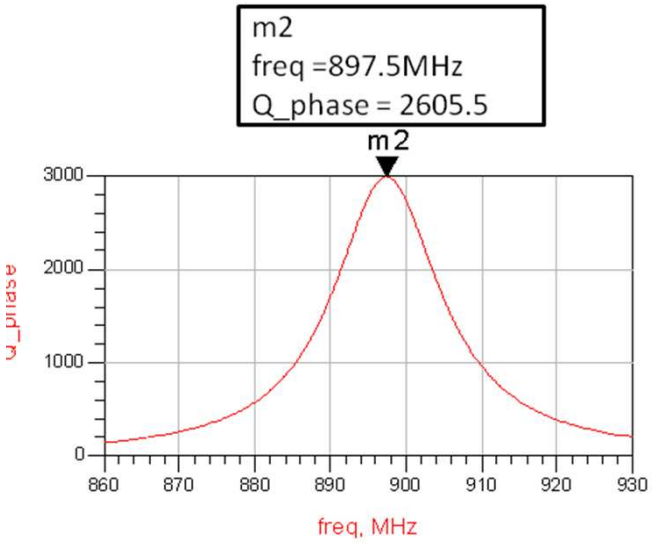

Figure 6.13: Q-Factor - unit cell

6.5 3 Unit Cells RX Filter Design - Simulation, Momentum, Measurement Results

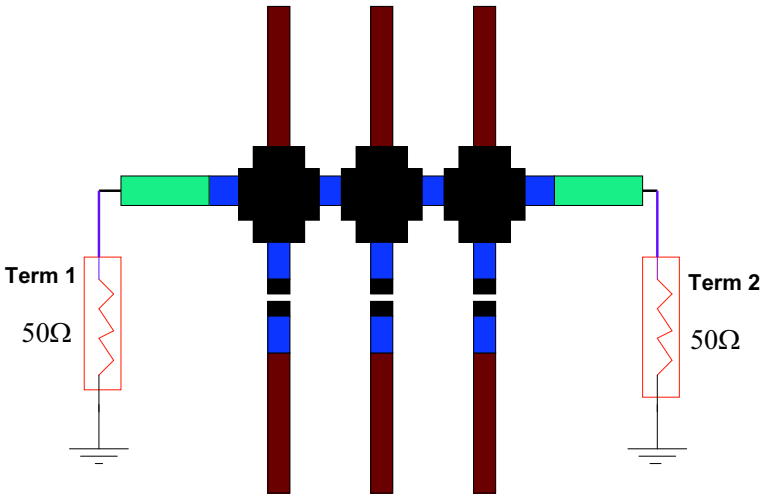

Figure 6.14: RX BPF Three Unit Cell

Fig. 6.14 represents a three unit cell CRLH MTM BPF RX filter in a shielded suspended substrate with match to the ports in 50Ω environment. The circuit design simulations are carried out in Agilent's ADS Software. Besides circuit simulator we have also simulated the layout in method of moments simulator (MoM) in the absence of any active devices, which is expected to reveal results closer to measurement. In this case, as the structure matches to 50Ω, there is no need of Impedance transformer as we have used in the case of TX-Filter.

6.5.1 Circuit Simulator Results

Three unit cell RX filter is simulated in ADS environment and like in TX filter here we also optimized the structure to the desired performance:

- Width of the slots
- Width and length of the side wings

- Number of unit cells
- Properties of the substrate (i.e. holder of the structure)
- Distance between slots (independent of the width of the side wings)
- Distance of the structure to the ground plane
- Distance of the substrate to the upper electrical shield
- Width of the strips.

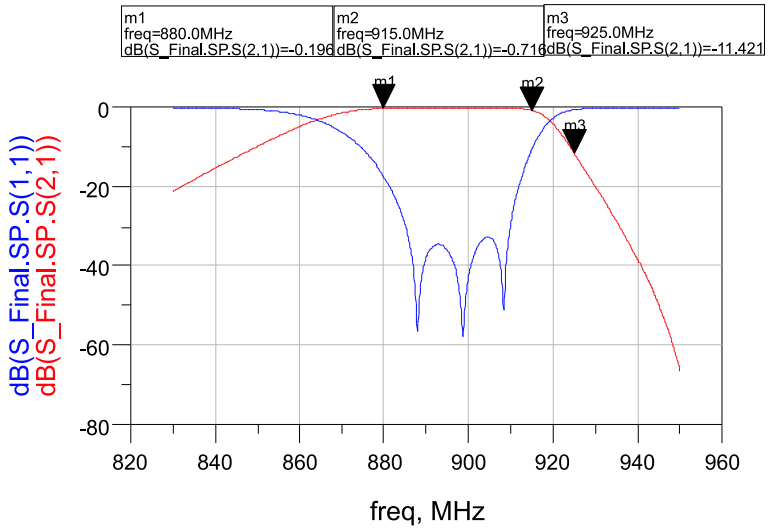

Figure 6.15: Rx BPF - CS results

The circuit simulator has an average insertion loss (ripple) less than -0.05 dB (880 MHz - 915 MHz) with a stopband of -17 dB with three poles within 35 MHz range and is depicted in fig. 6.15.

6.5.2 Momentum Simulator Results

Method of moments simulator results can be seen in fig. 6.16. On comparison with circuit simulator, the momentum results are -0.5 dB and -6 dB more in ripple and edges (stopband), which is again much better hope to go for measurement

board to prove the state of art CRLH MTM new RX structured filter and its applications in RF communication systems. The electric current distribution can be seen in fig. 6.17, which clearly shows, that these resonances has left handed behavior with a uniform homogenous current distribution. The right pole shows zeroth order resonance and thus the existance of bandgap due to unbalanced conditions.

Fig. 6.18 is a 3D figure which represents the suspended substrate housing which we have used during this design, the measurements of such housing is explained in the previous section.

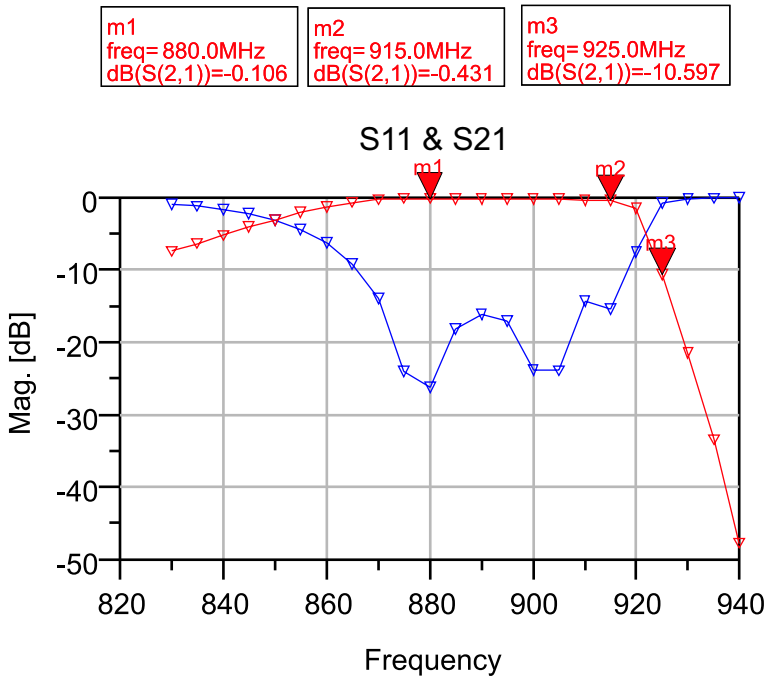

Figure 6.16: RX BPF - MoM results

6.5.3 Measurement Results

The layout board of dimension 14.8 cm x 27.8 cm in fig. 6.19 is fabricated using ROGERS RO4003 material with substrate thickness of 0.813 mm and conductor thickness of 0.1 mm respectively in a close conductive housing of shielded

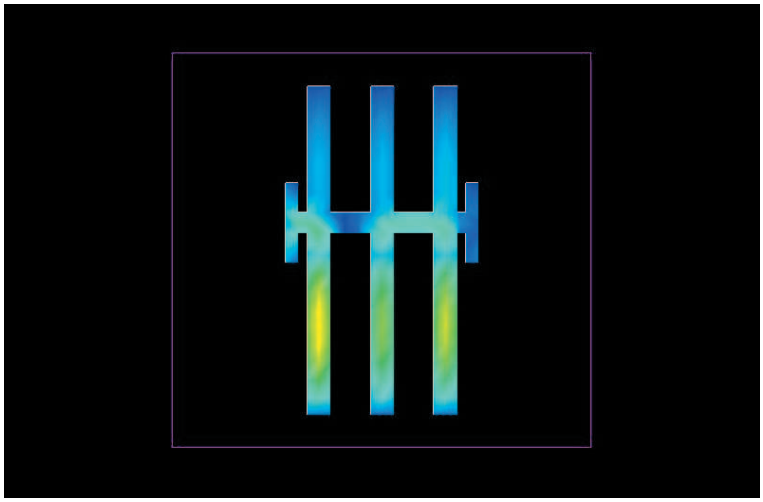

Figure 6.17: Electric current Field Distribution

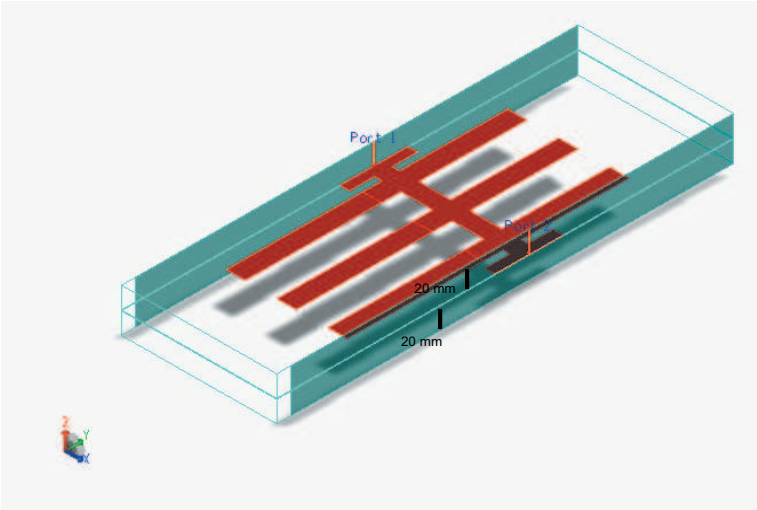

Figure 6.18: 3-Dimensional Housing Figure

suspended substrate, separated by 20 mm symmetric walls on top and bottom from the center of BPF, as depicted in 3D fig. 6.18. The cross-section can be seen in fig. 6.20, closed box view in fig. 6.21 respectively. The measurement board of MTM CRLH BPF results in fig. 6.22 and fig. 6.23 shows a stopband of nearly -10 dB at 903 MHz with an average passband less than -0.7 dB between 870 MHz -903 MHz within 35 MHz bandwidth approximately, the frequency range is dis-

placed about 10 MHz due to critical housing of the suspended substrate. The comparison between circuit simulator, momentum simulator and measurement results and are tabulated in table. 6.1. The obtained fabricated board results are almost -1dB, 0.1 dB higher in the stopband, passband in comparison with method of momentum analysis simulator than circuit simulator and hence satisfy our goal of reaching passband less than -1 dB. The ideal solution of momentum simulator optimization techniques which we adopted during TX-results also worked for RX board.

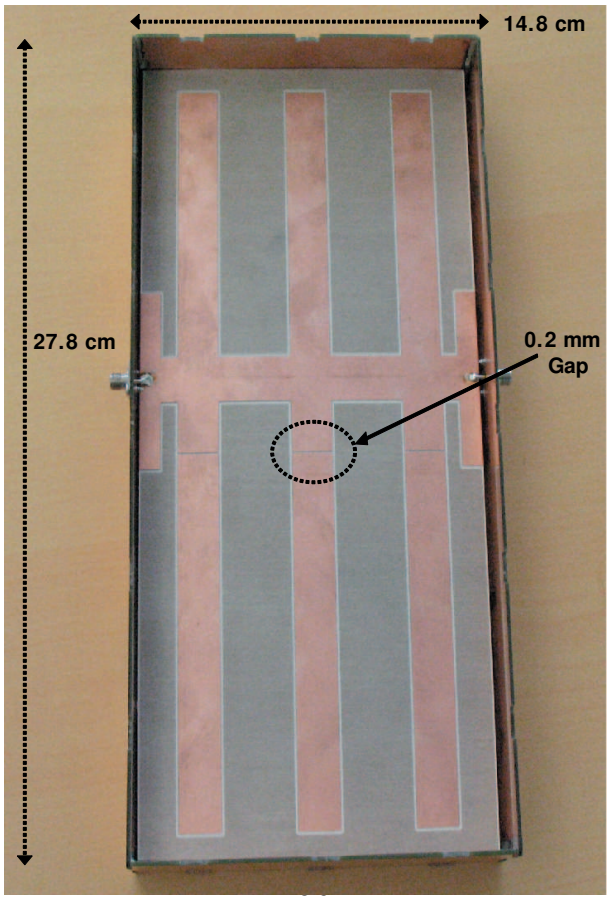

Figure 6.19: Meta RX-Filter -PCB Board

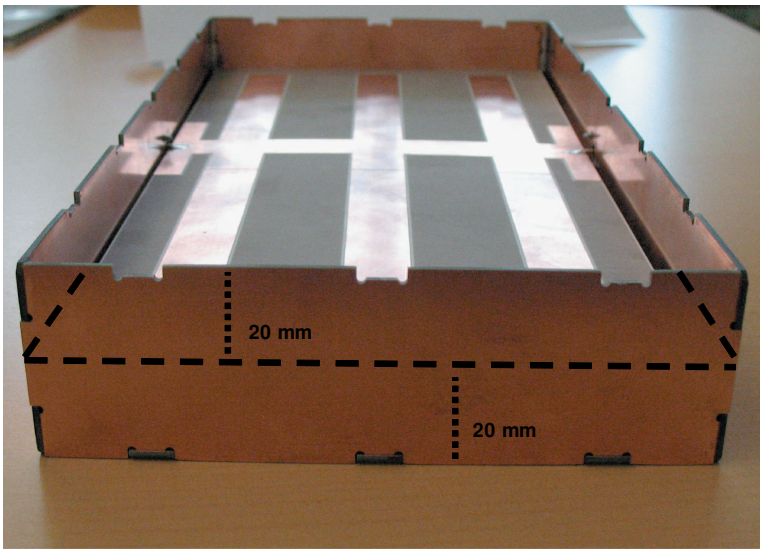

Figure 6.20: Meta RX-Filter - Side View

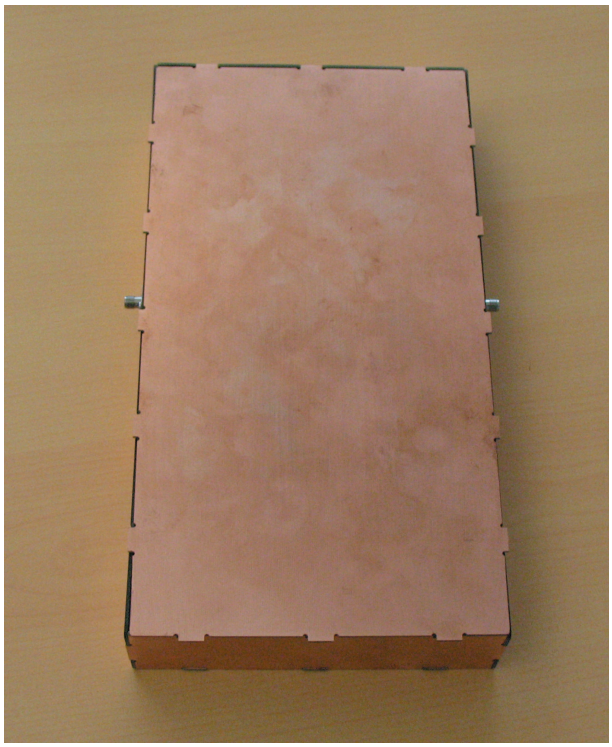

Figure 6.21: Meta RX-Filter - Closed View

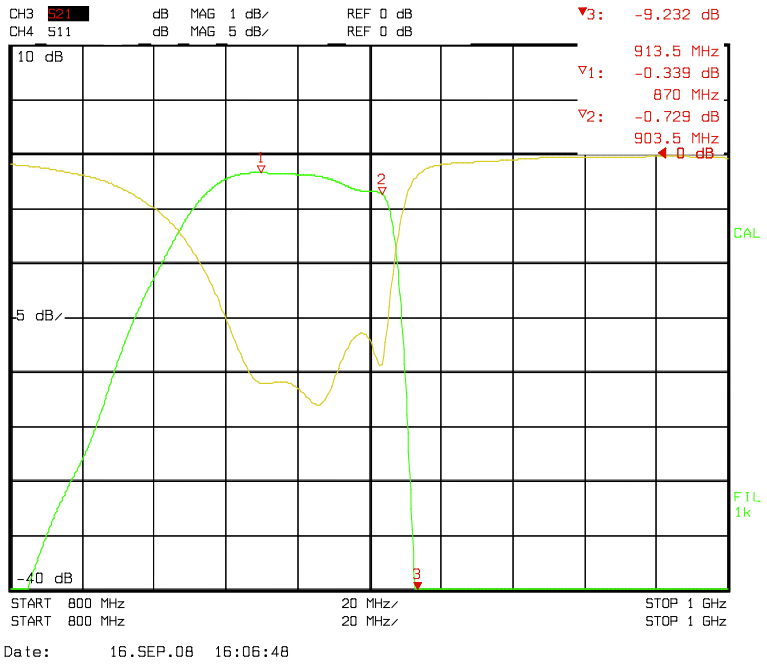

Figure 6.22: Meta RX-Filter - Measurement Results

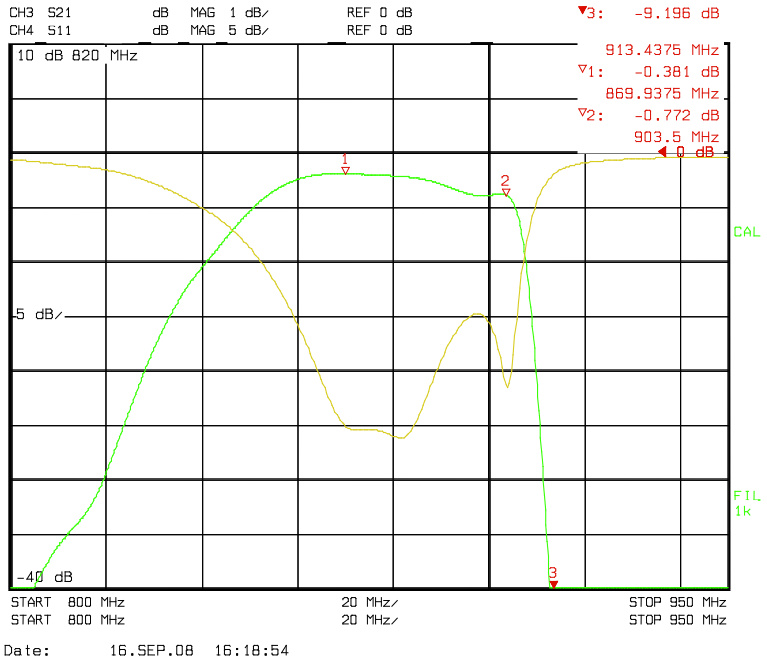

Figure 6.23: Meta RX-Filter - Measurement board Results - Clear View

Freq	CS Results	MoM Results	Measured Results
880 MHz Passband dB[S21]	-0.07 dB	-0.1 dB	-0.72 dB (870 MHz)
915 MHz Passband dB[S21]	-0.01 dB	-0.7 dB	-0.4 dB (903 MHz)
925 MHz Stopband dB[S21]	-17 dB	-11.4 dB	-9.2 dB (913 MHz)

Table 6.1: RX-Result Comparison Table

6.6 conclusion

It was shown by designing RX bandpass filter that, there is a possibility for the RX-filter behavior with left handed TLines. Suspended substrate implementation is very beneficial in terms of providing low insertion losses which is very much needed for E-GSM base stations. The obtained board measurement result is very good in agreement with momentum simulation results with respect to circuit simulator results.

Chapter 7

Conclusions and Discussion

7.1 conclusions

This thesis work has been carried out for the laid out objectives. The results and the comparisons have been discussed in the previous chapter. Now in this chapter, conclusions and the future opportunities by this work done are discussed.

The main objectives of the thesis are:

1. To Design duplex filters for the application of E-GSM 900 base stations using CRLH Metamaterial Structures.
2. To propose a different MTM filter structure with gaps and open stubs in comparison with the previously published MTM filter structures.
3. To impose microstrip suspended substrate technology for the design.
4. To prove the state of art Metamaterial structure and its applications at RF/Microwave frequencies.

As it was discussed earlier that LH transmission lines do not exist in real nature, we have used the quasi-lumped transmission lines (Artificial Structures) with elementary cells consisting of series capacitors and shunt inductors. We can design

filters by using numerous methods, but in this thesis work we have worked to prove that, there is a possibility to design RF filters using metamaterial structures.

7.1.1 Things learned and New

Things learned and new during this thesis work are:

1. Possibility to design TX/RX narrow bandpass filters with Left-Handed metamaterials in a planar microstrip technology.
2. Combination of microstrip gap capacitors and open stub inductors leads to CRLH MTM structures.
3. Proved the state of art balanced-structure metamaterials and its applications at RF/Microwave frequencies. Which clarifies the question that, whether balanced or unbalanced structures should be used.
4. Shortstubs ($\lambda/4$ Tlines) can be replaced with long openstubs ($\lambda/2$ Tlines), which has a virtually large-valued ground capacitor. Hence provides similar results.
5. Suspended substrate technology is an added advantage for achieving good results like reduced losses and enhances Q-factor.
6. Using planar microstrip technology for filter designs, we have attained Q-factors of nearly 5000. which is very high.
7. High power handling in comparison with coaxial filters.

7.2 Advantages and Drawbacks

We have met the goals successfully. But the accuracy has been compromised at some places as a matter of fact. This compromisation is unavoidable.

Advantages: During TX-BPF design. We have proved the new LH TL filter structure with microstrip gap capacitors and $\lambda/2$ TLines. For the three unit cells, we have successfully met our goal i.e insertion loss is less than -1 dB. The momentum simulator results are very near to fabricated board results (i.e. 1% - 2% deviation). Also suspended substrate technology implementation played an important role in attaining good results. Finally, we have shown the advantages of balanced structures in left-handed materials for TX BPF design.

Drawbacks: TX-BPF design. For three unit cells, the board size achieved is 33 cm x 37 cm, it means for more than 3 unit cells the size matters. Housing is critical. Stop band should still be sharper than what was achieved.

Advantages: During RX-BPF design. The proposed left-handed TL structure worked in showing RX filter characteristics. The measured results obtained with three unit cells are very close to simulation results and hence in meeting goal. In this case as well, suspended substrate implementation has given good results. Therefore, we have shown the advantages of balanced structures in Left-Handed materials for RX BPF design.

Drawbacks: RX-BPF design. There is a displacement of 10 MHz in the measurement results in comparison with the simulation results. Still the board size has to be reduced in order to fit on increase in number of unit cells. Housing is critical and hence the stop band needs to be sharper than achieved. Finally a duplexer cannot be made with two different sized bandpass filters, where the sizes need to fit.

7.3 future work

The left-handed bandpass filter design work can be continued by increasing the number of unit cells, decreasing the board size, goal with same sizes for TX and RX bandpass filters (for a perfect duplexer). Also the future work can be continued showing various RF applications using balanced structure CRLH metamaterials and hence to prove the state of art.

Bibliography

[1]. V.G.Veselago,*"The electrodynamics of substances with simultaneously negative values of ϵ and μ"* , Sov. Phys.-Usp., vol. 10, pp. 509-514, Jan-Feb. 1968.

[2]. J.B.Pendry, A.J.Holden, W.J.Stewart and I.Youngs *"Extremely low frequency Plasmons in metallic structures"* Phys. Rev. Lett., vol. 76, no. 25, pp. 4773-4776, June.1996

[3]. J.B.Pendry,A.J.Holden,D.J.Robbins,W.J.Stewart, *"Magnetism from conductors and enhanced nonlinear phenomena*" ,IEEE Trans.Microw. Theory Tech., vol.47, no.11, pp.2075-2084, Nov.1999.

[4]. D.R.Smith, W.J.Padilla, D.C.Vier, S.C.Nemat-Nasser, and S.Schultz, *"Composite medium with simultaneously negative permeability and permittivity"*, Phys. Rev. Lett., vol.84, no.18, pp.4184-4187, May 2000.

[5]. C.Caloz, H.Okabe, T.Iwai, and T.Itoh, *"Transmission line approach of left-handed (LH) materials"*, in USNC/URSI Nat.Radio Science Meeting, vol.1, Jun.2002, p.39.

[6]. G.V.Eleftheriades and k.G.Balmain *"Negative refraction Metamaterials, Fundamental Principles and Applications"*, in IEEE press, Wiley, Hoboken NJ 2005.

[7]. A.K.Iyer and G.V.Eleftheriades, *"Negative refractive index Metamaterial*

supporting 2-D waves", in IEEE MTT-S Int.Microwave Symp.Dig.,vol.2, Jun.2002, pp.1067 1070.

[8]. D.R.Smith and N.Kroll, *"Negative refractive index in left-handed materials"*, Phys.Rev.Lett.,vol.85, no.14, pp.2933-2936, Oct.2000.

[9]. A.Lai, T.Itoh, *"Composite Right/Left-Handed Transmission Line Metamaterials"*, IEEE Microwave Magazine, pp.34-50, Sept.2004.

[10]. I-H.Lin, M.DeVincentis, C.Caloz, T.Itoh, *"Arbitrary Dual-Band Components Using Composite Right/Left-Handed Transmission Lines"*, IEEE Transactions on Microwave Theory and Technique, Vol.52, No.4, April 2004.

[11]. C.Caloz, A.Sanada, T.Itoh, *"A novel Composite Right-/Left-Handed Coupled-Line Directional Coupler With Arbitrary Coupling Level and Broad Bandwidth"*, IEEE Transactions on Microwave Theory and Techniques, Vol.52, No.3, March 2004.

[12]. H.Okabe, C.Caloz, T.Itoh, *"A Compact Enhanced-Bandwidth Hybrid Ring Using an Artificial Lumped-Element Left-Handed Transmission-Line Section"*, IEEE Transactions on Microwave Theory and Technique, Vol.52, No.3, March 2004.

[13]. W.Menzel, A.Balalem *"Quasi-Lumped Suspended Stripline Filters and Diplexers"*, IEEE Trans. on MTT, vol.MTT-53, Oct.2005, pp.3230 3237.

[14]. J.E.Dean *"Suspended substrate stripline filters for ESM applications"*, IEE Proc.,Vol.132, Pt.F, July 1985, pp.257 - 266.

[15]. G.Fischer, *"Architectural benefits of wide band gap RF power transistors for frequency agile base station systems"*, IEEE MTT, 6th annual Wireless and Microwave Technology Conference, Clearwater, Florida, April.2004.

[16]. C.Caloz, T.Itoh *"Electromagnetic Metamaterials"*, IEEE press, Wiley, Hoboken NJ, 2006.

[17]. Ricardo Marques, Ferran Martin, Mario Sorolla *"Metamaterials with Negative Parameters"*, IEEE press, Wiley, Hoboken NJ, 2007.

[18]. Gunther Dehm-Andone, Grzegorz Adamiuk, Georg Fischer *"Using Metamaterial structures with frequency agile base stations"*, IEEE GEMIC 2006

[19]. Lei Zhu, Huamin Shi, Menzel.W, *"Coupling behaviors of quarter-wavelength impedance transformers for wideband CPW bandpass filter"*, Microwave and Wireless Components Letters, IEEE Volume.15, Issue.1, Jan.2005 Page(s)1315.

[20]. Bekheit, Amari, Menzel.W, *" Modelling and Optimization of Compact Microwave Bandpass Filters. Microwave Theory and Techniques"*, IEEE Transactions on Volume 56, Issue 2, Feb.2008 Page(s).420430

[21]. Anu Lehtovuori, Luis Costa, *" Model for Shielded Suspended Substrate Microstrip Line"*, Circuit Theory Laboratory Report Series, Helsinki University of Technology 1998.

[22]. Wen Zhang*"Optical activity and applications of planar chiral metamaterials"*, PhD thesis at University of Southampton, 2006.

[23]. Gunther Dehm, Grzegorz Adamiuk, Georg Fischer, Schenkel Horst *"Metamaterial Filter for use in a base station of a wireless communication systems"*, US patent WO2007/100324

[24]. Islam, R.; Eleftheriades, G.V *"Compact Negative-Refractive-Index Transmission-Line (NRI-TL) coupler, filter and diplexer "*, Antennas and Propagation International Symposium, 2007 IEEE 9-15 June 2007 Page(s):4957 - 4960

[25]. R. A. Shelby, D. R. Smith, and S. Schultz *"Experimental verification of a negative index of refraction"*, Science, 77:292, 2001.

[26]. J. Pacheco, T. M. Grzegorczyk, B.-I. Wu, Y. Zhang, and J. A. Kong. *"Power propagation in homogeneous isotropic frequency dispersive left-handed media"*, Phys. Rev.Lett., 89:257401, 2002.

[27]. J. B. Pendry. *"Negative refraction makes a perfect lens"*. Phys. Rev. Lett., 85:3966,2000.

[28]. R. Ziolkowski and E. Heyman *"Wave propagation in media having negative permittivity and permeability"*. Phys. Rev. E, 64:056625, 2001.

[29]. C. G Parazzoli, R. B. Greegor, K. Li, B. E. C. Koltenbah, and M. Tanielian. *"Experimental verification and simulation of negative index of refraction using Snell's law "*.Phys. Rev. Lett., 90:107401, 2003.

[30]. J. A. Kong, B.I.Wu, and Y. Zhang. *"A unique lateral displacement of a Gaussian beam transmitted through a slab with negative permittivity and permeability "*. Microwave Opt. Technol. Lett., 33(2):136139, April 2002.

[31]. J. Gerardin and A. Lakhtakia. *"Negative index of refraction and distributed Bragg reflectors"*. Microwave Opt. Technol. Lett., 34(6):409411, 2002.

[32]. A. Grbic and G. V. Eleftheriades. *"Experimental verification of backward-wave radiation from a negative refractive index metamaterial"*. J. Appl. Phys., 92(10):59305935,2002.

[33]. J. Lu, T. M. Grzegorczyk, Y. Zhang, J. Pacheco, B.-I. Wu, and J. A. Kong. *"Cerenkov radiation in materials with negative permittivity and permeability"*. Optics Express, 11(7):723734, 2003.

[34]. Hoang Van Nguyen, Christophe Caloz, *"Broadband Highly Selective Band-pass Filter based on a Tapered Coupled-Resonator CRLH Structure"*IEEE Transactions on Microwave Theory and Techniques, Vol.52, No.3, March 2004.

[35]. R. A. Shelby, D. R. Smith, S. C. Nemat-Nasser, and S. Schultz. *"Microwave transmission through a two-dimensional, isotropic, left-handed metamaterial "*. Appl. Phys.Lett., 78(4):489, 2001.

[36]. C. Caloz, A. Sanada, and T. Itoh. *"Microwave applications of transmission-line based negative refractive index structures "*. Proc. of Asia-Pacific Microwave Conf., Seoul, Korea, vol. 3, pp. 17081713, Nov. 2003.

[37]. A.Grbic and G. V. Eleftheriades.*"Growing evanescent waves in negativere-fractive index transmission line media "*. Appl. Phys. Lett.82(12):181517, 2003.

[38]. C. Caloz and T. Itoh.*"Novel microwave devices and structures based on the transmission line approach of meta-materials"*. IEEE-MTT Intl Symp., vol. 1, pp. 195198, Philadelphia, PA, June 2003.

[39]. M. D. Pozar *"Microwave Engineering"*. Third Edition, John Wiley & Sons, 2004.

[40]. A. Sanada, C. Caloz, and T. Itoh.*"Characteristics of the composite right/left-handed transmission lines,"*. IEEE Microwave Wireless Compon. Lett., vol. 14, no. 2, pp. 6870, February 2004.

[41]. G. L. Matthaei, L. Young, and E. M. T. Jones.*"Microwave Filters, Impedance-Matching Networks, and Coupling Structures"*. Artech House, Dedham, 1964.

[42]. C. Caloz and T. Itoh. *"Transmission line approach of left-handed (LH) structures and microstrip realization of a low-loss broadband LH filter"* A.IEEE Trans. Antennas Propagat., vol. 52, no. 5, May 2004

[43]. Lai, C. Caloz and T. Itoh. *"Transmission line based metamaterials and their microwave applications"* Microwave Mag., vol. 5, no. 3,pp. 3450, Sept. 2004.

[44]. Benedek, P. Silvester, P., *"Equivalent Capacitances for Microstrip Gaps and Steps Microwave Theory and Techniques"*, IEEE Transactions on Volume 20, Issue 11, Nov 1972 Page(s):729 733.

[45]. Reinhold Ludwig, Pavel Bretchko, Gene Bogdanov, *"RF Circuit Design: Theory and Applications"* Published by Pearson Prentice Hall, 2008.

[46]. Qizheng Gu *"RF system design of transceivers for wireless communications"* Published by Springer, 2005.

[47]. Wolfgang Sieber, Franz Rottmoser *"High frequency filter in a coaxial construction"* Patent No:20080024248, US patent 2008.

[48]. V. K. Varadan, Kalarickaparambil Joseph Vinoy, K. A. Jose *"RF MEMS and Their Applications"* John Wiley and Sons October 2002.

[49]. Shu, Yong-hui, Xiao-xia Qi. and Yun-ji Wang, *"Analysis Equation for Shielded Suspended Substrate Microstrip Line and Broadside-Coupled Stripline"*, IEEE MTT-S International Microwave Symposium Digest,

[50]. Changjun Lui, Wolfgang Menzel *"on the relation between a negative refractive index transmission line and chebyshev filter"*, IEEE International 37th European Microwave Conference, Munich, Germany Oct-2007.

Publications

[1]. Shaik Geelani, Georg Fischer, Jürgen Detlefsen, Horst Schenkel, *"Metamaterial Based Filters in Suspended Substrate*", International Metamaterial Conference Pamplona Spain, September 2008.

[2]. Shaik Geelani, Georg Fischer, Jürgen Detlefsen, Horst Schenkel *"Composite Right/Left Handed Metamaterial Structures for RF Narrow Bandpass Filter Design"*, IEEE 2008 International Workshop on Metamaterials, Nanjing China, November 2008.

[3]. Shaik Geelani, Georg Fischer, Jürgen Detlefsen, Horst Schenkel, *"Metamaterial Based RF Narrow Bandpass Filter Design in Microstrip Suspended Substrate*",EEE, RFM08 Malaysia, December 2008.

[4]. Shaik Geelani, Georg Fischer, Jürgen Detlefsen, *"Metamaterial RF Tx-Bandpass Filter Design for EGSM-900 Base stations"*, IEEE National workshop on Metamaterials and special materilas for electromagnetic applications and TLC - MMSM08, Naples. Italy Dec 2008.

[5]. Shaik Geelani, Horst Schenkel, *"Metafilter with asymmetric structure*" , Alcatel-Lucent, Bell-Labs, Germany - German patent DE SA00474EP, June 2008.

Composite Right/Left Handed Metamaterial Structures for RF Narrow Bandpass Filter Design

Geelani Shaik[1,3], Horst Schenkel[1]

Jürgen Detlefsen[3], Georg Fischer[2]

Alcatel-Lucent Bell Lab Technologies AG, Thurn and Taxis Strasse 10, 90411 Nuremberg, Germany[1]
gtumcher@alcatel-lucent.com, hschenkel@alcatel-lucent.com

Friedrich-Alexander-Universität Erlangen-Nürnberg, Lehrstuhl für Technische Elektronik Cauerstraße 9, 91058 Erlangen Germany[2]

Technical University of Munich, Lehrstuhl für Hochfrequenztechnik Fachgebiet HFS, 21 D-80333 Arcisstraße, München Germany3

***Abstract*— In this paper we have proposed Metamaterial based Composite Right-Left Handed transmission line new structure with microstrip gap capacitors and open stub inductors. By using this structure and also to check the possibility of performance, we have designed narrow bandwidth RF bandpass filter in shielded suspended substrate for EGSM base station applications (Tx band, 925MHz - 960MHz). To validate the proposed structured design and analysis, the layout board of bandpass filter was fabricated and measured. It is shown that the simulated and measured performances are good in agreement. For three unit cells within a narrow bandwidth of 35 MHz, the layout board of bandpass filter has achieved an insertion loss of nearly -0.7 dB and a stopband of -10 dB approximately.**

Index Terms— **Bandpass filter, Composite left/right handed metamaterials (CRLH), suspended substrate, microstrip gaps, open stubs.**

1. INTRODUCTION

C. Caloz and T. Itoh [1] in their publications presented periodical Composite Right/Left Handed [CRLH] Metamaterial [MTM] Transmission Line [TL] bandpass filter design with interdigital capacitors and short stub inductors for broad bandwidths, in their periodical structure they have got the same amount of left handed [LH]and right handed [RH] resonance frequencies dependently on the amount of cells. Islam/Eleftheriades [10] in their publications presented new metamaterial TL structures with interdigital capacitors and open stub inductors for narrow bandwidth bandpass filters. By taking their ideas in to consideration in this paper, we have proposed narrow bandwidth filter design using microstrip gap capacitors and open stubs inductors [10] which equates with CRLH MTM TL. Moreover, considering the flexibility of base stations where there is always need for high selective and low ripple bandpass filters. By designing a bandpass filter with this structure, it is shown that metamaterial structures can be of great advantage for building blocks in RF systems.

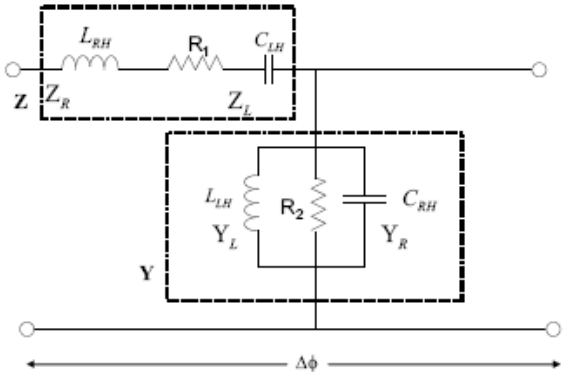

Fig. 1: MTM CRLH TL

LC equivalent CRLH TL in Fig. 1 can be implemented for bandpass filter which is fully characterized in terms of its propagation constant "β" and characteristic impedance "Z_c" in its passband. Where [2],

$$\beta = \sqrt{\frac{C_{RH}}{C_{LH}} + \frac{L_{RH}}{L_{LH}} + \frac{R}{R_2} - \omega^2 * L_{RH} * C_{RH} - \frac{1}{\omega^2 * L_{LH} * C_{LH}} + j * \left\{ \omega * \left[R_1 * C_{RH} + \frac{L_{RH}}{R_2} - \frac{R_1}{\omega^2 * L_{LH}} - \frac{1}{\omega^2 * R_1 * C_{LH}} \right] \right\}} \quad (1)$$

and

$$Z_C = \sqrt{\frac{L_{RH} + \frac{R_1}{j * \omega} - \frac{1}{\omega^2 * C_{LH}}}{C_{RH} + \frac{1}{R_2 * j * \omega} - \frac{1}{\omega^2 * L_{LH}}}} \quad (2)$$

Also the resonance frequencies of the serial (Eq. 3) and parallel part (Eq. 4) are very important parameters of the structure which defines the edges of the band gap.

978-1-4244-2609-6/08/$25.00 ©2008 IEEE

The series resonance frequency of the unit cell is given as [3],

$$f_{se} = \frac{1}{2\pi\sqrt{L_{RH}C}_{LH}} \quad (3)$$

The shunt resonance frequency of the unit cell is

$$f_{sh} = \frac{1}{2\pi\sqrt{L_{LH}C}_{RH}} \quad (4)$$

We have proposed two goals, first to prove the new structure and second to achieve insertion loss less than 1 dB in the desired bandwidth (925 MHz-960 MHz).

2. MICROSTRIP OPEN STUB AND GAP EQUIVALENT TO CRLH STRUCTURE

Fig.2 shows a microstrip MTM CRLH TL bandpass filter structure with series microstrip gap (slots) capacitor and shunt open stub inductor. The structure is the modelling of the metamaterial which is equivalent of CRLH TL of Fig. 1.

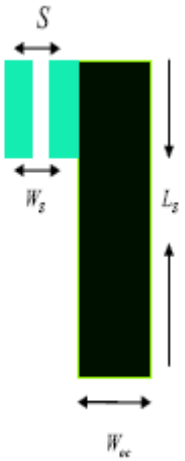

Fig. 2: MTM unit cell structure with gaps and open stubs

The metamaterial (or left handed) line is represented by periodical arrangement of serial capacity and shunt inductivity. The serial capacity is represented in the layout by slots and shunt inductivity by open stubs. The equivalent microstrip gap circuit is shown in Fig. 3 which is symmetric [4]. The position of the resonances in the frequency domain is determined by the length of the side wings which exhibits right handed inductance. By changing the length of the short wings (left and right wings between slots) we can also steer the position of the LH-resonances to each other. Moreover, the distance between the slots is mainly determined by the width of the side wings. It's not the rule, if the distance between the slots is different as the width of the side wings, and has a big influence on the behaviour. The width of the side wings has also huge influence on the bandwidth. The wider are the side wings the narrower the filter effect tends to be.

The side wing inductors are used for the presence of RH (Right Handed) inductance during low frequency approximations. In order to concentrate all the possible frequencies in a narrow frequency range, we have used the gaps (slots), where the width of the gaps steers the bandwidth of the filter. Smaller the capacity (width of the gap), the more narrow is the more narrow is the bandwidth [2].

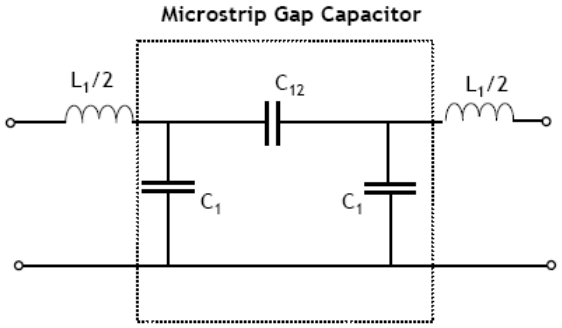

Fig. 3: Microstrip Gap Equivalent Circuit

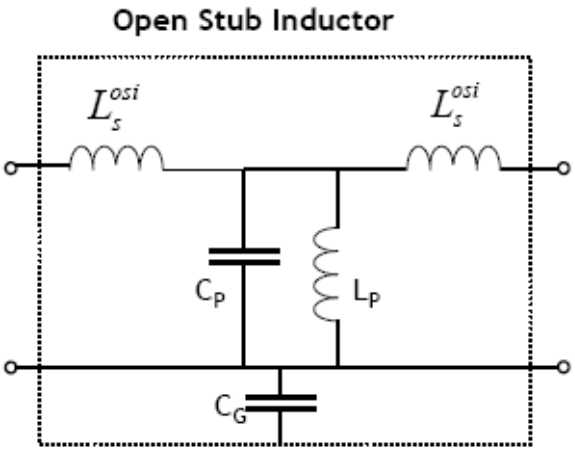

Fig. 4: Shunt open stub equivalent circuit

Fig.4 shows the equivalent of open stub inductor. To avoid via conductor in short stub inductors [1], we have implemented microstrip open stub inductors, long lengths of open stubs and homogenous current distribution could be a disadvantage. But could be of interest, if any solution arises during research to overcome the drawbacks.

For parameter extraction [From Fig:1, Fig:3 and Fig:4], neglecting extremely small inductance L_s^{oci}, we obtain four CRLH parameters.

$$L_{RH} = L_1/2 + L_1/2 = L_1 \quad (5)$$

$$C_{RH} = 2C_1 + C_P + C_G \quad (6)$$

$$L_{LH} = L_P \quad (7)$$

$$C_{LH} = C_{12} \quad (8)$$

Also, the values of gap width, spacing is optimized in Agilent's ADS software with goal constraints. The low-frequency approximation for the inductance of open stub [1] is,

$$L_L = -Z_C^{OS}\,(Cot\beta^{OS} l)/\omega \quad (9)$$

Where $\cot(\beta^{OS}.l)$ is the electrical length of stub.

The schematic of the new CRLH TL structured bandpass filter is shown in Fig. 5 which is in domain resonance frequencies and is added to impedance matching network for perfect 50Ω matching to the ports. The electrical distributions of the currents in Fig. 6 also shows the proof that, one of these resonances has common right handed behaviour and the second one left handed behaviour. Between these resonances must be the band gap. Therefore, this structure must be then the CRLH.

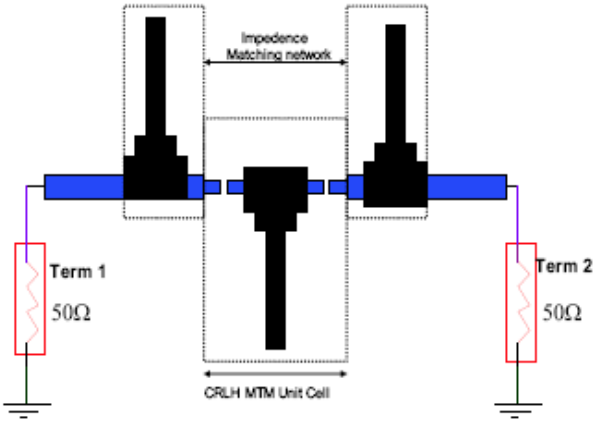

Fig. 5: Unit Cell with open stubs and gaps in Impedance matching

3. MICROSTRIP SUSPENDED SUBSTRATE IMPLEMENTATION TO CRLH BPF STRUCTURE

To achieve insertion loss less than 1 dB we have implemented suspended substrate structure. Suspended Strip line is an excellent transmission line media [5], increased cross-section together with a relative thin substrate are responsible for reduced ohmic and dielectric losses. Large portion of the fields in air results in low dispersion and hence the radiation is prevented with shielding [5], [6]. But also have the disadvantages of difficulties in miniaturization, critical housing technology and the increased complexity of utilizing hybrid elements [7]. It has been clear that, thinner and less lossy substrate decreases the insertion loss and narrows the bandwidth [15]. Rogers 4003 is a substrate material used with 0.813 mm as thickness in a symmetrical shielding between the walls [19]. Mechanical stability is a very important factor regarding suspended substrate housing, which makes to use the above quality substrate. Our MTM research has combined a vast area to accommodate suspended substrate for better results to reach our goal and hence to prove the state of art MTM structures. Pictorial representation of its block can be seen in Fig. 7

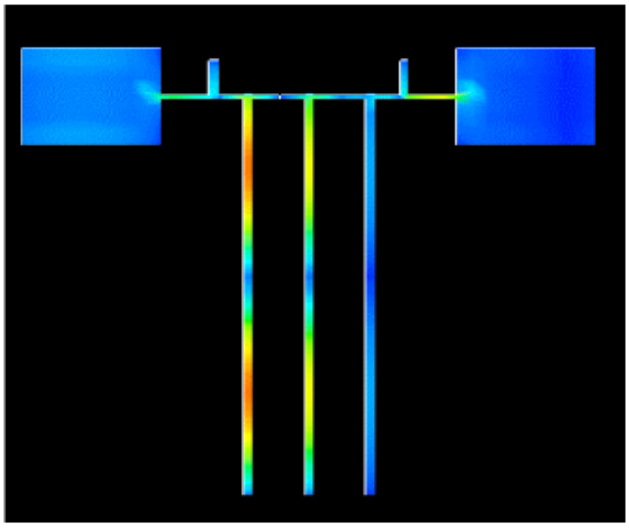

Fig. 6: Electrical Current Distribution

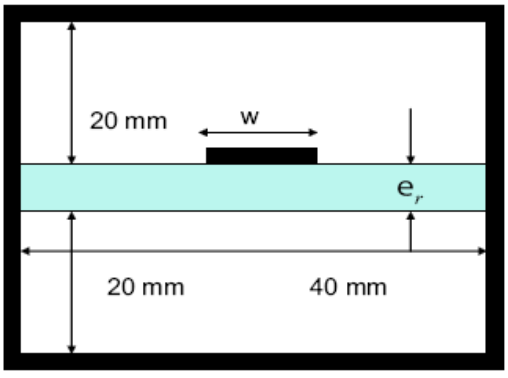

Fig. 7: Block of Microstrip Suspended Substrate

4. THREE UNIT CELL BANDPASS FILTER – SIMULATION AND MEASUREMENT RESULTS

Fig. 8 is a three unit cell CRLH MTM BPF filter in a Shielded suspended substrate with impedance transformers to match the ports in 50Ω environment. The circuit design simulations are carried out in Agilent's ADS Software. Besides circuit simulator we have also simulated the layout in method of momentum analysis simulator (MoM) in the absence of any active devices, which takes a closer look at measurement results.

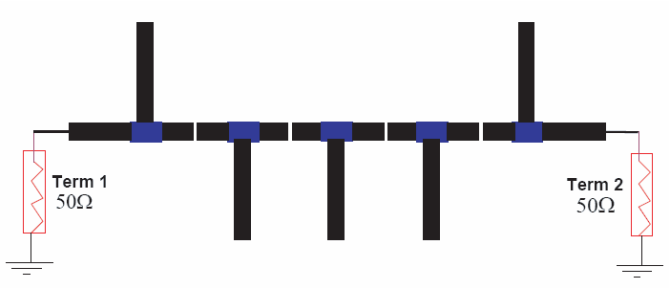

Fig. 8: Periodic Three Unit Cells BPF

We have many possibilities to optimise the structure to the desired performance:

- Width of the slots
- Width of the side wings
- Number of the cells
- Properties of the substrate (i.e. holder of the structure)
- Distance between slots (independent of the width of the side wings)
- Distance of the structure to the ground plane
- Distance of the substrate to the upper electrical shield
- Width of the stripes

The Circuit simulator has an average insertion loss (ripple) less than -0.25 dB (925MHz - 960 MHz) with a sharp stopband of -23 dB with three poles within 35 MHz range and is depicted in Fig. 9.

Method of momentum simulator analysis results can be seen in Fig.10, On comparison with circuit simulator, the momentum results are -0.3 dB and -13 dB more in ripple and edges (stopband), which is again much better hope to go for measurement board to prove the state of art CRLH MTM structure and its applications in RF communication systems.

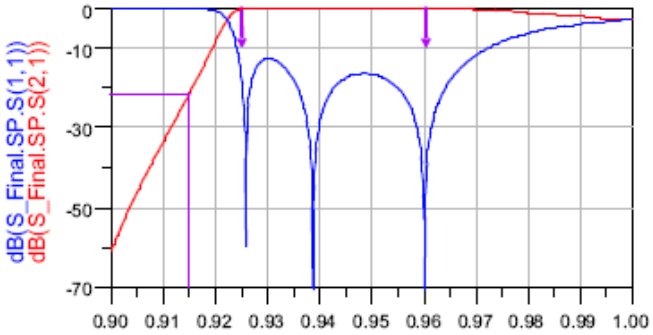

Fig. 9: Circuit Simulation Results

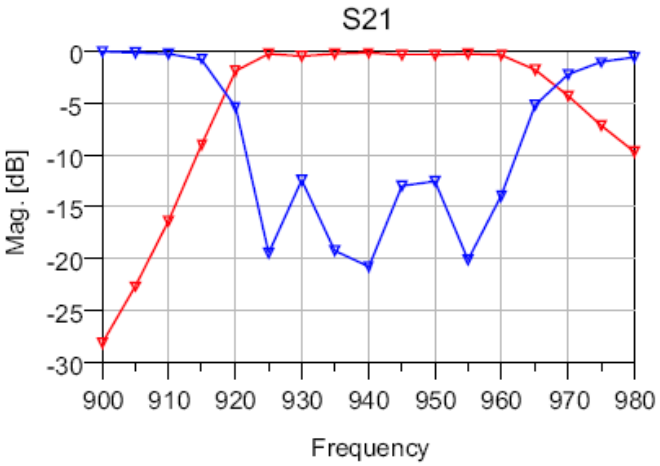

Fig. 10: Momentum Simulator Results - Three Unit Cells BPF

The layout board 33cm x 37cm in Fig.11 is fabricated using ROGER'S 4003 material with substrate thickness of 0.813mm and conductor thickness of 0.1mm respectively in a close conductive housing of shielded suspended substrate, separated by 20mm symmetric walls on top and bottom from the centre of BPF. The cross-section can be seen in Fig.12. The measurement board of MTM CRLH BPF results in Fig.13 shows a stopband of nearly -10 dB at 915 MHz with an insertion loss less than -0.7 dB between 925MHz - 960MHz within 35 MHz narrow bandwidth. Fig.14 shows the comparison between circuit simulator, momentum simulator and measurement results and is tabulated in Table.1. The obtained fabricated board results are almost equal in the stopband and 0.4 dB higher in the passband in comparison with method of momentum analysis simulator than circuit simulator and hence satisfy our goal of reaching passband less than -1 dB. This gives an idea that, the measurement results can be improved better with momentum simulator optimization techniques. Moreover sharper stopband can be achieved by increasing more number of unit cells [9] which is our future research task along with size reduction in the state of art MTM structures.

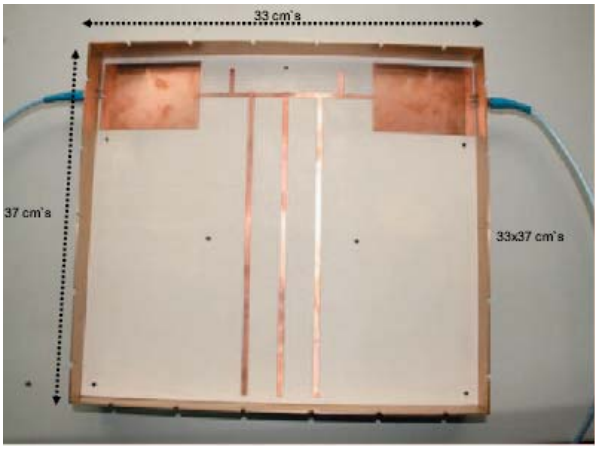

Fig. 11: Measurement Board 3 unit cell structure

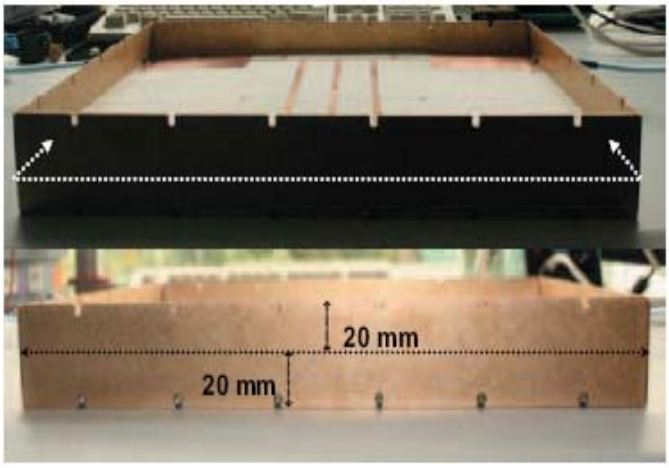

Fig. 12: Measurement Board - Cross-section

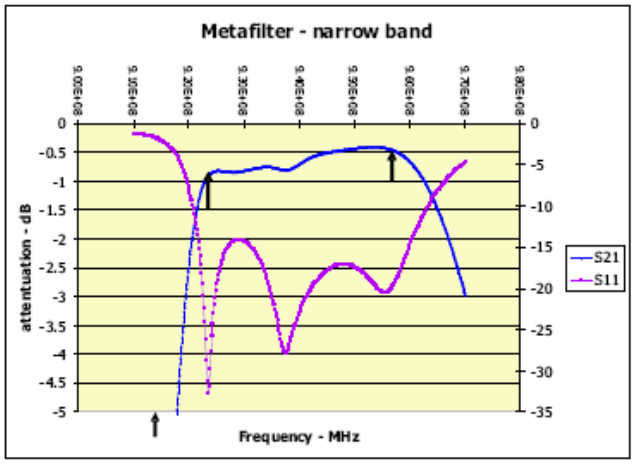

Fig. 13: Measurement Board Results – closer View

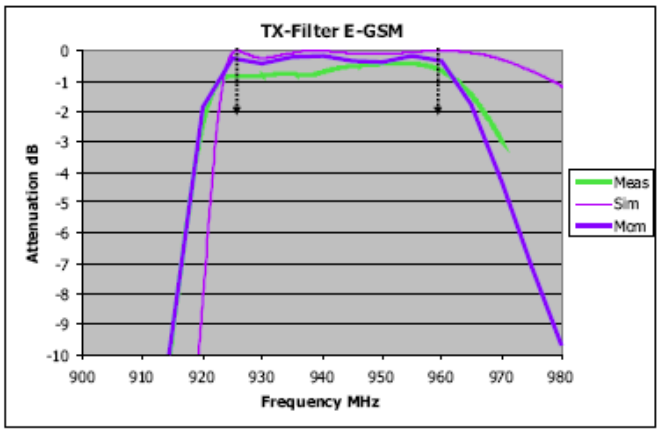

Fig. 14: Result Comparison

Freq	Circuit Simulator	Momentum Simulator	Measurement Board Results
925 MHz Passband dB[S21]	-0.07 dB	-0.25 dB	-0.7 dB
960 MHz Passband dB[S21]	-0.03 dB	-0.26 dB	-0.4 dB
915 MHz Stopband dB[S21]	-23 dB	-10 dB	-10 dB

Table. 1 : Result Comparison

5. CONCLUSION

It was shown by designing a narrow bandpass filter with proposed new CRLH structure that, Metamaterials are very beneficial in terms of providing low insertion losses which are very much needed for EGSM base station. The obtained board measurement result is very good in agreement with momentum simulation results with respect to circuit simulator. Future work on metamaterial CRLH structures for microwave filters will continue for much better results using new structure with microstrip gap capacitors and open stub inductors taking size reduction in to consideration.

6. ACKNOWLEDGEMENT

The author Shaik Geelani would like to thank his co-author, Prof. Georg Fischer for the creation of Doctorate opportunity as well to gain professional experience at Bell Labs Europe. He also would like to thank Bell Labs Nuremberg Team, especially Michael Doubrava and Dr. Michael Sollner for their support during the research.

Further he wants to thank the German Ministry of research and education (BMBF) for funding part of this work under MARIO project (Metamaterial based flexible duplex filters).

REFERENCES

[1] C. Caloz, T. Itoh, Electromagnetic Metamaterial, IEEE press, Wiley, Hoboken NJ, 2006

[2] Gunther Dehm-Andone, Grzegorz Adamiuk, Georg Fischer; Using Metamaterial structures with frequency agile base stations, IEEE GEMIC 2006.

[3] C. Caloz, H. Okabe, T. Iwai, and T. Itoh, “Transmission line approach of left-handed (LH) materials”, in USNC/URSI Nat. Radio Science Meeting, vol. 1, Jun. 2002, p. 39

[4] Benedek, P. Silvester, P., Equivalent Capacitances for Microstrip Gaps and Steps Microwave Theory and Techniques, IEEE Transactions on Volume 20, Issue 11, Nov 1972 Page(s):729 – 733.

[5] Bekheit, M.; Amari, S.; Menzel, W, Modelling and Optimization of Compact Microwave Bandpass Filters. Microwave Theory and Techniques, IEEE Transactions on Volume 56, Issue 2, Feb. 2008 Page(s):420 – 430

[6] W. Menzel, A. Balalem: Quasi-Lumped Suspended Stripline Filters and Diplexers. IEEE Trans. on MTT, vol.MTT-53, Oct. 2005, pp. 3230 – 3237

[7] Anu Lehtovuori and Luis Costa, Model for Shielded Suspended Substrate Microstrip Line, Circuit Theory Laboratory Report Series, Helsinki University of Technology 1998.

[8] A. Lai, T. Itoh, "Composite Right/Left-Handed Transmission Line Metamaterials", IEEE Microwave Magazine, pp.34-50, Sept. 2004.

[9] I-H. Lin, M. DeVincentis, C. Caloz, T. Itoh, "Arbitrary Dual-Band Components Using Composite Right/Left-Handed Transmission Lines", IEEE Transactions on Microwave Theory and Technique, Vol. 52, No.4, April 2004.

[10] Islam, R.; Eleftheriades, G.V.; Antennas and Propagation International Symposium, 2007 IEEE 9-15 June 2007 Page(s):4957 - 4960Compact Negative-Refractive-Index Transmission-Line (NRI-TL) coupler, filter and diplexer

[11] C. Caloz, A. Sanada, T. Itoh, "A novel Composite Right-/Left-Handed Coupled-Line Directional Coupler With Arbitrary Coupling Level and Broad Bandwidth", IEEE Transactions on Microwave Theory and Techniques, Vol. 52, No.3, March 2004.

Metamaterial Based RF Narrow Bandpass Filter Design In Microstrip Suspended Substrate

Geelani Shaik[1, 3], Georg Fischer[2]

Jürgen Detlefsen[3], Horst Schenkel[1]

Alcatel-Lucent Bell Lab Technologies AG, Thurn and Taxis Strasse 10, 90411 Nuremberg, Germany[1]
gtumcher@alcatel-lucent.com

Friedrich-Alexander-Universität Erlangen-Nürnberg, Lehrstuhl für Technische Elektronik Cauerstraße 9, 91058 Erlangen Germany[2]

Technical University of Munich, Lehrstuhl für Hochfrequenztechnik Fachgebiet HFS, 21 D-80333 Arcisstraße, München Germany[3]

Abstract— Composite Right-Left Handed Metamaterial based narrow bandwidth RF bandpass filter is designed for EGSM-900 base station (Tx band, 925MHz - 960MHz), using microstrip gaps and open stubs in a shielded microstrip suspended substrate. To validate the design and analysis, the layout board of bandpass filter was fabricated and measured. It is shown that the simulated and measured performances are good in agreement. For three unit cells within a narrow bandwidth of 35 MHz, the layout board of bandpass filter has achieved an insertion loss of nearly -0.7 dB and a stopband of -10 dB approximately. This could be of great advantages for all RF systems which uses transmitter and receiver bands simultaneously.

Index Terms— *Bandpass filter, Composite left/right handed metamaterials (CRLH), suspended substrate, microstrip gaps, open stubs.*

I. INTRODUCTION

Pendry et al. developed first practical application based on theoretical metamaterial research by Veselago [1] which was published in 1968. His theoretical result constitutes a metallic structure with negative permittivity [2] and negative permeability [3]. C.Caloz et al., Iyer and Eleftheriades followed with a transmission line [TL] approach on metamaterials [5], [6] and further theoretical expansions on CRLH (Composite Right/Left Handed) MTM (Metamaterial) structures [6]-[7]. The Caloz/Ithoh research group also applied these results in [8], [9] – [10] for bandpass filters (BPF). C.Caloz/T.Itoh in their publications [14] presented periodical MTM bandpass filter design with interdigital capacitors and short stub inductors for broad bandwidths, in this paper we have used microstrip gap (slots) capacitors and open stub inductors to design periodic CRLH MTM Tx-bandpass filters for the applications of basestations within the narrow bandwidth of 35 MHz. As the requirement for basestations that are more flexible leads to the need for high selective and low ripple bandpass filters.

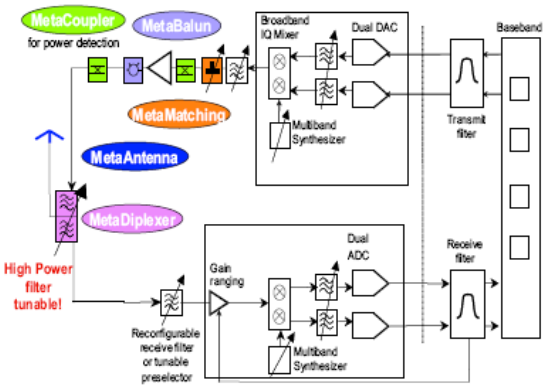

Fig. 1: Applications of metamaterials in RF Systems

By designing a bandpass filter it is shown that metamaterial structures can be of great advantage for building blocks in RF systems. Fig.1 gives a vision of applications explored using MTM structures [20]. At some locations static structures are sufficient, at other locations the MTM structures need to be tuned by either MEMS (Micro Electromechanical Systems) [20] or ferroelectric varactors like e.g. BST (Barium Strontium Titanate) component, however this approach has its merits given that the number of frequency bands opened for mobile communication is constantly increasing due to de-regulation and a further band cannot be added once a system is deployed.

2. CRLH METAMATERIAL THEORY ON FILTER APPLICATION

Fig. 2 shows the LC equivalent circuit model for the Ideal unit cell of a CRLH TL (Transmission Line). Considering the balanced condition of the circuit where the series resonance is equals to the parallel resonance i.e. $\omega_{se} = \omega_{sh}$ [14].

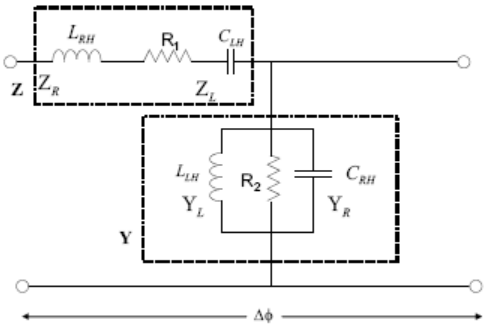

Fig. 2: MTM CRLH TL

The series resonance frequency of the unit cell is given as,

$$f_{se} = \frac{1}{2\pi\sqrt{L_{RH}C_{LH}}} \tag{1}$$

The parallel resonance frequency of the unit cell is

$$f_{sh} = \frac{1}{2\pi\sqrt{L_{LH}C_{RH}}} \tag{2}$$

Where L_{RH}, C_{LH}, L_{LH}, C_{RH} represents the left and right handed capacitors and inductors respectively.

Referring to the Fig.2, on the left hand side (LH),

When $\omega \to 0$, then $|Z| \to 1/(\omega_{C_L}) \to \alpha$ and

$|Y| \to 1/(\omega_{L_L}) \to \alpha$

We therefore have stopband behaviour due to the high pass nature of LH elements.

On the other side, which is right hand side (RH),

When $\omega \to \alpha$, then $|Z| \to \omega_{L_R} \to \alpha$ and

$|Y| \to \omega_{C_R} \to \alpha$

Again stopband behaviour is found due to the low pass nature of RH Elements. Between these two stop bands a perfectly matched passband can be achieved at balanced conditions [14].
So the LC equivalent CRLH TL can be implemented for bandpass filter which is fully characterized in terms of its propagation constant "β" and characteristic impedance "Z_C" in its passband.

For a lossy TL, [16]

$$\beta = \sqrt{\frac{C_{RH}}{C_{LH}} + \frac{L_{RH}}{L_{LH}} + \frac{R}{R_2} - \omega^2 * L_{RH} * C_{RH} - \frac{1}{\omega^2 * L_{LH} * C_{LH}} + j * \left\{\omega * \left[R_1 * C_{RH} + \frac{L_{RH}}{R_2} - \frac{R_1}{\omega^2 * L_{LH}} - \frac{1}{\omega^2 * R_1 * C_{LH}}\right]\right\}} \tag{3}$$

And

$$Z_C = \sqrt{\frac{L_{RH} + \frac{R_1}{j*\omega} - \frac{1}{\omega^2 * C_{LH}}}{C_{RH} + \frac{1}{R_2 * j * \omega} - \frac{1}{\omega^2 * L_{LH}}}} \tag{4}$$

Fig. 3 is the practical symmetric unit cell of an LC CRLH TL, where the Input and Output impedances are matched simultaneously with the same value and is preferred over asymmetric unit cell which has the opposite properties [14].

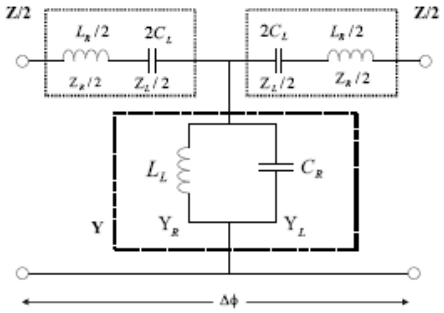

Fig. 3: Practical Symmetric BPF unit cell

3. MICROSTRIP OPEN STUB AND GAP EQUIVALENT TO CRLH STRUCTURE

Fig. 5 shows a typical microstrip MTM CRLH TL bandpass filter structure we have used in this paper and is constituted with microstrip gaps and open stubs [22]. The structure is the modelling of the metamaterial which is LC equivalent of Fig. 2. The metamaterial (or left handed) line is represented by periodical arrangement of serial capacity and shunt inductivity. The serial capacity is represented in the layout by slots

and shunt inductivity by open stubs. In order to concentrate all the possible frequencies in a narrow frequency range, we have used the gaps (slots), where the width of the gaps steers the bandwidth of the filter. Smaller the capacity (width of the gap), the more narrow is the bandwidth; the equivalent of this microstrip gap capacitor π-model can be seen in Fig.7. The Similar non biperiodical in Fig. 4 (i.e. periodical) circuit was presented by Prof. T. Itoh [14] in his publications. The difference was, that instead of slots he used interdigital capacitors and the arrangement was periodical. In his periodical structure he has got the same amount of LH and RH resonance frequencies dependently on the amount of cells. Also the resonance frequencies of the serial and parallel part (Fig.3) [16] are very important parameters of the structure because they define the edges of the band gap.

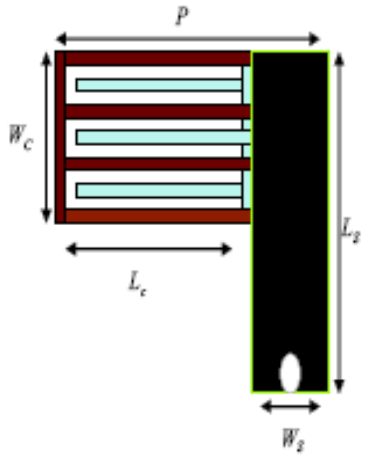

Fig. 4: MTM BPF with Interdigital capacitors

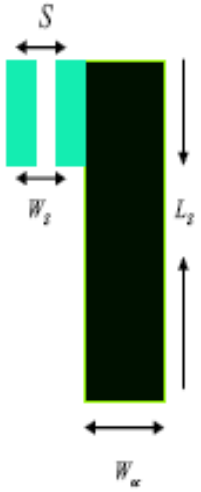

Fig. 5: MTM BPF with gaps and open stubs

The schematic of the new CRLH MTM TL structure is shown in Fig. 6 which is in domain resonance frequencies. The electrical distributions of the currents in Fig. 8 shows the proof that, one of these resonances has common right handed behaviour and the second one left handed behaviour. Between these resonances must be the band gap. Therefore, this structure must be then the CRLH (composed right left handed) structure. The position of the resonances in the frequency domain is determined by the length of the side wings which exhibits right handed inductance. By changing the length of the short wings (left and right wings between slots) we can also steer the position of the LH-resonances to each other. Moreover, the distance between the slots is mainly determined by the width of the side wings. It's not the rule, if the distance between the slots is different from the width of the side wings, and hence has a big influence on the behaviour. The width of the side wings has also huge influence on the bandwidth. The wider are the side wings the narrower the filter effect tends to be.

The π – model in Fig. 7 is a symmetric two-port network equivalent to the microstrip gap [15]. But the values of gap width, spacing is optimized in ADS with goal constraints and the inductance of the open stub values can be obtained as [14].

$$L_L = -\frac{Z_c^{oc}}{\omega}\cot\left(\beta^{oc}.l\right) \tag{5}$$

Where $\cot\left(\beta^{oc}.l\right)$ is the electrical length of stub [14]. It has been observed during simulation that, the unit cell impedance at the ports resembles as 75Ω, so impedance transformer [17] is used to step it down to 50Ω for perfect matching with the ports and is depicted in Fig. 6.

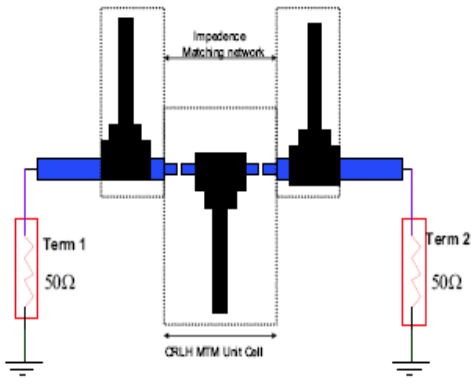

Fig. 6: MTM BPF unit cell Schematic with Gaps

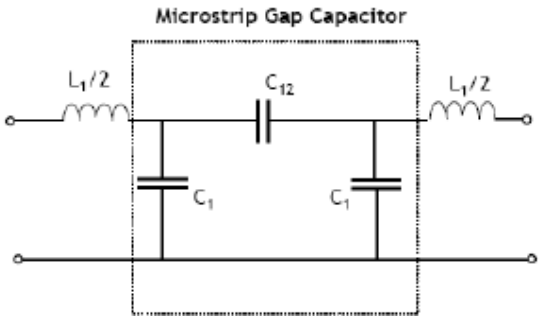

Fig. 7: π – Model microstrip gap

4. MICROSTRIP SUSPENDED SUBSTRATE IMPLEMENTATION

Suspended Strip line is an excellent transmission line media [18], increased cross-section together with a relative thin substrate are responsible for reduced ohmic and dielectric losses. Large portion of the fields in air results in low dispersion and hence the radiation is prevented with shielding [12], [13], [18]. But also have the disadvantages of difficulties in miniaturization, critical housing technology and the increased complexity of utilizing hybrid elements [19]. It has been clear that, thinner and less lossy substrate decreases the insertion loss and narrows the bandwidth [14]. Rogers 4003 is a substrate material used with 0.813 mm as thickness in a symmetrical shielding between the walls [19]. Mechanical stability is a very important factor regarding suspended substrate housing, which makes to use the above quality substrate.

Our MTM research has combined a vast area to accommodate suspended substrate for better results to reach our goal and hence to prove the state of art MTM structures. Pictorial representation of its block can be seen in Fig. 9

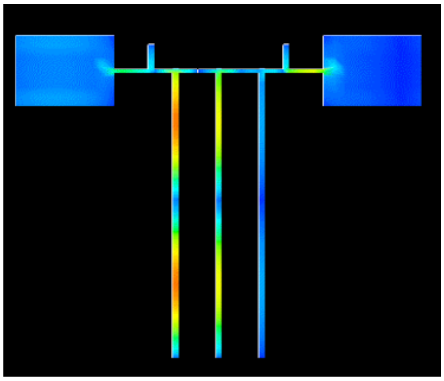

Fig. 8: Electric Current Distribution

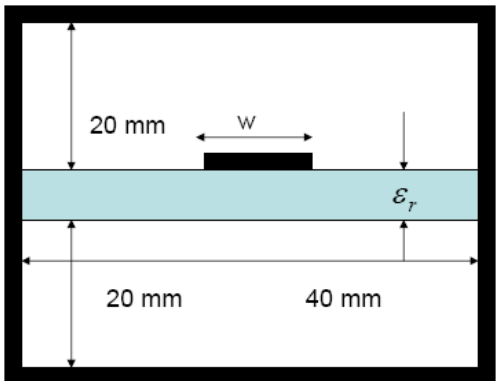

Fig. 9: Suspended Substrate Block

5. THREE UNIT CELLS BPF – SIMULATION AND MEASUREMENT RESULTS

Fig.10 is a symmetric three unit cell CRLH MTM BPF filter in a shielded suspended substrate with impedance transformers to match the ports in 50Ω environment. 3-Dimensional view of such arrangement can be seen in Fig.11. The circuit design simulations are carried out in Agilent's ADS software. Besides circuit simulator we have also simulated the layout in method of momentum analysis simulator (MoM) in the absence of any active devices, which takes us closer to measurement results. Also we have many possibilities to optimise the structure to the desired performance, such as,

Fig.10: Three Unit Cells MTM BPF

- Width of the slots
- Width of the side wings
- Number of the cells
- Properties of the substrate (i.e. holder of the structure)
- Distance between slots (independent of the width of the side wings)

- Distance of the structure to the ground plane
- Distance of the substrate to the upper and Lower electrical shielding
- Width of the strips.

Circuit simulator result has achieved an average insertion loss (ripple) less than -0.25 dB (925MHz - 960 MHz) with a sharp stopband of -23 dB within 35 MHz range depicted in Fig.12. Close ripple can be viewed in Fig.13. One can realize the concept in metamaterials, that the number of unit cells makes the edges sharper [14], but has influence in the increment of insertion loss.

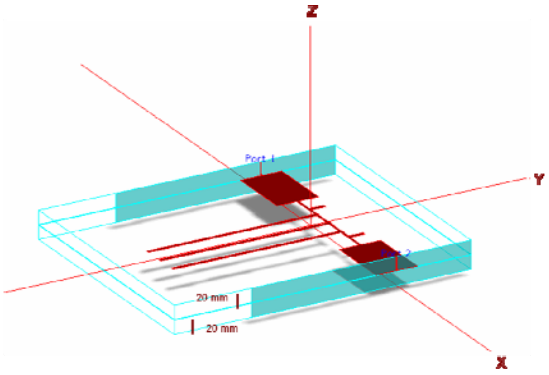

11: 3D View – 3 unit cells in shielding suspended substrate

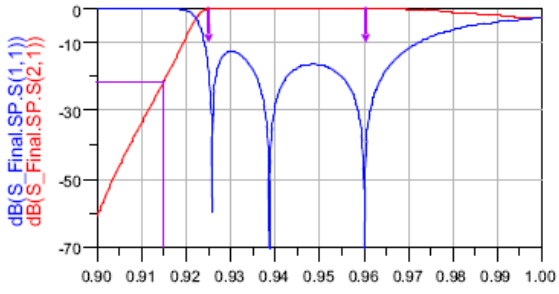

Fig. 12: Simulation Results

From simulation result with this structure it can be concluded that, with 11 unit cells less than -80 dB stopband can be achieved below -1 dB insertion loss.Method of momentum simulator analysis results can be seen in Fig.14 and Fig.15, On comparison with circuit simulator, the momentum results are -0.3 dB and -13 dB more in ripple and edges (stopband), which is again much better hope to go for measurement board to prove

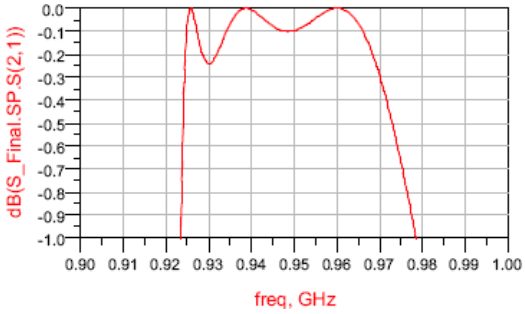

13: Simulation Results - Closer View

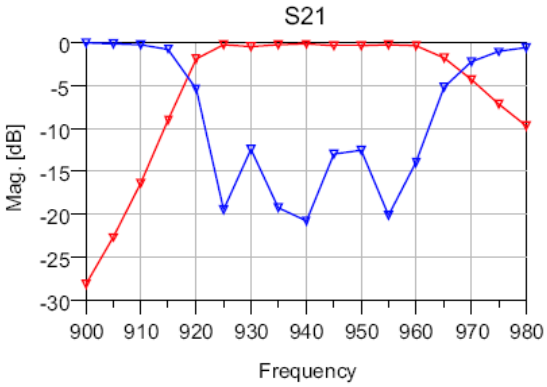

Fig. 14: Momentum Simulator Results

Fig. 15: Mom Result - Closer View

again much better hope to go for measurement board to prove the state of art CRLH MTM new structure and its applications in RF communication systems. The layout board 33cm x 37cm in Fig.16 is fabricated using ROGER'S 4003 material with substrate thickness of 0.813mm and conductor thickness of 0.1mm respectively in a close conductive housing [In Fig.17] of

shielded suspended substrate which is separated by 20mm symmetric walls on top and bottom from the centre of filter. The cross-section is shown in Fig.18.

The measurement board of MTM CRLH BPF results in Fig.19 shows a stopband of nearly -10 dB at 918 MHz with an average passband less than -0.76 dB between 928MHz -964MHz within 35 MHz bandwidth, the frequency range is displaced about 3-4 MHz due to critical housing of the suspended substrate, and can be adjusted by tuning the metallic housing screws to set our frequency range of design i.e. 925 MHz - 960 MHz respectively. The results in this range achieved -0.7 dB insertion loss in passband and -10 dB stop band at 915 MHz and can be seen in Fig.20.

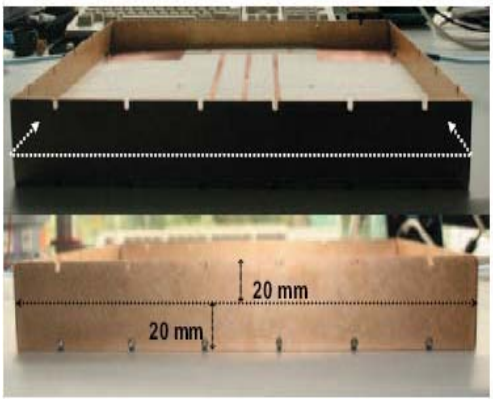

Fig. 18: Cross- Section

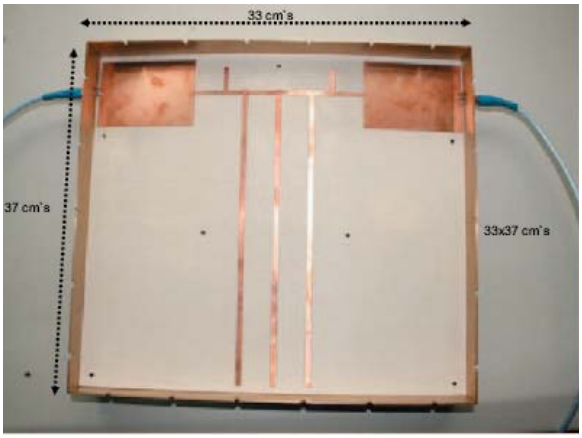

Fig. 16: Measurement Board: 3 Unit Cells

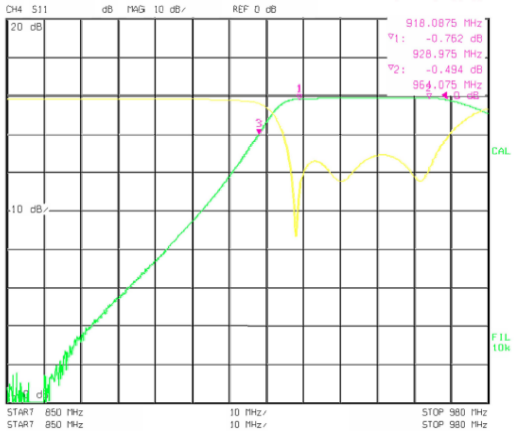

Fig. 19: Measurement Results Section

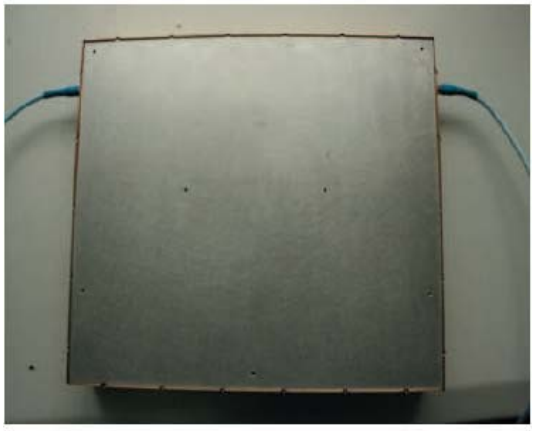

Fig. 17: Measurement board – Closed View

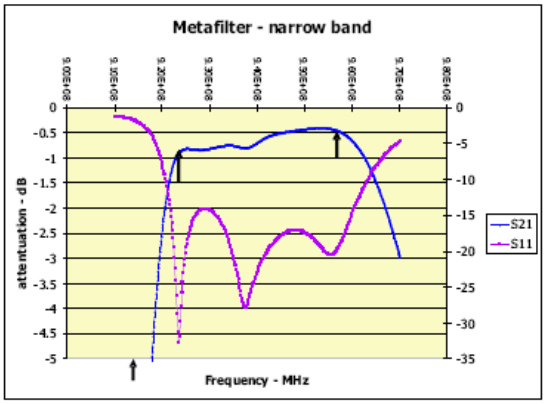

Fig. 20: (925 MHz-960 MHz) Range – Results

Freq	*Circuit Simulator*	*Momentum Simulator*	*Measurement Board Results*
925 MHz Passband dB[S21]	-0.07 dB	-0.25 dB	-0.7 dB
960 MHz Passband dB[S21]	-0.03 dB	-0.26 dB	-0.4 dB
915 MHz Stopband dB[S21]	-23 dB	-10 dB	-10 dB

Table.1: Result Comparison

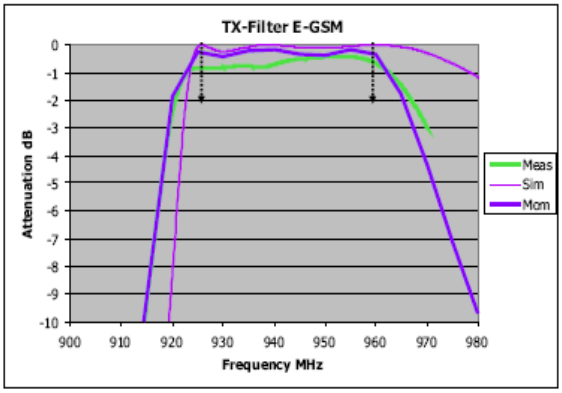

Fig. 21: Result Comparison

Fig.21 shows the Comparison between circuit simulator, momentum simulator and measurement results and is tabulated in table.1. The obtained fabricated board results are almost equal in the stopband and 0.4 dB higher in the pass band in comparison with method of momentum analysis simulator than circuit simulator and hence satisfy our goal of reaching passband less than -1 dB. This gives an idea that, the measurement results can be improved better with momentum simulator optimization techniques. Moreover sharper stopband can be achieved by increasing more number of unit cells [14] which is our future research task in the state of art MTM along with size reduction.

6. CONCLUSIONS

It was shown by designing Metamaterial BPF using gap capacitors and open stub inductors in suspended substrate that, Metamaterials are very beneficial in terms of providing low insertion losses which are very much needed for EGSM base stations. The obtained board measurement result is very good in agreement with momentum simulation results with respect to circuit simulator. Future work on metamaterial CRLH structures for microwave filters will continue for much better results taking size reduction in to consideration.

7. ACKNOWLEDGEMENT

The author Shaik Geelani would like to thank his co-author, Prof. Georg Fischer for the creation of Doctorate opportunity as well to gain professional experience at Bell Labs Europe. He also would like to thank Bell Labs Nuremberg Team, especially Michael Doubrava and Dr. Michael Sollner for their support during the research.

Further he wants to thank the German Ministry of research and education (BMBF) for funding part of this work under MARIO project (Metamaterial based flexible duplex filters).

REFERENCES

[1] V. G. Veselago, *"The electrodynamics of substances with simultaneously negative values of ε and μ",* Sov. Phys.-Usp., vol. 10, pp. 509-514, Jan.-Feb. 1968.

[2] J. B. Pendry, A. J. Holden, W .J. Stewart and I. Young's, *"Extremely low frequency Plasmon's in metallic microstructures",* Phys. Rev. Lett., vol. 76, no. 25, pp. 4773-4776, Jun. 1996

[3] J. B. Pendry, A. J. Holden, D. J. Robbins, and W.J. Stewart, *"Magnetism from conductors and enhanced nonlinear phenomena",* IEEE Trans.Microw. Theory Tech., vol. 47, no. 11, pp. 2075-2084, Nov. 1999

[4] D. R. Smith, W. J. Padilla, D. C. Vier, S. C. Nemat-Nasser, and S.Schultz, *"Composite medium with simultaneously negative permeability and permittivity",* Phys. Rev. Lett., vol. 84, no. 18, pp. 4184-4187, May 2000.

[5] C. Caloz, H. Okabe, T. Iwai, and T. Itoh, *"Transmission line approach of left-handed (LH) materials",* in USNC/URSI Nat. Radio Science Meeting, vol. 1, Jun. 2002, p. 39.

[6] A. K. Iyer and G. V. Eleftheriades, *"Negative refractive index Metamaterial supporting 2-D waves",* in IEEE MTT-S Int. Microwave Symp. Dig., vol. 2, Jun. 2002, pp. 1067 1070.

[7] D. R. Smith and N. Kroll, *"Negative refractive index in left-handed materials",* Phys. Rev. Lett., vol. 85, no. 14, pp. 2933-2936, Oct. 2000.

[8] A. Lai, T. Itoh, *"Composite Right/Left-Handed Transmission Line Metamaterials",* IEEE Microwave Magazine, pp.34-50, Sept. 2004.

[9] I-H. Lin, M. DeVincentis, C. Caloz, T. Itoh, *"Arbitrary Dual-Band Components Using Composite Right/Left-Handed Transmission Lines",* IEEE Transactions on Microwave Theory and Technique, Vol. 52, No.4, April 2004.

[10] C. Caloz, A. Sanada, T. Itoh, *"A novel Composite Right-/Left-Handed Coupled-Line Directional Coupler With Arbitrary Coupling Level and broad bandwidth",* IEEE Transactions on Microwave Theory and Techniques, Vol. 52, No.3, March 2004.

[11] H. Okabe, C. Caloz, T. Itoh, *"A Compact Enhanced-Bandwidth Hybrid Ring Using an Artificial Lumped-Element Left-Handed Transmission-Line Section",* IEEE Transactions on Microwave Theory and Technique, Vol. 52, No.3, March 2004.

[12] W. Menzel, A. Balalem: "Quasi-Lumped Suspended Stripline Filters and Diplexers", IEEE Trans. on MTT, vol.MTT-53, Oct. 2005, pp. 3230 – 3237.

[13] J. E. Dean: "Suspended substrate stripline filters for ESM applications". IEE Proc., Vol. 132, Pt. F, July 1985, pp.257 - 266.

[14] C. Caloz, T. Itoh, *"Electromagnetic Metamaterial",* IEEE press, Wiley, Hoboken NJ, 2006

[15] Benedek, P. Silvester, P., *"Equivalent Capacitances for Microstrip Gaps and Steps Microwave Theory and Techniques",* IEEE Transactions on Volume 20, Issue 11, Nov 1972 Page(s):729 – 733.

[16] Gunther Dehm-Andone, Grzegorz Adamiuk, Georg Fischer; *"Using Metamaterial structures with frequency agile base stations",* IEEE GEMIC 2006.

[17] Lei Zhu, Huamin Shi; Menzel:, *"W Coupling behaviours' of quarter-wavelength impedance transformers for wideband CPW bandpass filte"*., Microwave and Wireless Components Letters, IEEE Volume 15, Issue 1, Jan. 2005 Page(s):13 – 15.

[18] Bekheit, M.; Amari, S.; Menzel, "W, Modelling and Optimization of Compact Microwave Bandpass Filters. Microwave Theory and Techniques", IEEE Transactions on Volume 56, Issue 2, Feb. 2008 Page(s):420 – 430.

[19] Anu Lehtovuori and Luis Costa, *"Model for Shielded Suspended Substrate Microstrip Line",* Circuit Theory Laboratory Report Series, Helsinki University of Technology 1998.

[20] G. Fischer, *"Architectural benefits of wide band gap RF power transistors for frequency agile base station systems "*, IEEE MTT, 6th annual Wireless and Microwave Technology Conference, Clearwater, Florida, April 2004.

[21] Islam, R.; Eleftheriades, G.V, *"Compact-Negative-Refractive-IndexTransmission-Line (NRI-TL) coupler, filter and diplexer",* Antennas and Propagation International Symposium, 2007 IEEE 9-15 June 2007 Page(s):4957 - 4960

Metamaterial RF Tx-Bandpass Filter Design for EGSM-900 Basestations

Geelani Shaik[1,3], Horst Schenkel[1]

Jürgen Detlefsen[3], Georg Fischer[2]

Alcatel-Lucent Bell Lab Technologies AG, Thurn and Taxis Strasse 10, 90411 Nuremberg, Germany[1]
gtumcher@alcatel-lucent.com, hschenkel@alcatel-lucent.com

Friedrich-Alexander-Universität Erlangen-Nürnberg, Lehrstuhl für Technische Elektronik Cauerstraße 9, 91058 Erlangen Germany[2]

Technical University of Munich, Lehrstuhl für Hochfrequenztechnik Fachgebiet HFS, 21 D-80333 Arcisstraße, München Germany[3]

***Abstract*— In this paper RF Tx-band (925MHz-960MHz) bandpass filter for the application of EGSM-900 base stations is designed by using Complementary Right/Left handed metamaterial structured transmission lines with microstrip gaps and open stubs. To validate the design and analysis, the layout board of bandpass filter is fabricated and measured. With this new structure, It is shown that the simulated and measured results are very good in agreement. The layout board achieved an insertion loss of -0.7 dB with the stopband of nearly -10 dB within 35 MHz narrow band using three unit cells of metamaterial structure.**

Index Terms— **Bandpass filter, Composite left/right handed metamaterials (CRLH), suspended substrate, microstrip gaps, open stubs.**

I. INTRODUCTION

Pendry et al. developed first practical application based on theoretical metamaterial research by Veselago [1] which was published in 1968. His theoretical result constitutes a metallic structure with negative permittivity [2] and negative permeability [3]. C.Caloz et al., Iyer and Eleftheriades followed with a transmission line [TL] approach on metamaterials [5], [6] and further theoretical expansions on CRLH (Composite Right/Left Handed) MTM (Metamaterial) structures [6]-[7]. The Caloz/Ithoh research group also applied these results in [8],[9] –[10] for bandpass filters (BPF). C.Caloz et al/Itoh in their publications [14] presented periodical MTM bandpass filter design with interdigital capacitors and short stub inductors for broad bandwidths, in this paper we have used microstrip gaps (slots) and open stubs to design periodic CRLH MTM Tx-bandpass filters in the applications of basestations with the narrow bandwidth of 35 MHz.

As the requirement for basestations that are more flexible leads to the need for high selective and low ripple bandpass filters. By designing a bandpass filter it is shown that metamaterial structures can be of great advantage for building blocks in RF systems. Fig.1 gives a vision of applications explored using MTM structures [20]. At some locations static structures are sufficient, at other locations the MTM structures need to be tuned by either MEMS (Micro Electromechanical Systems) [20] or ferroelectric varactors like e.g. BST (Barium Strontium Titanate) component, however this approach has its merits given that the number of frequency bands opened for mobile communication is constantly increasing due to De-regulation and a further band cannot be added once a system is deployed.

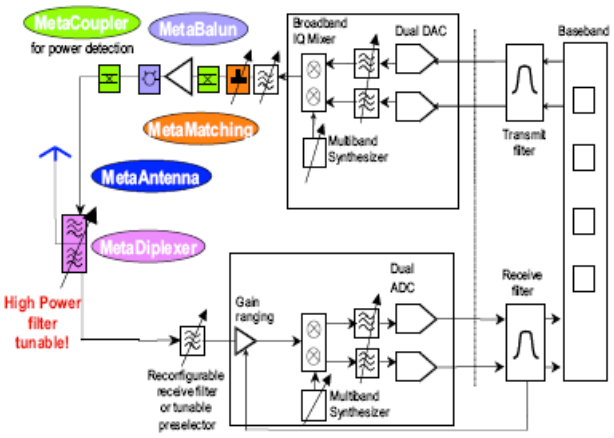

Fig. 1: Applications of metamaterials in RF Systems

2. MICROSTRIP OPEN STUB AND GAP EQUIVALENT TO CRLH STRUCTURE

Fig. 2 shows a typical microstrip MTM CRLH TL bandpass filter structure we have used in this paper and is constituted with microstrip gaps and open stubs. The structure is the modelling of the metamaterial and the equivalent of this new structure can bee seen in Fig. 3. The metamaterial (or left

handed) line is represented by periodical arrangement of serial capacity and shunt inductivity. The serial capacity is represented in the layout by slots and shunt inductivity by open stubs. In order to concentrate all the possible frequencies in a narrow frequency range, we have used the gaps (slots), where the width of the gaps steers the bandwidth of the filter. Smaller the capacity (width of the gap), the more narrow is the bandwidth [16]. The similar non biperiodical (i.e. periodical) circuit was presented by Prof. T. Itoh [14] in his publications. The difference was, that instead of slots he used interdigital capacitors and the arrangement was periodical. In his periodical structure he has got the same amount of LH and RH resonance frequencies dependently on the amount of cells. Considering the balanced condition of the circuit from Fig.3, where the series resonance is equals to the shunt resonance i.e. $\omega_{se} = \omega_{sh}$ [14]

The series resonance frequency of the unit cell is given as,

$$f_{se} = \frac{1}{2\pi\sqrt{L_{RH}C_{LH}}} \qquad (1)$$

The shunt resonance frequency of the unit cell is

$$f_{sh} = \frac{1}{2\pi\sqrt{L_{LH}C_{RH}}} \qquad (2)$$

By periodical arrangement of the cells we get the amount of LH-resonances propotional to the number of cells.

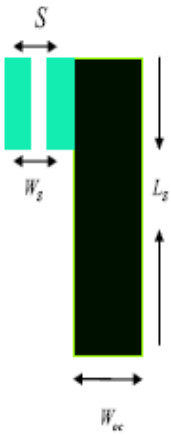

Fig. 2: MTM unit cell structure with gaps and open stubs

Periodicity in MTM is just convenience, from a fabrication point of view its easier to design and build a MTM by repeating periodically a unique cell than by collection of different cells.

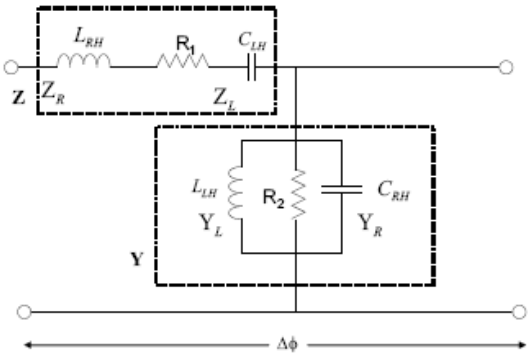

Fig. 3: Lossy CRLH TL

LC equivalent CRLH TL in Fig. 2 can be implemented for bandpass filter which is fully characterized in terms of its propagation constant "β" and characteristic impedance "Z_c" in its passband. Where [16],

$$\beta = \sqrt{\frac{C_{RH}}{C_{LH}} + \frac{L_{RH}}{L_{LH}} + \frac{R}{R_2} - \omega^2 * L_{RH} * C_{RH} - \frac{1}{\omega^2 * L_{LH} * C_{LH}} + j * \left\{ \omega * \left[R_1 * C_{RH} + \frac{L_{RH}}{R_2} - \frac{R_1}{\omega^2 * L_{LH}} - \frac{1}{\omega^2 * R_1 * C_{LH}} \right] \right\}} \qquad (3)$$

And

$$Z_C = \sqrt{\frac{L_{RH} + \frac{R_1}{j*\omega} - \frac{1}{\omega^2 * C_{LH}}}{C_{RH} + \frac{1}{R_2 * j * \omega} - \frac{1}{\omega^2 * L_{LH}}}} \qquad (4)$$

By reducing the capacity in serial branch we reduce the distance between resonances in the frequency domain. But the values of gap width, spacing is optimized in Agilent's ADS software with goal constraints. The low-frequency approximation for the inductance of open stub [14] is,

$$L_L = -Z_C^{OS} (Cot\beta^{OS} l)/\omega \qquad (5)$$

Where $\cot(\beta^{OS} l)$ is the electrical length of stub [14].

The schematic of the new CRLH MTM TL structure is shown in Fig.4 which is in domain resonance frequencies. The electrical distributions of the currents in Fig. 5 shows the proof that, one of these resonances has common right handed behaviour and the second one left handed behaviour. Between these resonances must be the band gap. Therefore, this structure must be then the CRLH (composed right left handed) structure. The position of the resonances in the frequency domain is determined by the length of the side

wings. By changing the length of the short wings (left and right wings between slots) we can also steer the position of the LH-resonances to each other and moreover, the distance between the slots is mainly determined by the width of the side wings. It is not the rule, if the distance between the slots is different as the width of the side wings which has a big influence on the behaviour. The width of the side wings has also huge influence on the bandwidth. The wider are the side wings the narrower the filter effect tends to be.

It has been observed during simulation that, the unit cell impedance at the ports resembles as 75 Ω, so the impedance transformer [17] is used to step it down to 50 Ω for perfect matching with the ports and can be seen in the same Fig. 4

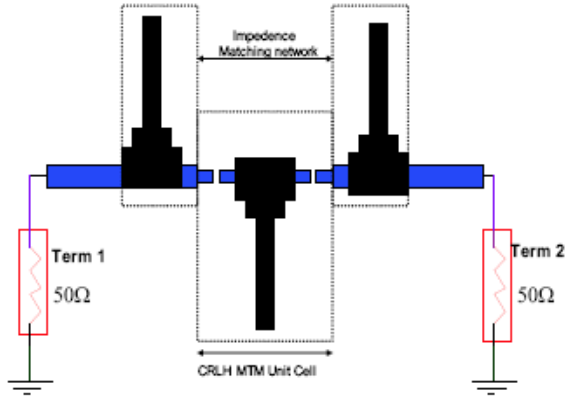

Fig. 4: Unit Cell with open stubs and gaps in Impedance matching

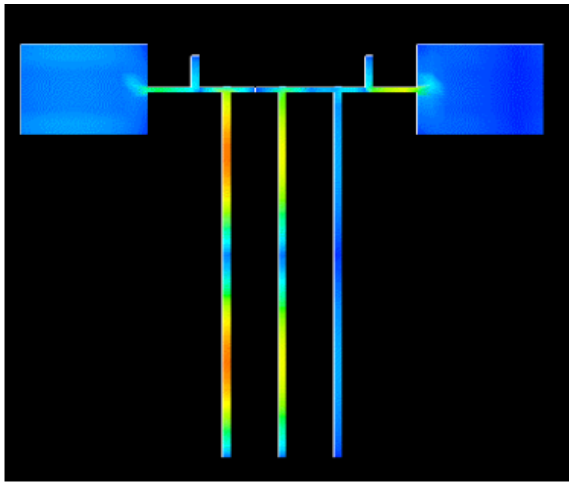

Fig.5: Electrical Current Distribution

3. MICROSTRIP SUSPENDED SUBSTRATE IMPLEMENTATION TO CRLH STRUCTURE

Suspended Strip line is an excellent transmission line media [18], increased cross-section together with a relative thin substrate are responsible for reduced ohmic and dielectric losses. Large portion of the fields in air results in low dispersion and hence the radiation is prevented with shielding [12], [13], [18]. But also have the disadvantages of difficulties in miniaturization, critical housing technology and the increased complexity of utilizing hybrid elements [19]. It has been clear that, thinner and less lossy substrate decreases the insertion loss and narrows the bandwidth [14]. Rogers 4003 is a substrate material used with 0.813 mm as thickness in a symmetrical shielding between the walls [19]. Mechanical stability is a very important factor regarding suspended substrate housing, which makes to use the above quality substrate. Our MTM research has combined a vast area to accommodate suspended substrate for better results to reach our goal and hence to prove the state of art MTM structures.. Pictorial representation of its block can be seen in Fig. 6

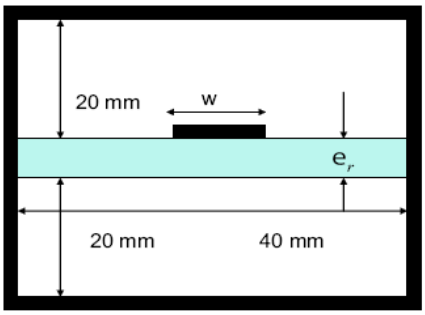

Fig. 6: Block of Microstrip Suspended Substrate

We have many possibilities to optimise the structure to the desired performance:

- Width of the slots
- Width of the side wings
- Number of the cells
- Properties of the substrate (i.e. holder of the structure)
- Distance between slots (independent of the width of the side wings)
- Distance of the structure to the ground plane
- Distance of the substrate to the upper and Lower electrical shielding
- Width of the strips

4. THREE UNIT CELL BANDPASS FILTER – SIMULATION AND MEASUREMENT RESULTS

Fig.7 is a symmetric three unit cell CRLH MTM BPF filter in a shielded suspended substrate with impedance transformers to match the ports in 50Ω environment. The circuit design simulations are carried out in Agilent's ADS software. Besides circuit simulator we have also simulated the layout in method of momentum analysis simulator (MoM) in the absence of any active devices, which takes us closer to measurement results.

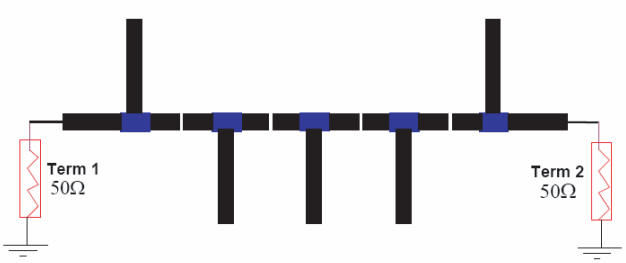

Fig. 7: Periodic Three Unit Cells BPF

Circuit simulator results are obtained with an average insertion loss (ripple) less than -0.25 dB (925MHz - 960 MHz) with a sharp stopband of -23 dB within 35 MHz range in Fig.8. Close ripple can be viewed in Fig.9. One can realize the concept in metamaterial, that the number of unit cells makes the edges sharper [14], but has influence in the increment of insertion loss. From simulation result with this structure it can be concluded that, with 11 unit cells less than -80 dB stopband can be achieved below -1 dB insertion loss.

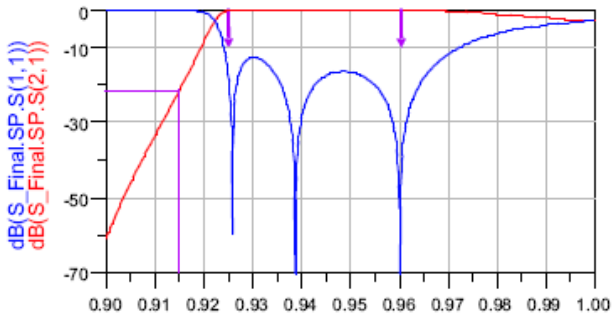

Fig. 8: Circuit Simulation Results

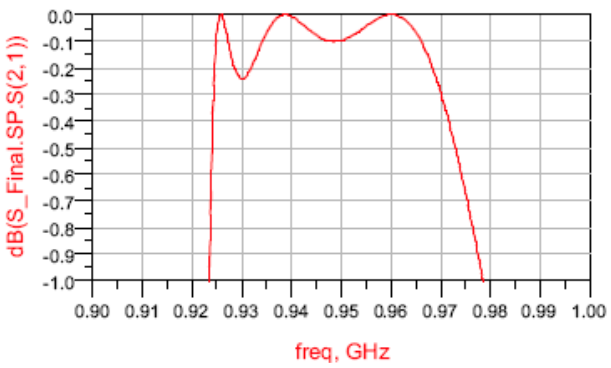

Fig. 9: Circuit Simulation Result – Closer View

Method of momentum simulator analysis results can be seen in Fig.10 and Fig.11, On comparison with circuit simulator, the momentum results are -0.3 dB and -13 dB more in ripple and edges (stopband), which is again much better hope to go for measurement board to prove the state of art CRLH MTM new structure and its applications in RF communication systems.

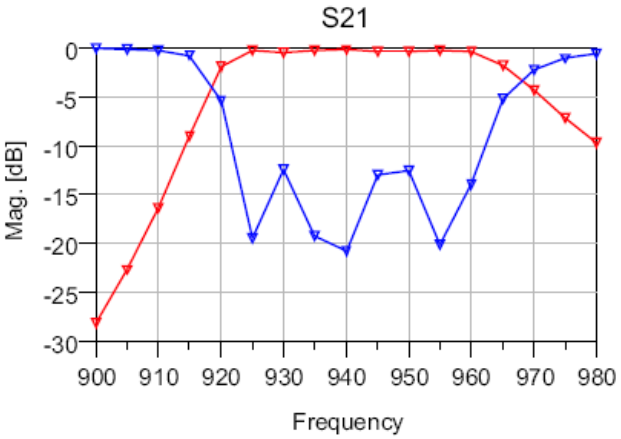

Fig. 10: Momentum Simulator Results - Three Unit Cells BPF

Fig. 11: Momentum Simulator Results – closer View

The layout board 33cm x 37cm in Fig.12 is fabricated using ROGER'S 4003 material with substrate thickness of 0.813mm and conductor thickness of 0.1mm respectively in a close conductive housing [In Fig.13] of shielded suspended substrate which is separated by 20mm symmetric walls on top and bottom from the centre of filter. The cross-section is depicted in Fig.14

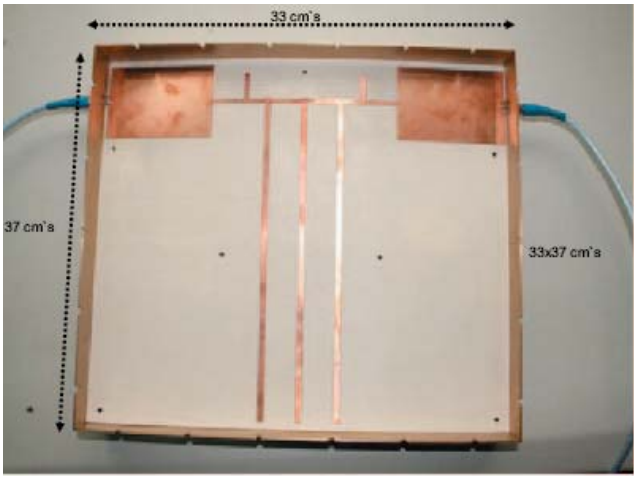

Fig. 12: Measurement Board 3 unit cell structure

Fig. 13: Measurement Board- Closed view

The measurement board of MTM CRLH BPF results in Fig.15 shows a stopband of nearly -10 dB at 918 MHz with an average passband less than -0.76 dB between 928MHz - 964MHz within 35 MHz bandwidth, the frequency range is displaced about 3-4 MHz due to critical housing of the suspended substrate, and can be adjusted by tuning the metallic housing screws to set our frequency range of design i.e. 925 MHz - 960 MHz respectively. The results in this range has -0.7 dB insertion loss and -10 dB stop band at 915 MHz and can be seen in Fig.16.

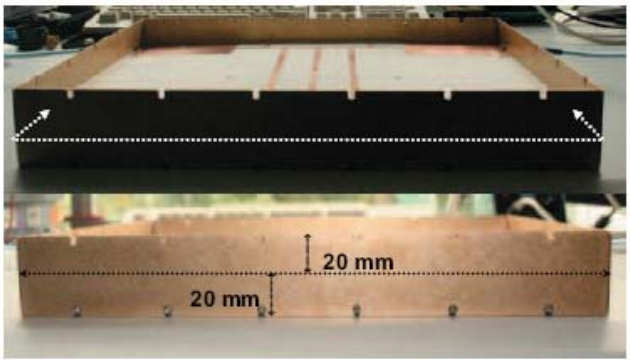

Fig. 14: Measurement Board - Cross-section

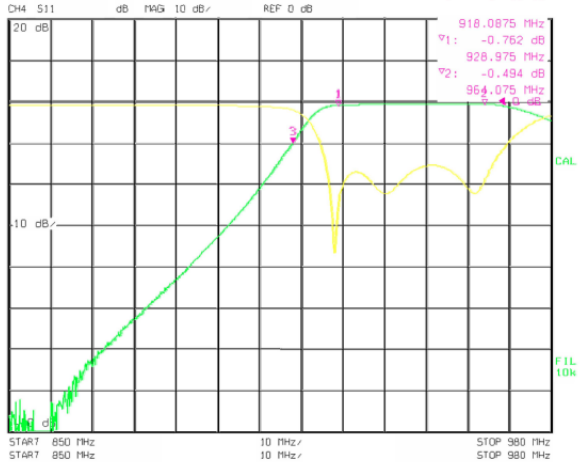

Fig. 15: Measurement Results

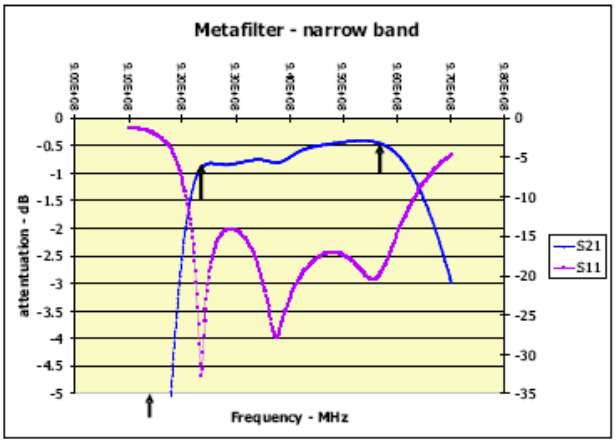

Fig. 16: Measurement Board Results – closer View

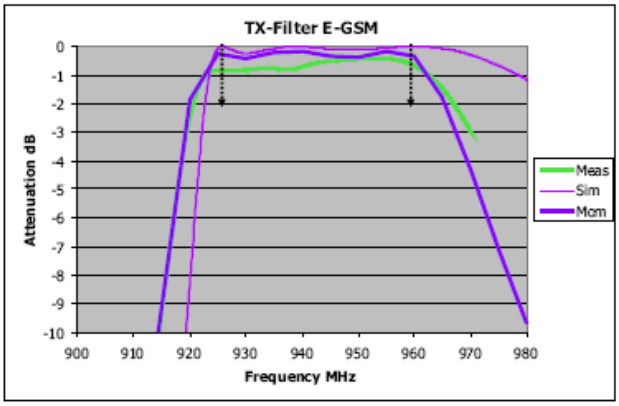

Fig. 17: Result Comparison

Fig.17 shows the comparison between circuit simulator, momentum simulator and measurement results and is tabulated below. The obtained fabricated board results are almost equal in the stopband and 0.4 dB higher in the pass band in comparison with method of momentum analysis simulator than circuit simulator and hence satisfies our goal of reaching passband less than -1 dB. This gives an idea that, the measurement results can be improved better with momentum simulator optimization techniques. Moreover sharper stopband can be achieved by increasing more number of unit cells [14] which is our future research task in the state of art MTM structures.

Freq	Circuit Simulator	Momentum Simulator	Measurement Board Results
925 MHz Passband dB[S21]	-0.07 dB	-0.25 dB	-0.7 dB
960 MHz Passband dB[S21]	-0.03 dB	-0.26 dB	-0.4 dB
915 MHz Stopband dB[S21]	-23 dB	-10 dB	-10 dB

Table. 1 Result Comparison

5. CONCLUSION

It was shown by designing a bandpass filter, metamaterial CRLH structures are very beneficial in terms of providing low insertion losses which are very much needed for EGSM base station. The obtained board measurement result is very good in agreement with momentum simulation results with respect to circuit simulator results. Future work on metamaterial CRLH structures for microwave filters will continue for much better results using our new structure with open stubs and gaps taking size reduction and cost in to consideration.

6. ACKNOWLEDGEMENT

The author Shaik Geelani would like to thank Prof. Georg Fischer for the creation of Doctorate opportunity aswell to gain professional experience at Bell Labs Europe. He also would like to thank Bell Labs Nuremberg Team, especially Dr. Michael Doubrava and Dr. Michael Sollner for their support during the research.

Further he wants to thank the German Ministry of research and education (BMBF) for funding part of this work under MARIO project (Metamaterial based flexible duplex filters).

REFERENCES

[1] V. G. Veselago, “The electrodynamics of substances with simultaneously negative values of ε and μ ”, Sov. Phys.-Usp., vol. 10, pp. 509-514, Jan.-Feb. 1968.

[2] J. B. Pendry, A. J. Holden, W .J. Stewart and I. Young’s, “Extremely low frequency Plasmon’s in metallic microstructures”, Phys. Rev. Lett., vol. 76, no. 25, pp. 4773-4776, Jun. 1996

[3] J. B. Pendry, A. J. Holden, D. J. Robbins, and W.J. Stewart, “Magnetism from conductors and enhanced nonlinear phenomena”, IEEE Trans.Microw. Theory Tech., vol. 47, no. 11, pp. 2075-2084, Nov. 1999

[4] D. R. Smith, W. J. Padilla, D. C. Vier, S. C. Nemat-Nasser, and S.Schultz, “Composite medium with simultaneously negative permeability and permittivity”, Phys. Rev. Lett., vol. 84, no. 18, pp. 4184-4187, May 2000.

[5] C. Caloz, H. Okabe, T. Iwai, and T. Itoh, “Transmission line approach of left-handed (LH) materials”, in USNC/URSI Nat. Radio Science Meeting, vol. 1, Jun. 2002, p. 39.

[6] A. K. Iyer and G. V. Eleftheriades, “Negative refractive index Metamaterial supporting 2-D waves”, in IEEE MTT-S Int. Microwave Symp. Dig., vol. 2, Jun. 2002, pp. 1067 1070.

[7] D. R. Smith and N. Kroll, “Negative refractive index in left-handed materials”, Phys. Rev. Lett., vol. 85, no. 14, pp. 2933-2936, Oct. 2000.

[8] A. Lai, T. Itoh, "Composite Right/Left-Handed Transmission Line Metamaterials", IEEE Microwave Magazine, pp.34-50, Sept. 2004.

[9] I-H. Lin, M. DeVincentis, C. Caloz, T. Itoh, "Arbitrary Dual-Band Components Using Composite Right/Left-Handed Transmission Lines", IEEE Transactions on Microwave Theory and Technique, Vol. 52, No.4, April 2004.

[10] C. Caloz, A. Sanada, T. Itoh, "A novel Composite Right-/Left-Handed Coupled-Line Directional Coupler With Arbitrary Coupling Level and

[11] Broad Bandwidth", IEEE Transactions on Microwave Theory and Techniques, Vol. 52, No.3, March 2004.
[12] H. Okabe, C. Caloz, T. Itoh, "A Compact Enhanced-Bandwidth Hybrid Ring Using an Artificial Lumped-Element Left-Handed Transmission-Line Section", IEEE Transactions on Microwave Theory and Technique, Vol. 52, No.3, March 2004.
[13] W. Menzel, A. Balalem: Quasi-Lumped Suspended Stripline Filters and Diplexers. IEEE Trans. on MTT, vol.MTT-53, Oct. 2005, pp. 3230 – 3237.
[14] J. E. Dean: Suspended substrate stripline filters for ESM applications. IEE Proc., Vol. 132, Pt. F, July 1985, pp.257 - 266.
[15] C. Caloz, T. Itoh, Electromagnetic Metamaterial, IEEE press, Wiley, Hoboken NJ, 2006
[16] Benedek, P. Silvester, P., Equivalent Capacitances for Microstrip Gaps and Steps Microwave Theory and Techniques, IEEE Transactions on Volume 20, Issue 11, Nov 1972 Page(s):729 – 733.
[17] Gunther Dehm-Andone, Grzegorz Adamiuk, Georg Fischer; Using Metamaterial structures with frequency agile base stations, IEEE GEMIC 2006.
[18] Lei Zhu, Huamin Shi; Menzel:, W Coupling behaviours' of quarter-wavelength impedance transformers for wideband CPW bandpass filter., Microwave and Wireless Components Letters, IEEE Volume 15, Issue 1, Jan. 2005 Page(s):13 – 15.
[19] Bekheit, M.; Amari, S.; Menzel, W, Modelling and Optimization of Compact Microwave Bandpass Filters. Microwave Theory and Techniques, IEEE Transactions on Volume 56, Issue 2, Feb. 2008 Page(s):420 – 430.
[20] Anu Lehtovuori and Luis Costa, Model for Shielded Suspended Substrate Microstrip Line, Circuit Theory Laboratory Report Series, Helsinki University of Technology 1998.
[21] G. Fischer, Architectural benefits of wide band gap RF power transistors for frequency agile base station systems, IEEE MTT, 6th annual Wireless and Microwave Technology Conference, Clearwater, Florida, April 2004.

Resume

Educational Qualifications

PhD in Electrical/Electronics Engineering **March 2009**
Friedrich-Alexander-University, Erlangen – Nurnberg
(Title *"High Q-factor Metamaterial duplex filters in suspended substrate technology"*)

M.S., Electronics and Telecommunication Engineering **Aug. 2005**
University of Gavle, Sweden - Specialization in RF/Microwave Engineering

Masters, Physics **Sep. 1998**
University of Bhopal, Bhopal, India - Specialization in Electronics.

Bachelor of Science, Electronics **June 1996**
Sri Krishna Devaraya University, Anantapur, India

Working Experience

Alcatel-Lucent Bell-Labs, Nuremberg, Germany **Sep. 2006 – Nov. 2008**
PhD, Research Engineer RF Design

Maxplanck Institute for semiconductors, Munich, Germany **Jan. 2006 – April. 2006**
Research Assistant

Infineon Technologies, Munich, Germany **Sep. 2004 - Sep. 2005**
Research Student RF Design

Syed Hashim College of Science and Technology, **Dec. 1998 - March 2003**
Hyderabad, India
Teaching Assistant

Personal Data

Nationality : Indian
Date of Birth : 17 June 1976
Contact : tsjeelani@gmail.com